CNNM/PRL/ARL15 complex regulates magnesium homeostasis and TRPM7

Yevgen Zolotarov

Department of Biochemistry
Faculty of Medicine
McGill University
Montréal, QC, Canada

August 2022

A thesis submitted to McGill University in partial fulfillment of the requirements of the Degree of Doctor of Philosophy

I dedicate this thesis to my father. He instilled the love of science in me since a young age. We had bookshelves upon bookshelves filled with books on mathematics, physics, astronomy, biology, and science fiction that I started reading as soon as I could read. His kindness and joyful attitude will stay with me forever. He left us too soon.

Table of Contents

Abstract

Magnesium is crucial for numerous metabolic pathways and is required for general health. For instance, all free ATP is stabilized by a Mg^{2+} ion and ribosomes have more than a hundred magnesium binding sites. Furthermore, translation and transcription depend on this cation and yet the regulation of magnesium homeostasis remains only partially explained. To further elucidate the function of CNNMs in magnesium homeostasis, we identified a novel role of ARL15 as an interacting partner of CNNMs. They co-localized in the perinuclear region where ARL15 modulates N-glycosylation of CNNMs. This in turn affects Mg^{2+} influx and ATP production in kidney cancer cells. TRPM7, the ubiquitous divalent cation channel, was also identified as a putative interacting partner of ARL15. As a follow-up to this study, we uncovered a novel role of CNNMs as negative regulators of TRPM7. The presence of ARL15 significantly increased the binding between CNNMs and TRPM7. The binding of PRL-2 to CNNM3 resulted in a change in the subcellular localization of the latter. TRPM7 and CNNM3 affected the expression of PRL-1/2 in opposite ways, which in turn affected TRPM7 downstream signaling. The regulatory binding between TRPM7 and CNNM3 is modulated by either ARL15 or PRL-1/2 interactions with CNNM3, which are in turn affected by the changes in magnesium levels. The novel layers of Mg^{2+} regulation uncovered in this thesis can be targeted to improve magnesium absorption in hypomagnesemia patients. Additionally, our results uncover important possibilities to impede the metabolic processes of cancer cells, thereby preventing their spread.

Résumé

Le magnésium est crucial pour plusieurs voies métaboliques et est requis pour la santé générale. Par exemple, tout l'ATP libre est stabilisé par un ion de Mg^{2+}, et les ribosomes ont plus de cent sites de liaison pour de ce cation. Bien que les processus de transcription et de traduction dépendent du magnésium, la régulation de son homéostasie n'est que partiellement élucidée. Pour comprendre davantage la fonction des CNNMs dans cette homéostasie, nous avons identifié un nouveau rôle de ARL15 comme partenaire d'interaction des CNNMs. Ils co-localisent dans la région périnucléaire, où ARL15 module la N-glycosylation des CNNMs, affectant ainsi l'afflux de Mg^{2+} et la production d'ATP dans les cellules cancéreuses du rein. Le canal des cations divalents TRPM7 a aussi été identifié comme partenaire d'interaction putatif de ARL15. Nous avons de plus découvert un nouveau rôle des CNNMs en tant que régulateurs négatifs de TRPM7. La présence de ARL15 augmente la liaison entre les CNNMs et TRPM7. La liaison de PRL-2 entraîne un changement de localisation subcellulaire de CNNM3. TRPM7 et CNNM3 affectent l'expression de PRL-1/2 de manière opposée, ce qui module la signalisation en aval de TRMP7. La liaison régulatrice entre TRPM7 et CNNM3 est modulée par l'interaction de ARL15 ou de PRL-1/2 avec CNNM3, qui est alors affectée par un changement du niveau de magnésium. Dans ces études, nous avons découvert de nouvelles strates de régulation de l'homéostasie du magnésium et de TRMP7. Les niveaux de régulation de Mg^{2+} découverts dans cette thèse peuvent êtres ciblés pour améliorer l'absorption de magnésium dans les patients souffrant d'hypomagnésémie. En outre, nos résultats ouvrent d'importantes possibilités pour freiner le métabolisme des cellules tumorales, empêchent ainsi leur propagation.

Acknowledgements

I am immensely grateful to my supervisor, Dr. Michel Tremblay, for his kindness, guidance, support, and trust. He accepted a student coming from an unrelated field into cancer research and let me explore novel ideas. I am extremely thankful to my friend and mentor Serge Hardy. He taught me and guided me throughout my PhD, and I will cherish all the numerous discussions we shared over many pints of beer. I am lucky to have interacted with all the past and current students and post-docs with whom I shared many lunches and happy hours that made life in the lab much more fun: João, Elie, Teri, Emily, Mathilde, Jacob, Chuhan, Alex, Ana, Hira, Tiffanie, Simon, Tzvet, Shan, Mark, Capucine, Zuzet, Alberto and Belma. I want to thank Noriko for her kindness and expertise with microscopy and for making beautiful figures. This work would be impossible without all the collaborators at McGill and outside. I am especially thankful to Chao Ma and Jeroen de Baaij for their hard work and contributions to our first paper. Work in the lab was made possible by our incredible support staff: Jean-François, Isabelle, and Jacinthe. I want to thank several members of the Sonenberg lab for their friendship and insight: Ritchie, Gyan and Mehdi. My sister and my parents were always there for me. I formed multiple great relationships in Michel's lab, where I met a lot of great people. The most important of them is the one I built with the love of my life and now my wife – Valerie. Her positive attitude, joyful outlook, and constant support and love made my life infinitely better.

Abbreviations

APC	ATP-Mg/P_i carriers
ARF	ADP-ribosylation factor
ARFGEF	ARF guanine nucleotide exchange factor 1
ARL15	ADP-ribosylation factor-like 15
AMP	adenosine monophosphate
ADP	adenosine diphosphate
ATP	adenosine triphosphate
BioID	proximity-dependent biotin identification
CBS	cystathionine β-synthase
CNNM	cyclin and CBS domain divalent metal cation transport mediator
CTP	cytidine triphosphate
DCT	distal convoluted tubule
DMSO	dimethyl sulfoxide
DNA	deoxyribonucleic acid
DPAGT1	dolichyl-phosphate N-acetylglucosaminephosphotransferase 1
EMC	ER membrane complex
Endo H	endoglycosidase H
ER	endoplasmic reticulum
ERK1/2	extracellular signal-regulated kinase 1/2
FCCP	carbonyl cyanide-*p*-trifluoromethoxyphenylhydrazone
GFP	green fluorescent protein
GlcNAc	N-acetylglucosamine
GTP	guanosine triphosphate
GWAS	genome-wide association study
HDL	high-density lipoprotein
HIP14(L)	Huntingtin-interacting protein 14 (like)
IP	immunoprecipitation
ITP	inosine triphosphate

LMAN	lectin, mannose binding 1
MAGT1	magnesium transporter 1
MMGT1	membrane magnesium transporter 1
$[Mg^{2+}]_e$	extracellular magnesium concentration
$[Mg^{2+}]_i$	intracellular magnesium concentration
mTORC	mechanistic target of rapamycin
NAFLD	non-alcoholic fatty liver disease
NASH	non-alcoholic steatohepatitis
ORF	open reading frame
OST	oligosaccharyltransferase
PNGase F	peptide:N-glycosidase F
PRL	phosphatase of regenerating liver
PTP	protein tyrosine phosphatase
RDA	recommended dietary allowance
RMSD	root-mean-square deviation
RNA	ribonucleic acid
RPN	ribophorin
siRNA	small interfering RNA
SLC	solute carrier
TAL	thick ascending limb of the loop of Henle
TCGA	The Cancer Genome Atlas
tRNA	transfer RNA
TRPM	transient receptor potential cation channel subfamily M
UDP-GlcNAc	uridine diphosphate *N*-acetylglucosamine
uORF	upstream open reading frame
XMEN disease	X-linked immunodeficiency with Mg^{2+} defect, Epstein-Barr virus (EBV) infection and neoplasia disease
ZDHCC	zinc finger DHHC-type palmitoyltransferase

List of figures

Supplementary Figures

List of tables

Supplementary Tables

Preface and contributions

The thesis is written in the manuscript format with results presented in two chapters (Chapter 2 and Chapter 3).

Chapter 2 – ARL15 modulates magnesium homeostasis through N-glycosylation of CNNMs

Yevgen Zolotarov*, Chao Ma*, Irene González-Recio, Serge Hardy, Gijs A.C. Franken, Noriko Uetani, Femke Latta, Elie Kostantin, Jonathan Boulais, Marie-Pier Thibault, Jean-François Côté, Irene Díaz Moreno, Antonio Díaz Quintana, Joost G.J. Hoenderop, Luis Alfonso Martínez-Cruz, Michel L. Tremblay†, Jeroen H.F. de Baaij†

Cellular and Molecular Life Sciences (2021) 78: 5427–5445

Contribution to original knowledge: In this paper we identified a novel role of a poorly described small GTPase ARL15 in magnesium homeostasis regulation. Interactions of ARL15 with CNNM family members were established and the effect on N-glycosylation of CNNM3 was described. ARL15 was found to significantly affect magnesium uptake and ATP production.

Contribution of authors: Y.Z., C.M., S.H., J.H., M.L.T. and J.d.B. designed the research studies, Y.Z., C.M., I.D.M., A.D.Q., G.A.C.F., I.G.R., E.K., F.L., J.B., M.-P.T., L.A.M.C., J.F.C., N.U., S.H., J.H., M.L.T. and J.d.B. conducted experiments and/or analyzed data. Specifically, Y.Z. identified the interactions between ARL15 and CNNMs, the changes in N-glycosylation and ATP production, and conducted the experiments in figures 2.1 D, E; 2.5; 2.6 B and Supp. Fig. 2.5. Y.Z., C.M., S.H., M.L.T. and J.d.B. wrote the manuscript.

Chapter 3 – CNNMs and their interacting partners regulate TRPM7

Yevgen Zolotarov*, Serge Hardy*, Noriko Uetani, Jacob A.C. Coleman, Simon Roitman, Michel L. Tremblay

Manuscript in preparation

Contribution to original knowledge: In this manuscript we described the involvement of ARL15 in CNNM•TRPM7 interactions. CNNMs were identified as inhibitors of TRPM7 activity on multiple levels: magnesium uptake, cell morphology and downstream signaling. Dynamic interactions between CNNMs and TRPM7 that were regulated by ARL15 and PRL-1/2 in response to changes in magnesium levels were elucidated.

Contribution of authors: Y.Z., S.H., and M.L.T. designed the research studies, Y.Z., S.H., N. U., J.A.C.C. and S. R. performed the experiments and analyzed the data. Specifically, Y.Z. identified the interactions between TRPM7, CNNMs and ARL15 and the function of ARL15 in strengthening these interactions, and conducted the experiments in figures 3.1; 3.3; 3.5, Supp. Fig. 3.1; 3.2 D; 3.3. Y.Z. and S.H. wrote the manuscript.

Chapter 1

Literature review

Magnesium

Magnesium (Mg^{2+}) is the second most abundant divalent cation in the human body. It is involved in hundreds of enzymatic reactions, including such vital processes as transcription and translation [1]. Currently, 200 pathways and processes are listed on HMDB under magnesium (https://hmdb.ca/metabolites/HMDB0000547, accessed on 16 Aug 2021, Ref. [2]). Notable among them are glycolysis, gluconeogenesis, citric acid cycle and fatty acid metabolism, demonstrating the importance of magnesium in such crucial biochemical pathways. Given the vast range of reactions that involve magnesium it is not surprising that multiple human diseases are associated with magnesium imbalance [3].

Magnesium in biochemistry and molecular biology

Most ATP in the cell is found in the form of Mg•ATP where the two positive charges of a magnesium ion neutralize negative charges on phosphate groups of adenosine triphosphate [4]. Magnesium can be found in bidentate or tridentate phosphate coordination, where either two or three phosphate groups are neutralized by Mg^{2+} [5]. Similarly, GTP is found in the Mg•GTP form [6]. Enzymatic reactions involving hydrolysis of ATP or GTP require a magnesium ion [7, 8]. Apart from binding free nucleotide di- and triphosphates, magnesium also binds RNA and DNA polynucleotides. Binding of Mg^{2+} to RNA results in stabilization of its structure, decreased degradation and increased catalysis [9]. The process of transcription itself involves Mg^{2+} since up to six magnesium ions compensate negative charges of $(PO_2)^-$ oxygens on the backbone of tRNA molecules [10]. Protein synthesis is also dependent on magnesium since multiple Mg^{2+}

ions are found within the structure of ribosomes where they are involved in proper folding and stability of rRNA, and interaction between rRNA and ribosomal proteins [11, 12]. In bacteria, a single ribosome contains at least 170 magnesium ions and depletion of magnesium results in reduction of ribosome synthesis and increase in magnesium transporters translation [13]. Similarly to prokaryotes, eukaryotic cells respond to magnesium deprivation by upregulating transcription and translation of genes involved in magnesium transport and regulation [14–19].

Magnesium transporters and transport mediators

Apart from the TRPM6/7 magnesium channels and the CNNM family of magnesium transport mediators, which will be discussed in greater detail below, multiple proteins have been described as magnesium transporters. The SLC41 family, MRS2 and putative magnesium transporters are discussed in this section.

SLC41 family

The solute carrier 41 (SLC41) family consists of three members (SLC41A1, SLC41A2, SLC41A3) that have been described as magnesium transporters [20]. SLC41A1 has been described more specifically as a Na^+/Mg^{2+} exchanger that is involved in Mg^{2+} efflux [21]. However another study has shown that the activity of SLC41A1 does not depend on sodium [16]. Rather, the authors demonstrated that a low magnesium diet affects the function of mitochondria by decreasing the activity of Krebs cycle components, which was rescued by *Slc41a1* knockout in mouse cardiomyocytes [22]. *Slc41a1* expression is sensitive to depletion of magnesium, where significant increase in its mRNA levels was

observed in kidney cortex and distal convoluted tubule cells cultured in low extracellular magnesium [23]. In polarized cells SLC41A1 is found at the basolateral membrane, where it could participate in the extrusion of Mg^{2+} from kidney cell cytoplasm into the bloodstream [16]. SLC41A2 is not as well studied as SLC41A1, but it has also been shown to be involved in magnesium transport. In TRPM7 knockout cells, overexpression of SLC41A2 rescued the proliferation arrest and increased magnesium uptake [24]. *Slc41a3* was identified, together with *Cnnm2* and *Trpm6*, to have increased expression in the distal convoluted tubule (DCT) in mice fed a Mg^{2+}-deficient diet [25]. *Slc41a3*$^{-/-}$ mice were shown to have hypomagnesemia and had an increase in *Trpm6* and *Slc41a1* magnesium transporter expression to compensate for the knockout of *Slc41a3* [15]. In contrast with SLC41A1 and SLC41A2, which are expressed at the plasma membrane, SLC41A3 is expressed at the inner mitochondrial membrane, where it acts as a Na^{+}/Mg^{2+} exchanger and participates in Mg^{2+} extrusion [26].

MRS2 and mitochondria

Whereas SLC41A3 participates in mitochondrial magnesium efflux, MRS2 plays a role of the sole magnesium transporter that participates in Mg^{2+} influx in mitochondria, a process which was first identified in yeast [27] and then confirmed in human cells [28, 29]. A recent study has shown that lactate drives the release of magnesium from the ER and the consequent mitochondrial Mg^{2+} influx, which requires Mrs2 [30]. The transporter involved in the efflux of magnesium from the ER is still unknown. ATP13A4 has been proposed as a potential ER Mg^{2+} transporter but its function has not been confirmed [31]. The lactate study has also shown that *Mrs2* knockout (KO) mice were protected

from LPS-induced septic shock due to the reduction in leukocyte infiltration and attenuation of proinflammatory cytokine release [30]. In addition, phosphorylation of pyruvate dehydrogenase was higher in *Mrs2* WT than in KO hepatocytes, which resulted in decreased mitochondrial bioenergetics, and the differences between the two genotypes were increased upon lactate treatment [30]. Pyruvate dehydrogenase is inhibited by phosphorylation, which results in a decrease of acetyl-CoA entering the TCA cycle [32]. This was a surprising finding since a previous study has shown no changes in pyruvate concentration upon *Mrs2* knockout but a decrease in TCA cycle metabolites such as malate, citrate, *cis*-aconitate and succinate [33]. Various studies have as well demonstrated that Mg^{2+} enhances the activity of pyruvate dehydrogenase and other dehydrogenases that participate in the TCA cycle [34]. Mitochondrial ATP-Mg/P_i carriers (APCs, SLC25A23-25 and SLC25A41) are involved in indirect transport of magnesium in and out of mitochondria, but their effect on Mg^{2+} dynamics is not well understood [35].

Putative magnesium transporters

Multiple other proteins have been ascribed the role of magnesium transporters with insufficient evidence [31, 36]. The function of most of them has not been well studied and their effect on magnesium homeostasis is not understood. The function of MAGT1 and MGMT1 has been elucidated and they were shown not be magnesium transporters but rather proteins involved in proper processing and N-glycosylation of membrane proteins [37, 38].

Magnesium in health and disease

Given the importance of magnesium in such a wide range of biochemical processes it is not surprising to see that it is involved in multiple human diseases. Magnesium is absorbed from food in the intestine, where most of the absorption takes place through a paracellular pathway in the small intestine, while fine control of magnesium uptake takes place in the large intestine through a transcellular pathway [3]. Magnesium is filtered through the kidneys and the regulation of magnesium in the body takes place though fine-tuned reabsorption in the DCT of the nephron [3].

Magnesium deficiency

Normal serum magnesium levels are defined as 0.7-1.0 mmol/L [39]. According to epidemiological surveys conducted in different countries magnesium deficiency is a frequently observed issue. Fewer than 25% of respondents in the USA National Health and Nutrition Examination (2001–2010) met the recommended dietary allowance (RDA) of magnesium [40] and 2.5%-15% are estimated to have hypomagnesemia [39]. In a German survey, hypomagnesemia was observed in 14.5% of people in a population of 16000 individuals [41]. In an Iranian population, 14.6% of individuals had a sub-optimal magnesium level below 0.8 mmol/L [42]. In Canada, magnesium RDA stands at 320 mg/day for adult females, 360 mg/day for pregnant females and 420 mg/day for adult males (https://www.canada.ca/en/health-canada/services/food-nutrition/healthy-eating/dietary-reference-intakes/tables/reference-values-elements-dietary-reference-intakes-tables-2005.html, accessed on September 9, 2021). Food sources high in magnesium include nuts and seeds, beans and tofu, and whole grains [43]. However,

comparing content of magnesium in food with actual consumption shows that a much lower amount of magnesium is consumed than listed in food micronutrients tables, which is attributed to its loss during cooking [44]. Vegetarians were shown to consume 80% more magnesium, on average, compared to omnivores [45]. The standard American diet supplies inadequate amounts of several vitamins and minerals, including magnesium, which can result in hypomagnesemia and related conditions [46].

Diseases linked with magnesium perturbations

Multiple adverse conditions are associated with hypomagnesemia, with some of them listed in Table 1. For example, dietary magnesium is inversely correlated with incidence of depression [47, 48], and supplementation with magnesium chloride for 6 weeks was enough to improve multiple self-reported parameters in adults with mild-to-moderate depression [49].

Populations with low serum or dietary magnesium present higher incidence of prediabetes and diabetes [50], imbalanced cholesterol [51], higher markers of adiposity and higher serum glucose levels [52]. These are associated with the incidence of stroke, which is reduced in a dose-dependent manner in population with increasing magnesium intake [53]. Magnesium supplementation results in a clinically significant reduction in blood pressure [54] and improvement in many other health parameters, such as hyperglycemia and hypertriglyceridemia, and results in decreased incidence of type 2 diabetes [55]. Metformin treatment, a widely-used diabetes therapy is associated with reduced serum magnesium levels and results in a reduced expression of TRPM6, a

magnesium transporter, which could partly explain the link between diabetes and hypomagnesemia [56].

In mice with progeria, magnesium supplementation improved their antioxidant and ATP status, as well as their longevity [57].

The importance of magnesium in health is highlighted in the papers mentioned above, which reinforces the need to study magnesium transporters and modulators involved in its homeostasis.

Table 1.1: Association of hypomagnesemia with various conditions

Disease	Reference
Arrhythmia	[58, 59]
Asthma	[60, 61]
Ataxia	[62, 63]
Depression and anxiety	[47, 49, 64]
Fibromyalgia	[65]
Hypertension	[66–68]
Hypothyroidism, Hashimoto thyroiditis	[69]
Inflammation	[70]
Metabolic syndrome and obesity	[55]
Migraine	[71]
NAFLD, NASH	[72, 73]
Preeclampsia	[74]
Seizures and epilepsy	[75–78]
Stroke	[79, 80]
Type 2 diabetes	[81]

ARL15

Biochemical properties and function of ARL15 are not well understood. Initial information on ARL15 came from a series of genome-wide association studies (GWAS) which identified its link with adiponectin levels [82–84], type 2 diabetes [84–86], serum lipid

levels [87], rheumatoid arthritis [88, 89] and blood pressure [90]. Of note, a GWAS performed in the Japanese population could not confirm the association of ARL15 with type 2 diabetes [91]. The association of ARL15 with adiponectin and lipid levels, as well as type 2 diabetes was elucidated in the study which showed that in adipocytes, knockdown of ARL15 resulted in reduced adiponectin production and secretion, and pre-adipocyte differentiation [92]. This makes sense since adiponectin plays an important role in glucose uptake and fatty-acid oxidation [93]. Reduction of adiponectin levels is linked with insulin resistance, type 2 diabetes, hypertension and dyslipidemia [93]. A post-translation S-palmitoylation modification of ARL15 was recently identified on Cys22 and 23, which was responsible for its proper localization to the Golgi during adipogenesis [94]. Since S-palmitoylation is a reversible post-translational modification, this dynamic process could be regulated to affect ARL15's localization.

A link between ARL15 and kidney function was uncovered in a GWAS meta-analysis which identified a relationship between a SNP in an intron of ARL15 and the estimated glomerular filtration rate, which is a measure of kidney function [95]. Further, the connection between magnesium and ARL15 was unraveled in a GWAS meta-analysis that identified two genes to be linked with kidney magnesium handling: ARL15 and TRPM6, a magnesium channel [96]. A recent study identified ARL15, CNNMs and TRPM7 to form a native complex, where ARL15 was responsible for inhibiting magnesium influx through TRPM7 [97].

Interestingly, ARL15 appears to be crucial for development since its knockout in mice is embryonically lethal [98].

PRLs

The phosphatase of regenerating liver (PRL) family is composed of three members: PTP4A1 (PRL-1), PTP4A2 (PRL-2) and PTP4A3 (PRL-3). They are dual specificity phosphatases, albeit their enzymatic activity is very low compared to other phosphatases, partly due to the presence of an alanine immediately after $C(X)_5R$ motif instead of serine/threonine found in other PTPs (Fig. 1.1A) [99]. The phosphatase activity of PRLs can be regulated through the formation of disulfide bond between cysteine 49 and cysteine 104 (numbering based on PRL-1/3), with reduced PRL having a much higher activity [100]. Rat PRL-1 was first identified as an immediate-early gene following a partial hepatectomy that resulted in rapid liver regeneration, giving the name to this phosphatase family [101]. PRLs share high sequence identity (>78%), with PRL-3 being more distant from PRL-1 and -2 (Fig. 1.1B). They are unique among phosphatases in having a CAAX prenylation motif at their C-terminal (where C is a cysteine, A is an aliphatic amino acid and X can be any amino acid), which localizes PRLs to membranes [102] (Fig. 1.1A). Following prenylation, the AAX peptide is cleaved in the ER by RCE1 prenyl endopeptidase [103]. Deletion of the CAAX motif results in nuclear localization of PRLs, which was initially hypothesized to be due to the presence of a potential bipartite nuclear localization signal formed by the polybasic region [104, 105], later shown not to be involved in nuclear localization [106]. PRL-1 and -2 are expressed in all tissues whereas PRL-3 is mostly expressed in the heart, skeletal muscle and the prostate [102]. PRLs are overexpressed in multiple cancers and, more recently, a link with magnesium homeostasis was established [102].

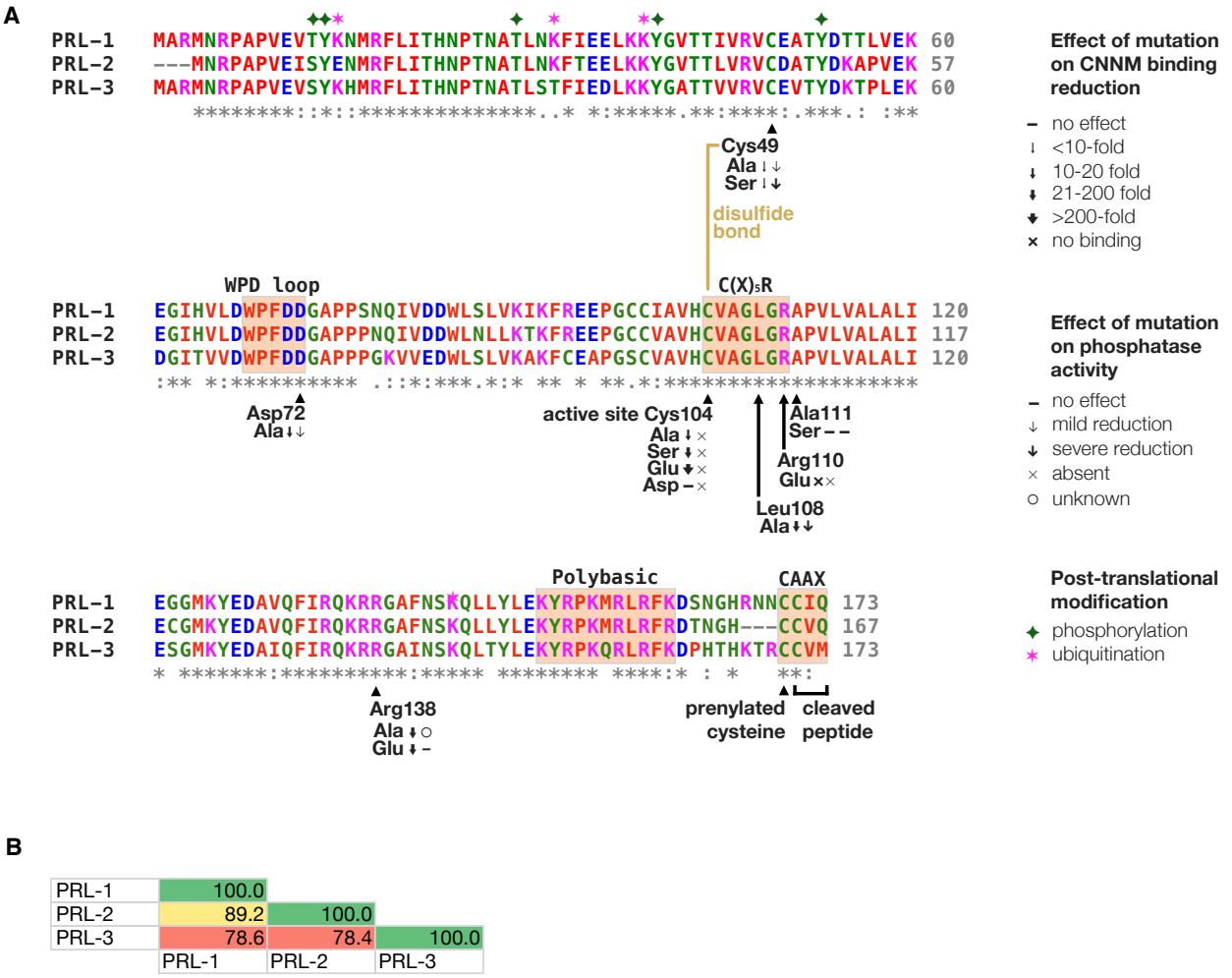

Figure 1.1: Alignment and comparison of PRL proteins
A: Clustal Omega [107] alignment of human PRL proteins with PRL3 CNNM binding and phosphatase activity data adapted from [108, 109], numbering based on PRL3. Post-translational modification data obtained from PhosphoSitePlus [110]. B: Amino acid identity between PRLs based on the alignment.

Role in cancer

The first PRL associated with cancer progression was PRL-3 which was linked with colorectal cancer liver metastases [111]. Since then, PRLs have been linked with development of primary tumours and metastases [102]. PRL-3 expression is much lower in most tissues than that of PRL-1 and PRL-2. However, in transformed tissues, its

expression levels increase significantly [111]. Amplification and high mRNA levels of *PTP4A* genes in different cancers is observed on average at ~5% for *PTP4A1* and *PTP4A2* (Fig. 1.2). In general, *PTP4A3* shows higher levels of amplification/high mRNA than *PTP4A1* and *2*, at 14.2% of samples, with highest levels in ovarian serous cystadenocarcinoma and uveal melanoma (Fig. 1.2). A similar proportion (22.3%) of diverse human tumour samples were identified as PRL-3 positive using immunohistochemistry [112]. Similarities between *PTP4A1* and *2* mRNA regulation, and their contrast with *PTP4A3*, could be explained in part by the presence of an analogous regulatory uORF in the 5′ UTR of *PTP4A1* and *2*, that is absent in *PTP4A3* [18]. In addition, only the 5′ UTR of *PTP4A3* contains repeated GCCCAG motifs, which are involved in translational repression by PCBP1 [112].

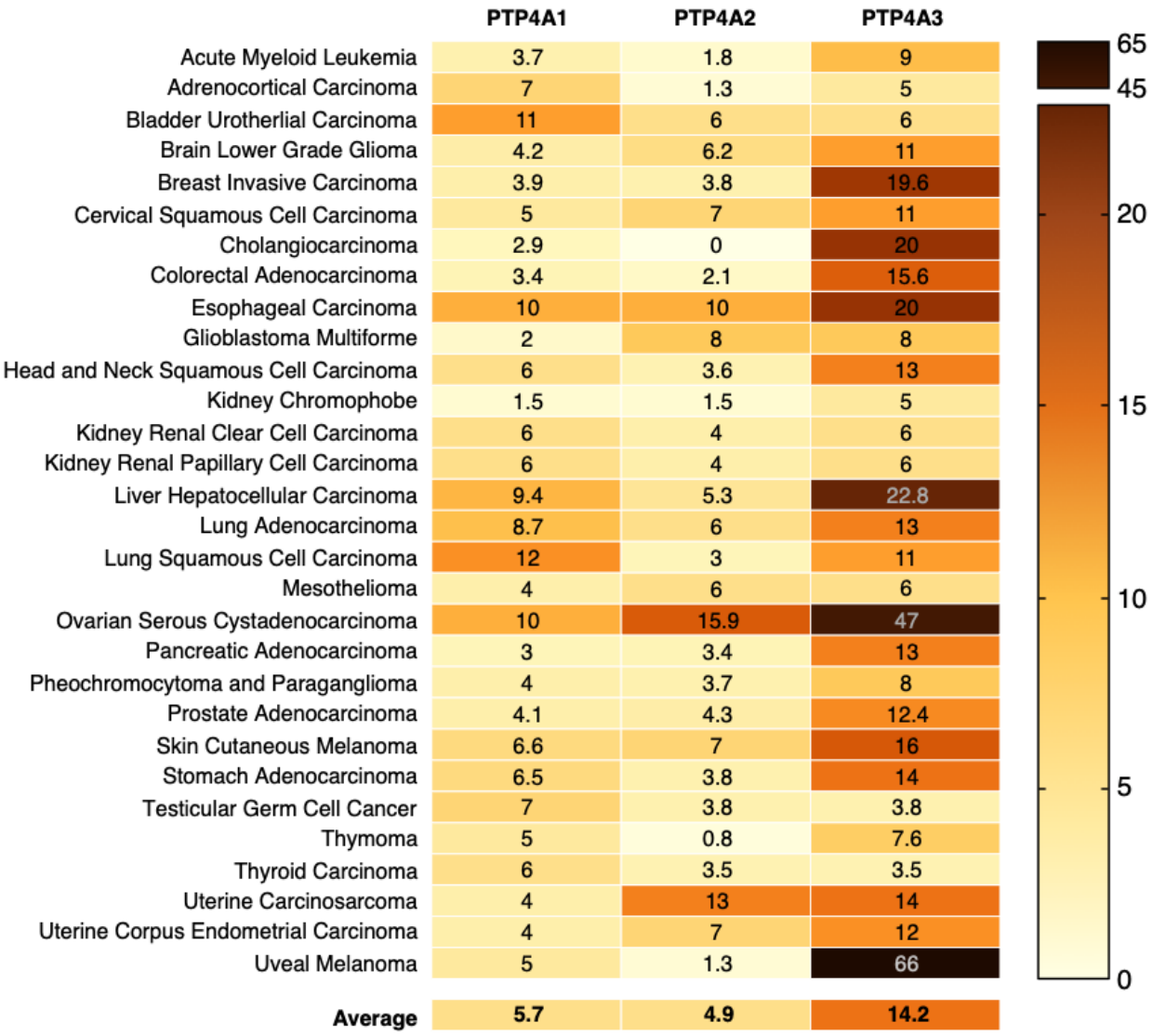

Figure 1.2: Proportion of cancer patients with amplifications or high mRNA levels of *PTP4A* gene family in TCGA

Multiple papers have linked high PRL-3 expression to worsened patient outcomes in various cancers, such as colorectal, ovarian, breast and lung [113–116]. Overexpression of PRL-2 was linked with breast cancer progression and it was observed that *PTP4A2* mRNA levels are higher in tumour and more so in lymph nodes, compared to normal breast tissue [117]. In another breast cancer study, the association with

disease-free survival with PRL-3 was only observed in patients who had developed lymph nodes metastases, and no association was observed for PRL-1 or PRL-2 [118]. This could explain why no significant association between breast cancer survival and *PTP4A* gene expression was observed in the TCGA pan-cancer dataset (Fig. 1.3). Ovarian cancer patients with detectable PRL-3 protein expression fared significantly worse than those with undetectable PRL-3 [119]. mRNA levels of *PTP4A1* and *PTP4A2* in ovarian cancer effusions were inversely correlated with overall survival [120]. However, there was no significant link between *PTP4A* mRNA levels and patients' survival in the TCGA pan-cancer dataset (Fig. 1.3). The expression of *PTP4As* is significantly associated with survival of patients with two types of kidney cancer: clear cell and papillary (Fig. 1.3). Curiously, *PTP4A1* is associated with improved survival in clear cell renal carcinoma, in contrast with *PTP4A2* and *PTP4A3*. For papillary renal cell carcinoma, high expression of *PTP4A1* and *PTP4A3* is associated with reduced survival. Interestingly, no publications to date have associated *PTP4As* expression with clear cell and papillary renal cancers. An association of *PTP4A3* with two different types of kidney cancer has been established: upper tract urothelial carcinoma [121] and Wilms' tumour [122]. This discrepancy could be partly explained by the lack of significant correlation between *PTP4A* mRNA and protein levels in different tissues [123]. Lack of correlation between *PTP4A3* mRNA and protein levels was also observed in various cancer cell lines [112].

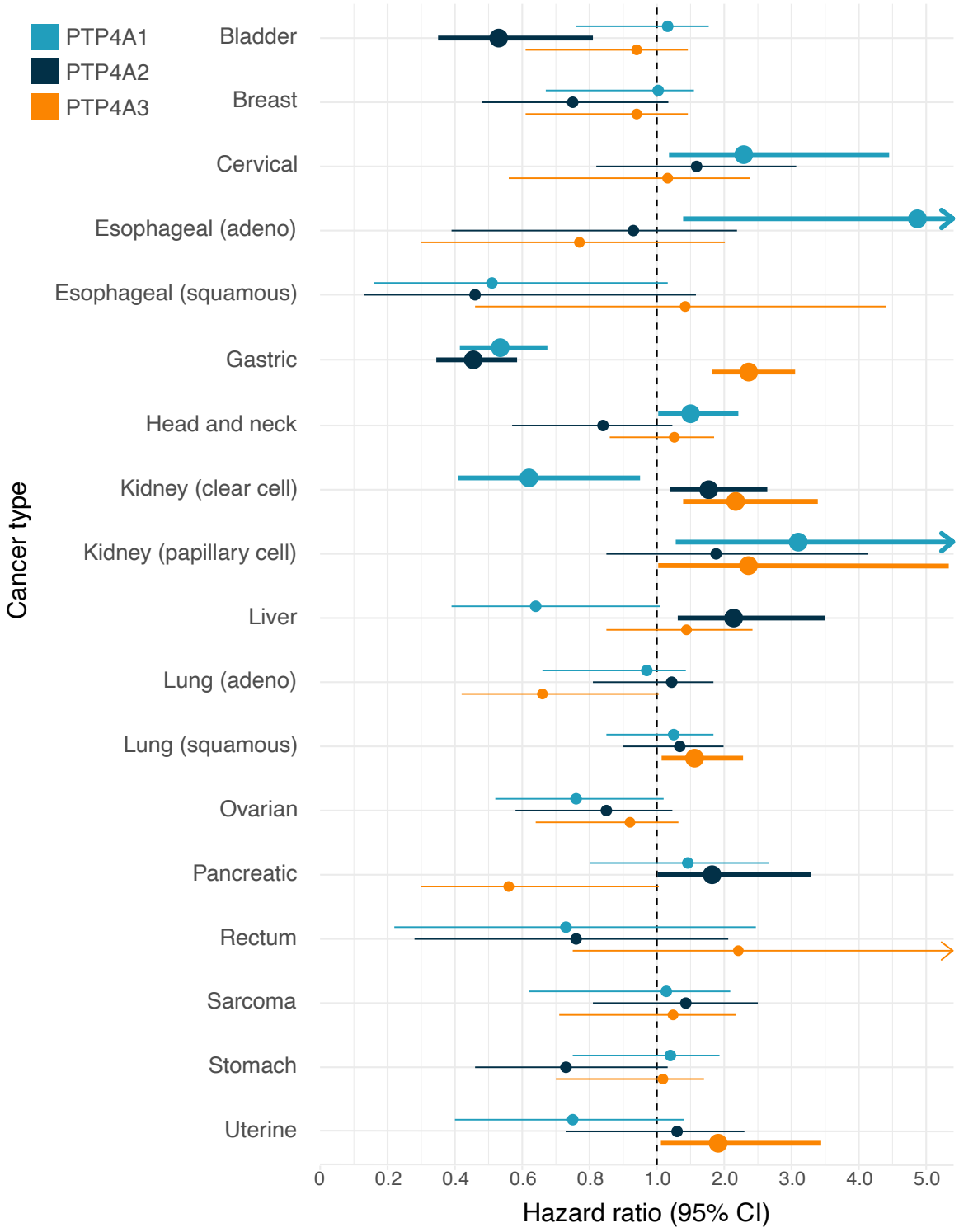

Figure 1.3: Hazard ratio of death in cancers with *PTP4A* gene expression KM-plotter was used to obtain hazard ratio statistics comparing cancer patients' survival in the upper and lower *PTP4A* expression quartiles [124, 125]. Thick lines indicate cases where expression of a specific *PTP4A* gene had a significant effect on survival based on the log-rank P value < 0.05.

The involvement of PRL-3 in tumour proliferation, angiogenesis, migration and metastasis has been studied extensively and multiple pathways affected by PRL-3 overexpression have been identified (reviewed in [126, 127]). These include pathways signalling through Rho GTPases, CSK/FAK/SRC/Rac, PI3K/AKT/PTEN, Ras/MEK/ERK1/2, p53, integrin, β-catenin and tensin/paxillin/vinculin [126, 128, 129]. For example, both PRL-1 and -3 were associated with increased cell motility and metastatic tumour formation in mice, and cells expressing catalytically dead (C104S mutation) PRL-3 exhibited reduced motility [130]. While multiple putative targets of PRLs have been identified, few have been confirmed by independent labs [102]. For instance, PTEN downregulation and consequent oncogenesis has been linked with both PRL-2 [131] and PRL-3 [132].

The link between PRLs and hematologic cancers has long been established. For example PRL-3 was found to be overexpressed in and involved in progression of Hodgkin's lymphoma [133, 134], T-cell lymphoblastic leukemia [135, 136], acute myeloid leukemia [137–139] and chronic myeloid leukemia [140]. Its oncogenic effects have been linked with dysregulation of various signaling pathways through such targets as β-catenin [139], SRC [135] and STATs [141–143]. STAT5 itself has been shown to promote PRL-3 expression in AML [137]. In a zebrafish model of T-cell lymphoblastic leukemia, prl-3 overexpression by itself did not increase the chance of establishing leukemia, however overexpression of myc and prl-3 together resulted in a significantly higher number of fish with leukemia, compared to myc alone [136]. In this study, PRL-3 was called a "collaborating oncogenic driver" and not an oncogene as in the study above,

which is in line with previous studies showing that PRLs alone are not sufficient to drive tumorigenesis but are necessary to enhance and maintain a transformed phenotype.

A recent study has shown that PRL-3 causes cells to be addicted to an acidic extracellular environment [144]. This is accomplished through the increase of intracellular magnesium, which in turn stimulates ATP and ROS production. Concomitant activation of TRPML lysosomal calcium channel results in lysosomal exocytosis, which allows for proton extrusion [144]. An acidic tumour microenvironment is linked with cancer growth and metastasis [145] and therefore the decrease in extracellular pH due to exocytosis of H^+ in PRL-3-overexpressing cells helps explain PRLs' effect on cancer proliferation. Another recent study showed that PRL-3 overexpression increases cancer cell survival in response to hypoxia mimicking $CoCl_2$ by acting as the phosphatase of p38 MAPK [146]. Phosphorylation of p38 MAPK under stress conditions, such as hypoxia and ROS production, leads to apoptosis [147], and its direct dephosphorylation by PRL-3 leads to survival and increased metastasis formation [146]. Interestingly, neither PRL-1 nor PRL-2 had an effect on p38 MAPK phosphorylation [146].

CNNMs

CNNMs (cyclin and CBS domain divalent metal cation transport mediator or cyclin M) have previously been named Ancient Conserved Domain Proteins (ACDPs) due to the high degree of conservation of their domains in all trees of life [148]. Homologs of CNNMs have been recently identified in fungi and plants and have been shown to be crucial for high magnesium tolerance [149]. Even though CNNMs contain a cyclin box sequence that has homology to cyclin proteins [148], a role in cell cycle progression has

not been observed for these proteins [150]. CNNMs share a conserved domain architecture composed of an N-terminal extracellular domain, CNNM (InterPro domain ID: IPR002550) (which until recently has been known as DUF21 (domain of unknown function 21)), Bateman module composed of 2 CBS domains (IPR044751) and a putative cyclic nucleotide-binding homology (CNBH) or cNMP-like domain (IPR018490) (Fig. 1.4) [151].


L48P
D63E
F93Lfs31X
N-glycosylation
E122K
Y189C
L161P
L170P
S269W
F272L
S196P
S200Y/P
R236Q/W
Y314X
V324M
V326L
L330F
E357K
L324P
L418P
L359P
G364Vfs9X
R407L
P409L
L438Pfs9X
G492C
T568I
D426
G433
T495I
V499M
R519X
extended loop
Y581X
N594S
R605X
S795L
R797X
Q717X
CNNM1
CNNM2
CNNM3
CNNM4
CNNM
CBS1
CBS2
CNBH

◂ Figure 1.4: Alignment of human CNNM proteins
Clustal Omega [107] alignment of human CNNM proteins with following annotations: CNNM, CBS1, CBS2 and CNBH [152, 153] domains highlighted below the sequence alignment; CNNM2 hypomagnesemia-causing and CNNM4 Jalili syndrome mutations are highlighted in tan ( ) and teal ( ) and indicated above the alignment; mutations in CNNM3 loop are indicated in pink ( ); black triangles (▼) indicate residues involved in magnesium coordination based on prokaryotic CNNM homolog structures [154, 155]
* - identical, : - similar, . – somewhat similar amino acids.

Human diseases

Mutations in CNNM2 and CNNM4 have been linked with hypomagnesemia [156–160] and Jalili syndrome [161–176], respectively (Fig. 1.4). Two types of hypomagnesemia are caused by various mutations in CNNM2: hypomagnesemia 6, renal (HOMG6, OMIM: 613882) and hypomagnesemia, seizures and mental retardation 1 (HOMGSMR1, OMIM:616418). Mutations in CNNM4 cause Jalili syndrome (OMIM:217080), which is characterized by cone-rod dystrophy and amelogenesis imperfecta, a tooth formation disorder. In this disorder, magnesium deficiency causes a disbalance of cations and results in malformation of photoreceptor cells and necrosis in pigment epithelial cells, and it is linked with diabetic retinopathy [177, 178]. A mutation in CNNM4 results in tooth malformation, and disbalance in magnesium and calcium in the teeth manifested in higher magnesium content in the enamel and lower content in the dentin [179]. Additionally, CNNM4 knockout mice exhibit hypomineralization of tooth enamel [180]. On the other hand, CNNM1 and CNNM3 have not been associated with human genetic disorders.

Whereas genetic mutations cause specific human disorders, overexpression of CNNMs has an effect on the growth of malignant cells. Work in breast cancer cells lines

demonstrated that overexpression of CNNM4 in MCF7 cell line resulted in close to 100% cell death, whereas overexpression of the Q730X mutant had no such effect [181]. In two other breast cancer cell lines, T47D and BT20, the opposite effect of CNNM4 was observed, where its knockdown resulted in growth suppression [181]. CNNM3 overexpression in DB-7 mouse mammary cancer cells resulted in increased colony formation and tumour mass [182]. CNNM4 knockout in mice results in increased proliferation and decreased differentiation of colon epithelia which resulted in increased colon tumour formation in the AOM/DSS murine model [183]. A recent link between CNNM4 and non-alcoholic steatohepatitis (NASH) was uncovered – CNNM4 is overexpressed in that condition and results in depletion of magnesium from the liver [184]. Concomitantly, lipid accumulation in hepatocytes was found to be reversed with liver-targeted *CNNM4* siRNA in mice [184].

CNNMs and magnesium flux

There is a debate in the field of CNNM studies on whether these proteins are magnesium transporters or transport mediators [185–188].

CNNM4 shows a basolateral expression pattern in colon epithelial cells where it acts as a sodium-coupled magnesium extruder [180]. S200Y and L324P CNNM4 mutations, associated with Jalili syndrome, prevented magnesium efflux [180] (Fig. 1.4). While CNNM4 appears to act as a magnesium transporter in the colon and small intestine, CNNM2 participates in magnesium reabsorption in the kidney [156]. Basolateral expression of CNNM2 is observed in the thick ascending limb of Henle's loop (TAL) and in the distal convoluted tubule (DCT) of the kidney nephron, and shows a

similar pattern of expression to TRPM6 [156]. Both genes are upregulated in response to low magnesium exposure [156].

CBS domains of CNNM1, 2 and 4 bind ATP in the presence of magnesium but show no binding without magnesium [189]. In two studies, no binding of CNNM3 to ATP was observed, regardless of the presence of Mg^{2+} [153, 189]. However, another study produced a crystal structure of CNNM3 Bateman module bound to ADP, which the authors state is probably due to a mixture of crystallized proteins bound to AMP and ATP, since no ADP was present in the buffer [108]. Additionally, ADP was captured without the presence of magnesium. Lack of CBS domains resulted in a loss of magnesium efflux capacity without affecting CNNM cell surface localization [189].

A mutation within the CBS2 domain of CNNM2 and CNNM4 (T568I and T495I, respectively) has been linked with human genetic disorders and has been shown to abrogate magnesium efflux [156, 163, 189]. The T/I mutation prevents the interaction between the CNNM Bateman module and Mg^{2+}-bound nucleotides [189, 190]. Binding of nucleotides to the Bateman module results in a significant conformational change from a twisted to a flat conformation [190]. Unexpectedly, while not being able to bind nucleotides, the T/I mutation mimics the conformational change induced by nucleotide binding [190]. Similarly, binding of PRLs to the Bateman module induces a shift to the flat conformation [108, 191]. Additionally dimerization of CNNM Bateman modules requires Mg•ATP (AMP and ADP are not sufficient) and the binding of PRL enhances it [153]. CNNM4 Jalili syndrome-causing mutations R407 and P409 located in the vicinity of T495 disrupt contacts with Mg•ATP [163, 172]. These CNNM4 mutations (P407L, R409L and T495I) also prevent dimerization of Bateman modules [153]. Given the

presence of disease-causing mutations in the CNNM2/4 Bateman module and its importance in magnesium transport it's not unreasonable to hypothesize that it acts as a sensor of intracellular magnesium concentration. When magnesium concentration is high ATP production increases resulting in an abundance of Mg•ATP which then binds the Bateman domain and affects its conformation. The shift from twisted to flat structure affects the movement of the transmembrane domain, allowing the exchange of Na^{+}/Mg^{2+}. In the alternate version, where CNNMs do not act as direct magnesium transporters but rather as magnesium homeostasis mediators, the shift in conformation would affect the interaction of CNNMs with either ARL15, PRLs or TRPM7 to affect magnesium flux. The P/L, R/L and T/I mutations that permanently lock the Bateman module in an Mg•ATP-associated-like state would dysregulate the fine control of intracellular magnesium flux and thus result in hypomagnesemia or Jalili syndrome. PRLs themselves could represent an additional layer of magnesium regulation since their active site cysteine phosphorylation is sensitive to the presence of magnesium, which affects their interaction with CNNMs, which in turn enhances the dimerization of the Bateman module and shifts it to a flat conformation, which has downstream effects on Mg^{2+} flux.

Two recent papers [154, 155] identified a magnesium coordinating pocket in the transmembrane region of a bacterial (TpCorC in *Thermus parvatiensis*) and archaeal (MtCorB in *Methanoculleus thermophilus*) CNNM homologs. In addition, magnesium indicator-loaded liposomes with reconstituted bacterial and archaeal CNNM orthologs produced an increase in the fluorescent signal when Mg^{2+} was added, which points towards the orthologs being true magnesium transporters [155]. These new papers by

Huang *et al*. and Chen *et al.* increase the epistemic probability of CNNMs being true transporters. Five amino acids (CNNM2: S269, S273, N323, G356 and E357) were identified as Mg^{2+}-coordinating residues (Fig. 1.4, black triangles). Two out of five have been previously linked with hypomagnesemia [157] with two additional mutations in the vicinity of magnesium-coordinating sites (F272L and V324M) recently identified [158, 159]. The first two serine mutations were linked with Jalili syndrome in CNNM4 [162, 176]. Mutating any of these residues in TpCorC either prevented cell surface expression or resulted in a decrease in magnesium efflux [154]. Curiously, 3 out of 5 magnesium-coordinating residues are not conserved in CNNM3 (Fig. 1.4). One study has not observed any effect of CNNM3 on magnesium flux [189], while another showed that it had a significant effect on magnesium uptake [192]. An inhibitor (IGN95a) of TpCorC was identified to bind in the Mg•ATP-binding site of its Bateman module and decreases ATP binding and magnesium efflux [193]. IGN95a has a dissociation constant (K_d) of 47.0 μM for the Bateman module, which is ~100-fold higher than that of ATP (~0.5 μM) making it a poor inhibitor and despite structural similarity of between the CNNM2/4 and TpCorC Bateman modules, IGN95a exhibited very weak binding to CNNM2/4 [193].

MtCorB undergoes a large shift in its cytoplasmic region upon R235L mutation which prevents it from binding Mg•ATP, mimicking the Jalili syndrome R407L mutation observed CNNM4 [155]. This shift results in a loss of dimeric torus structure between the Bateman domains of each subunit. This is the first such shift in CBS observed in CBS1 and 2 domains. If CNNMs were to undergo a similar rearrangement, it might result in a loss of interaction with proteins that depend on the proper orientation of CBS-pair domain. The advantage of this study is that almost the complete protein was crystallized

in its apo and holo states, which had not been achieved previously. The novel shift in structure could be explained by the presence of additional domains that interact with the Bateman domain, as well as the transmembrane region that could influence the movement of the cytoplasmic portion of the protein. One disadvantage is that putative prokaryotic CNNM homologs do not contain a cyclic nucleotide-binding homology domain (CNBH) but rather a "transporter-associated domain" of distinct sequence (InterPro IPR005170) and thus they are not perfect analogs of CNNMs.

PRL/CNNM interactions

Several years ago, our laboratory has uncovered a new mechanism of action of PRLs – they interact with CNNMs and regulate magnesium flux [192]. This study has shown, using the AP-MS technique, that PRL-2 interacts with all four members of the CNNM family and that this interaction is involved in the regulation of magnesium flux and cell growth in a mouse model of mammary cancer [192]. A single mutation in the glycine 433 residue (G433D) at the base of the extended loop of CNNM3 CBS2 motif (Fig. 1.4) was enough to abolish its interaction with RPL-2, resulting in decreased magnesium influx and reduction of mammary cancer tumour formation in mice [192]. A follow-up study by Kostantin *et al.* showed that another mutation at the tip of the extended loop, aspartate 426 (D426A), also completely abolished the interaction between CNNM3 and PRL-2 and reduced murine mammary cancer growth [182]. Another study showed that PRL-1 and PRL-3 interact with CNNM4, and affect magnesium efflux and tumour growth [194]. CNNMs are unique among CBS-domain-containing proteins in having an extended loop, which has co-evolved with PRLs [192]. Abovementioned studies confirmed the

importance of this loop and of the PRL active site in magnesium uptake and tumour growth. Multiple X-ray crystallography studies showed that PRLs and CNNMs interact through the entry of the CNNM extended loop into the catalytic pocket of PRL [108, 191, 195]. The active site cysteine can be phosphorylated during the dephosphorylation reaction and the newly-formed phosphocysteine intermediate has a long half-life due to the very low phosphatase activity of PRLs [195]. Interestingly, magnesium deprivation reduces formation of phosphocysteine [109, 195], which prevents CNNMs from binding PRLs, while the formation of a disulfide bond between C101 and C46 in PRL-2 decreases its affinity to CNMM3 CBS domain by 200-fold [195]. Compared to wild-type PRL-3, active-site-disrupting cysteine mutations (C104S and C49S) (Fig. 1.1) prevented interaction with CNNM4, and had reduced cell magnesium content and tumour growth [194]. Unlike the C/S mutation, the catalytic cysteine was found to be not essential for CNNM binding when it was mutated to alanine [195] and this mutation was later shown to decrease binding by 16-fold, compared to a 1400-fold decrease with the C/S mutation [108]. Multiple residues in the active site of PRL-3 were mutated and most of them significantly decreased the interaction with CNNMs, with R110E mutation completely abrogating this interaction [108]. The R138E mutation severely reduced PRL-3 binding to CNNM but still retained wild-type phosphatase activity (Fig. 1.1) [108]. The A111S, a mutation which restores the serine found in most other phosphatases had no effect on CNNM binding and significantly increased the steady-state kinetics but had the same burst phase as wild-type PRL-3 [108]. The distinct effect of PRLs on cancers was traditionally understood from the point of view that they behave as phosphatases, however recent studies on PRLs and CNNMs indicate that their interaction may play a

more important role. Mutations in CNNM3 that prevent binding to PRLs have been shown to reduce tumour growth in mouse studies (CNNM3 G433D [192] and D426A [182]). Mutations in PRL-3 which prevented its binding to CNNMs had a similar effect [194], however the lack of phosphatase activity induced by these mutations could not be excluded as playing a major role in reducing tumour growth. A recent study demonstrated that C104D mutation in PRL-3 had a negligeable effect on CNNM binding but it abrogated its phosphatase activity, whereas the C104E mutation didn't bind CNNMs and had no phosphatase activity (Fig. 1.1) [109]. When B16 melanoma cell lines expressing PRL-3 WT, C/D or C/E mutants were injected in mice, there was no difference in the number of nodules formed in the lungs between WT and C/D [109]. However, C/E formed significantly fewer nodules, similar to the R138E mutation that had very weak CNNM binding but almost wild-type level of phosphatase activity [109]. These findings indicate that the phosphatase activity of PRLs is not necessary for magnesium flux regulation and tumour formation, but its ability to bind CNNMs is crucial.

Regulation of PRL by CNNM and magnesium

While the interaction between PRLs and CNNMs regulates the flux of magnesium, magnesium and CNNMs themselves regulate PRL levels. It was shown that magnesium deprivation increases PRL-1/2 levels in multiple cancer cell lines [192]. Overexpression of wild-type CNNM3, but not of PRL-binding deficient G433D and D426A mutants, increased PRL-1/2 levels [182, 192]. On the other hand, overexpression of TRPM7, a magnesium channel, reduced PRL-1/2 levels [18]. It was demonstrated that magnesium deprivation increases PRL-1/2 levels through upregulation of translation of their mRNA

[18]. In physiological magnesium conditions, ribosomes stall at the conserved upstream open reading frame (uORF) in the PTP4A1/2 mRNA 5′ UTR, which prevents their translation, once magnesium levels decrease, ribosomes resume scanning along the mRNA and reinitiate translation at the main ORF [18]. Decreasing extracellular magnesium reduces ATP production [18] and the decrease in mitochondrial magnesium influx has a similar effect [33]. AMPK is activated by a reduction of ATP to ADP/AMP ratio, which leads to mTORC2 activation [196]. This interplay results in upregulation of PTP4A1/2 translation under low magnesium-induced energetic stress [18]. Thus, PRL-1/2 respond to intracellular magnesium changes to regulate its flux.

Magnesium channels TRPM6 and TRPM7

Transient receptor potential melastatin 6 and 7 (TRPM6 and TRPM7) are nonselective divalent cation channels that are permeable to magnesium, calcium and zinc [197, 198]. They are well studied proteins with more than a thousand articles published that mention them in their title or abstract on PubMed (queried on January 13, 2022). This section will focus on their activity related to magnesium transport specifically.

TRPM6/7 are unique among channels in that they contain a functional C-terminal kinase domain [197, 199]. The function of the kinase domain has long been debated, but in mice expressing a truncated version of the TRPM7 channel lacking the kinase domain, mineral homeostasis was not affected [198]. Global ablation of both *Trpm6* and *7* is embryonically lethal in mice [200, 201]. *Trpm6*-deficient adult mice on a high-magnesium diet survived significantly longer than on regular chow [201]. In HAP1 haploid leukemia cells, *Trpm7* knockout resulted in a reduction of magnesium and zinc uptake [198].

Surprisingly, ablation of *Trpm7* in mouse kidneys did not affect either serum or urine levels of divalent cations [198]. However, the knockout in the intestine resulted in growth retardation and early death, probably due to the deficiency of magnesium, zinc and calcium [198]. Zinc deficiency was observed earlier and its extent was larger than that of calcium or magnesium and KO mouse lifespan was increased with zinc and magnesium supplementation [198]. Levels of *Trpm6* and *Slc41a1* and *a2* were significantly upregulated in knockout mice [198]. One important aspect of this study is in showing that TRPM7 has a preference for zinc transport, even under physiological magnesium concentration, which is 500 times higher than that of zinc. *Trpm6* knockout in mouse kidneys resulted in reduced magnesium in the bone, but not in the serum or urine [201]. In contrast, *Trpm6* intestinal knockout resulted in a much larger decrease of magnesium in bone and also reduced magnesium in the serum and urine [201]. Wild-type mice fed a diet supplemented with three different magnesium compounds had a significantly longer lifespan than mice on standard chow [201].

While TRPM6/7 channels are expressed on the cell surface, the majority of the protein is observed in intracellular vesicles of uncertain function [202–204]. One study proposed that TRPM7 localizes to unique intracellular vesicles that function as a store of zinc, which is released in response to reactive oxygen species [205]. Curiously, these are proposed to be a novel type of intracellular vesicle distinct from lysosomes, endosomes, and various transport vesicles. Neither magnesium nor calcium was found in these vesicles, which raises the question of regulation of the channel specificity to zinc.

Mutations in TRPM6 have been linked with the human disorder of hypomagnesemia 1, intestinal (HOMG1, OMIM: 602014). A recent study identified two families with variants that either affect splicing of TRPM7 mRNA or its channel activity which resulted in hypomagnesemia with secondary hypocalcemia [206].

Regulation of TRPM6 and TRPM7

TRPM7 is regulated by intracellular magnesium and Mg•ATP, the physiological form of ATP [197]. When intracellular magnesium is depleted, the channel is activated within two minutes [207]. On the other hand, channel activity was almost completely supressed with 6 mM Mg•ATP and 3 mM $[Mg^{2+}]_i$; Mg•GTP had a similar suppressive effect as Mg•ATP, while ITP and CTP had a lower effect [197]. Due to the channel's sensitivity to ATP and GTP levels, this mode of regulation links magnesium transport by TRPM7 to cellular energy.

Magnesium is not just involved in regulating the channel directly – translation of TRPM7 is regulated by Mg^{2+} [208] in a similar manner to the regulation of PRL-1/2 [18]. mRNAs of TRPM7 and PRL-1/2 contain two uORFs that respond to high levels of magnesium by downregulating their translation [18, 208]. Conversely, in low magnesium, the translation is upregulated. In both cases, the uORFs are highly conserved and mutating them abolishes the magnesium-sensitive regulation [18, 208]. What remains to be understood is how exactly does magnesium regulate the translation through uORFs: are there magnesium-sensitive RNA-binding proteins, are the uORF peptides translated, perhaps the mRNA secondary structure is involved?

Apart from magnesium and Mg•ATP, there are other modes of regulation of TRPM6/7 activity. PIP_2 hydrolysis by phospholipase C (PLC) has been shown to inactivate TRPM6 [209] and TRPM7 [210]. Carbachol, an activator of muscarinic receptors which in turn activate PLC, supresses conductance of TRPM6/7. PLC interacts with TRPM6/7 through its kinase domain [209, 210] and, in B cells, TRPM7 has been shown to modulate PIP_2 production and hydrolysis [211]. Curiously, the interaction with PLC was not necessary for TRPM6 regulation [209]. Specific cytoplasmic residues were found in TRPM6 and TRPM7 to be required for PIP_2 interaction. Mutating them resulted in decrease in current amplitude [209]. Mg^{2+} influx was also directly inhibited by PIP_2 depletion [209]. PLC activity itself is inhibited by increasing magnesium concentration due to charge shielding of negatively charged PIP_2 with positively charged divalent cations [212].

EGF signalling through EGFR has been shown to activate TRPM6 currents by increasing the mobility of the channel in the membrane and changing its localization from intracellular to the cell surface [213]. This activation of TRPM6 involves a Src→PI3K→Rac1 signalling cascade, and a constitutively active Rac1 mutant G12V increased TRPM6 currents [213]. In mice with a postnatal knockout of *Trpm6*, *Egfr* expression was significantly reduced in the liver [201]. Surprisingly, the effect of EGF was only evident for TRPM6 and not TRPM7, in this study. Yet there's contradicting data. An earlier paper showed that EGFR actually inhibits TRPM7 currents by activating PLCγ, which is involved in PIP_2 hydrolysis [210]. Another report indicated that in A549 lung cancer cells EGFR actually stimulates cell surface expression of TRPM7 and increases TRPM7 currents [214]. Moreover, in vascular smooth muscle cells, TRPM7 expression

is increased after EGF stimulation, which in turn increases intracellular magnesium levels and ERK-1/2 phosphorylation, in a TRPM7-dependent manner [215]. Furthermore, EGF increases the interaction between EGFR and TRPM7 and the abovementioned effects were not observed for TRPM6 [215]. The discrepancy in these results could be due to the use of different cell models. Nevertheless, there is a link between EGF and magnesium homeostasis in humans – a mutation in EGF has been found to cause hypomagnesemia 4, renal (OMIM: 611718) and that specific mutation fails to induce TRPM6 currents compared to WT EGF [216]. Additionally, cancer patients receiving treatment with the EGFR inhibitor cetuximab develop hypomagnesemia [216].

TRPM6/7 also regulate their own activity. In general, they are present as homotetramers and their kinase domain can be involved in autophosporylation [217]. TRPM6 and TRPM7 can also form heterotetramers and can cross-phosphorylate, however the importance of this phosphorylation is not well understood [218]. Using manganese to study TRPM6/7 activity, one study has shown that TRPM7 results in higher influx than TRPM6, while 6 and 7 co-overexpression resulted in an additive effect [219]. A mutation in TRPM6 causing hypomagnesemia (S141L) prevented it from interacting with TRPM7 and reduced manganese uptake compared to wild-type TRPM6 [219].

TRPM7 is N-glycosylated [202] but effect and regulation of its glycosylation has not been investigated. TRPM7 is the best studied magnesium transporter to date and yet much remains to be understood about its interaction and regulation.

N-linked glycosylation

Asparagine (N)-linked glycosylation, or N-glycosylation, is a post-translation protein modification found in all domains of life [220]. It is important for proper localization, folding, secretion and function of proteins. N-glycosylation begins in the endoplasmic reticulum (ER) lumen, where the $Glc_3Man_9GlcNAc_2$ [221] oligosaccharide is transferred from dolichol phosphate to the glycosylation sequon of proteins [222]. This reaction is catalyzed by the oligosaccharyltransferase (OST) complex [220]. The sequon is a conserved sequence of three amino acids N-X-S/T, where N represents asparagine, X could be any amino acid except proline, followed by either serine (S) or threonine (T). N-linked glycans transferred to nascent polypeptides in the ER are trimmed by glucosidase I and II, which remove terminal glucose residues, and by ER α-mannosidase I, which removes a mannose, resulting in a $Man_8GlcNAc_2$ [223] glycan. Once the protein with this glycan is shuttled into the Golgi, more mannose sugars can be added to the glycan resulting in a high-mannose form, alternatively Golgi α-mannosidase I will trim three more mannose residues to produce $Man_5GlcNAc_2$. Multiple glycosyltransferases then further modify the glycan expanding the range of possible glycoforms from hybrid to complex oligosaccharides [224]. This complex orchestration of multiple enzymes produces a plethora of possible glycans with varying functions. To date, the glycan repository GlyTouCan has described more that 120 thousand different glycans that were identified experimentally [225].

N-glycosylation regulates trafficking and plasma membrane localization of numerous receptors and transporters. Multiple members of the transient receptor

potential (TRP) channel family are N-glycosylated and their function depends on correct glycosylation [226]. For example, TRPM8, is N-glycosylated and mutations in the glycosylation sites result in reduction of its sensitivity to cold and cooling compounds [227]. Another member of the TRP family, TRPP2, requires N-glycosylation for proper biogenesis, otherwise it undergoes lysosomal degradation [228]. In the case of TRPM4B, the complex glycoform was prevalent at the cell surface compared to the high-mannose glycoform but mutating the N-glycosylation site did not abolish the function of the channel [229]. N-glycosylation of a mechanosensitive ion channel Piezo1 affects its trafficking and function, and it was hypothesized that this is linked with interactions the ECM [230].

The N-glycome is affected in many malignancies and this results in changes in cancer severity [231–233]. Inhibition of N-glycosylation in multiple carcinoma types through either mannoside acetyl-glucosaminyltransferase 5 knockout or 2-deoxy-D-glucose treatment resulted in improved CAR T cell accessibility, increased solid tumour infiltration and decreased tumour size [234].

A surprising recent finding identified small non-coding RNAs that present the same types of N-glycans found on proteins and that are exposed on the cell surface [235]. Their function remains unknown, opening more novel avenues in N-glycan research.

Link between N-glycosylation, magnesium and putative magnesium transporters

The transfer of GlcNAc phosphate from UDP-GlcNAc to dolichol phosphate by DPAGT1 is the first committed step in the formation of a core N-glycan [236]. UDP-GlcNAc is also necessary for complex glycan branching and sialylation [237]. Mutations in DPAGT1 in

the proximity of the magnesium-binding site result in a severe congenital disorder of glycosylation, type Ij (OMIM: 608093), with patients dying within their first year [238] or demonstrating fetal akinesia [239]. The enzymatic activity of wild-type and mutant DPAGT1 was sensitive to changes in Mg^{2+} concentration [238]. In *Mrs2* knockdown cells, in which mitochondrial magnesium uptake is abolished, the concentration of UDP-GlcNAc is significantly reduced [33].

A number of proteins have been ascribed the role of magnesium transporters, which was either not confirmed or shown to be erroneous [31, 36]. Prime among them is MAGT1, which stands for magnesium transporter 1 and which it most assuredly is not. It was first identified as a member of the oligosaccharyltransferase (OST) complex based on its homology with yeast OST proteins and was named IAP [240]. Then it was identified in a screen of magnesiotropic genes and characterized in *Xenopus laevis* oocytes where its overexpression resulted in magnesium uptake, and as such it was named MAGT1 [241]. Later, it was shown that when either MAGT1 or its homologue TUSC3 are overexpressed in HEK293 cells, no increase in magnesium uptake was observed, but MAGT1 expression increased when cells were grown without magnesium. Knockdown of MAGT1 and TUSC3 resulted in decreased magnesium uptake [242]. However, recent cryo-EM structures have shown that MAGT1 forms part of the oligosaccharyltransferase complex OST-B, it is embedded into the ER membrane and participates in protein N-glycosylation [38]. Another study has shown that MAGT1 is localized in the ER and that it affects protein N-glycosylation in a STT3B-dependent manner, playing the role of oxidoreductase [243]. Hemizygous mutations in MAGT1 cause congenital disorder of glycosylation, type Icc (OMIM: 301031) and XMEN (X-linked immunodeficiency with Mg^{2+}

defect, Epstein-Barr virus (EBV) infection and neoplasia) disease (OMIM: 300853). One of the phenotypes observed in XMEN disease is lack of magnesium influx in T cells in response to antigen receptor stimulation, which was initially attributed to the mutation in MAGT1 which was understood to be a magnesium transporter [244]. However, later evidence showed that patients with XMEN disease and MAGT1 mutation-associated congenital glycosylation disorder suffer from N-linked glycosylation reduction and exhibit an upregulation of TUSC3, potentially as a compensatory mechanism [245, 246]. Magnesium deprivation in T cells results in reduction of N-glycosylation of specific receptors such as NKG2D and CD70 and reduced cytotoxicity of T and NK cells, which could explain the susceptibility of XMEN patients to viral infections [246]. Recently, MAGT1 expression was restored using CRISPR knock-in in human hematopoietic cells from an XMEN patient and they observed increase in N-glycosylation of NKG2D and CD70 and restoration of cellular function [247]. All this data supports MAGT1 being an integral part of the OST and early observations about magnesium uptake could be explained by improper N-glycosylation of magnesium transporters, which would affect their localization and function.

Another gene, *Mmgt1*, or membrane Mg^{2+} transporter 1, was miscategorized as a magnesium transporter by the same group that named MAGT1, which identified it in a screen of magnesium-responsive genes in the kidney cortex of mice with hypomagnesemia [248]. Having only two transmembrane helices, it's hard to imagine how it would function as a transporter. MMGT1 was later identified to be involved with ER-associated degradation (ERAD) and was called TMEM32 [249]. Subsequently, it was shown to be an integral part of the ER membrane protein complex (EMC) involved in the

membrane insertion of tail-anchored membrane proteins, which is required for their N-glycosylation [250]. EMC is necessary for correct insertion of the first transmembrane domain of proteins and cooperates with SEC61, which correctly orients further transmembrane domains [251]. SEC61 interacts with OST which ensures proper protein N-linked glycosylation [252]. Other culprits in misidentified magnesium transporter studies are HIP14 and HIP14L [253], which have been shown to be palmitoyl acyltransferases that participate in reversible S-palmitoylation of proteins, which is necessary for correct trafficking and plasma membrane localization [254]. MAGT1 and MMGT1 participate in proper membrane orientation and N-glycosylation of proteins, while HIP14 and HIP14L participate in protein S-palmitoylation. Thus emerges an explanation of mischaracterization of these proteins as magnesium transporters: all these proteins could be involved in correct localization of magnesium transporters at the plasma membrane where they consequently affect magnesium transport. In the EMC studies, MMGT1 was designated as EMC5, however, like MAGT1, the original name persists and is recognized as the official gene name by the HUGO gene nomenclature committee. This results in these proteins still being described as magnesium transporters and numerous papers are published every year with these erroneous descriptions.

Chapter 2

ARL15 modulates magnesium homeostasis through N-glycosylation of CNNMs

Yevgen Zolotarov*, Chao Ma*, Irene González-Recio, Serge Hardy, Gijs A.C. Franken, Noriko Uetani, Femke Latta, Elie Kostantin, Jonathan Boulais, Marie-Pier Thibault, Jean-François Côté, Irene Díaz Moreno, Antonio Díaz Quintana, Joost G.J. Hoenderop, Luis Alfonso Martínez-Cruz, Michel L. Tremblay†, Jeroen H.F. de Baaij†

* These authors contributed equally to the preparation of the manuscript
† These are co-corresponding authors

Cellular and Molecular Life Sciences (2021) 78: 5427–5445

Abstract

Cyclin M (CNNM1-4) proteins maintain cellular and body magnesium (Mg^{2+}) homeostasis. Using various biochemical approaches, we have identified members of the CNNM family as direct interacting partners of ADP-ribosylation factor-like protein 15 (ARL15), a small GTP-binding protein. ARL15 interacts with CNNMs at their carboxyl-terminal conserved cystathionine-β-synthase (CBS) domains. *In silico* modeling of the interaction between CNNM2 and ARL15 supports that the small GTPase specifically binds the CBS1 and CNBH domains. Immunocytochemical experiments demonstrate that CNNM2 and ARL15 co-localize in the kidney, with both proteins showing subcellular localization in the endoplasmic reticulum, Golgi apparatus and the plasma membrane. Most importantly, we found that ARL15 is required for forming complex N-glycosylation of CNNMs. Overexpression of ARL15 promotes complex N-glycosylation of CNNM3. Mg^{2+} uptake experiments with a stable isotope demonstrate that there is a significant increase of $^{25}Mg^{2+}$ uptake upon knockdown of ARL15 in multiple kidney cancer cell lines. Altogether, our results establish ARL15 as a novel negative regulator of Mg^{2+} transport by promoting the complex N-glycosylation of CNNMs.

Introduction

Mg^{2+} is an essential cation for all living organisms. Mg^{2+} deficiency, therefore, causes organ dysfunction and is associated with a wide range of human diseases [3]. As co-factor of ATP, Mg^{2+} is involved in over 600 enzymatic reactions and as such it plays important roles in a plethora of biological mechanisms including DNA transcription, protein synthesis and energy metabolism [3]. For example, decreased intracellular Mg^{2+} levels suppress cell cycle progression and are consequently associated with cell growth impairment [255]. Recent studies therefore have focused on intracellular Mg^{2+} concentration as a central mechanism for cellular metabolism and proliferation [18].

Among the various mechanisms of Mg^{2+} sensing and transport, proteins of the Cyclin M (CNNM) family were shown to play an important role in the intracellular sensing of the Mg^{2+} availability [151, 256]. The CNNM family has 4 members in mammalians, which are highly conserved but have different tissue distribution [18, 151, 195, 256]. CNNM1, CNNM2 and CNNM4 have highest expression levels in brain, kidney and intestine, respectively whereas CNNM3 shows a ubiquitous expression pattern [257]. Genetic defects of CNNMs have been demonstrated to be causative for disease. Mutations in *CNNM2* are causative for a multi-organ syndrome comprising intellectual disability, seizures and renal Mg^{2+} wasting [OMIM: #616418] [157]. Patients with CNNM4 mutations suffer from Jalili syndrome, consisting of cone-rod dystrophy and amelogenesis imperfecta [OMIM: #217080] [162].

CNNMs interact with phosphatases of the regenerating liver (PRL-1-3) via the cystathionine-β-synthase (CBS) domain of CNNMs [102, 192]. CNNMs and PRLs have

been associated with progression of breast and colon cancers [192, 194]. Although the exact function of CNNM proteins is under debate [185, 258], it has been shown that engineered and naturally occurring mutations in CNNMs result in decreased Mg^{2+} transport in both cell and animal models [157, 192].

Recently, a large GWAS identified the ADP-ribosylation factor-like protein 15 (*ARL15*) locus to be associated with urinary Mg^{2+} excretion [96]. ARL15 is structurally similar to Ras-related GTP-binding proteins, which regulate intracellular vesicle trafficking [259, 260]. Within the kidney, ARL15 is highly expressed in the thick ascending limb (TAL) and distal convoluted tubule (DCT), like CNNM2, where Mg^{2+} reabsorption is tightly regulated [96]. However, the exact function of ARL15 and the mechanism by which ARL15 regulates renal Mg^{2+} handling are still unknown.

In this study, we identified CNNMs as direct interacting partners of ARL15 by binding to the CBS1 domain of CNNM2. We demonstrate that ARL15 is a negative regulator of cellular Mg^{2+} transport through its modulation of CNNMs N-glycosylation and the direct correlation of its expression to levels of intracellular Mg^{2+}.

Results

ARL15 is a new binding partner of CNNMs

To identify protein interactions of CNNMs, pull-down of mouse CNNM2 carboxyl (C)-terminal region was performed followed by mass spectrometry (Fig. 2.1A). Given that CNNM2 is known to regulate Mg^{2+} reabsorption in the DCT segment of the nephron, DCT-enriched kidney lysates were used. Twenty-four interacting partners of CNNM2 were detected, including ARL15 (Fig. 2.1B). Since ARL15 has been shown to be involved in urinary Mg^{2+} excretion [96], we decided to further explore this particular interacting partner. To confirm the interaction between ARL15 and CNNMs, BioID of ARL15 was performed and we identified 221 proteins as potential interacting partners of ARL15 and CNNM2, CNNM3 and CNNM4 were among them (Supp. Fig. 2.1). GO biological process overrepresentation analysis indicated that Mg^{2+} homeostasis is one of the most highly enriched processes (Fig. 2.1C). Immunoprecipitation demonstrated that CNNM3 and ARL15 interact endogenously (Fig. 2.1D). To further confirm this association, co-immunoprecipitation assays were performed with overexpressed ARL15 and the four members of the CNNM family. ARL15 binding was observed to a similar extent for each CNNM protein (Fig. 2.1E). Endogenous PRL-1 and PRL-2, which are well described interacting partners of CNNMs that regulate Mg^{2+} flux [192, 194], also co-precipitated with CNNMs and ARL15 (Fig. 2.1E). The above data indicates that ARL15 is a novel interacting partner of the four members of the CNNM family of Mg^{2+} modulators.

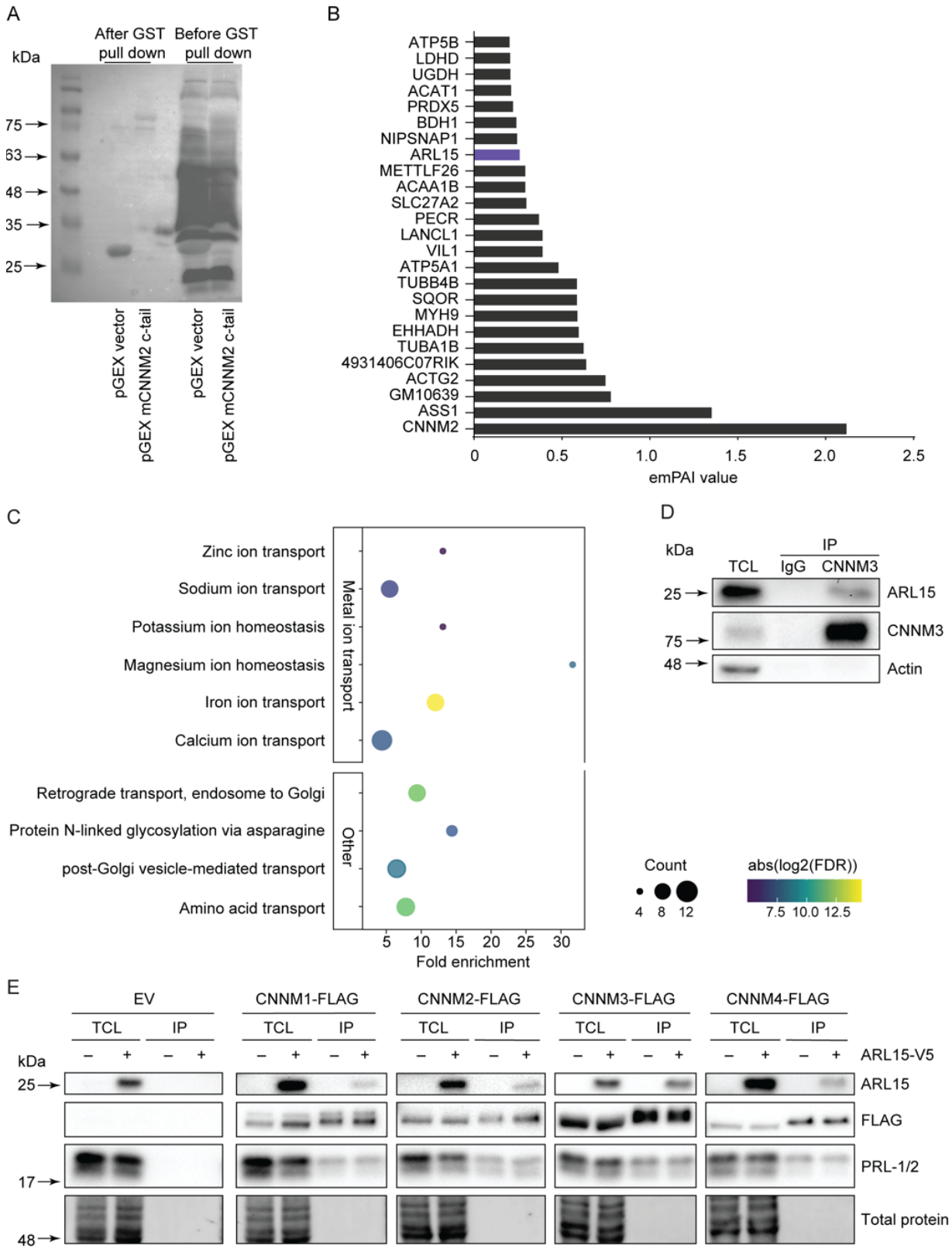
A
After GST pull down
Before GST pull down
kDa
75
63
48
35
25
pGEX vector
pGEX mCNNM2 c-tail
pGEX vector
pGEX mCNNM2 c-tail
B
ATP5B
LDHD
UGDH
ACAT1
PRDX5
BDH1
NIPSNAP1
ARL15
METTLF26
ACAA1B
SLC27A2
PECR
LANCL1
VIL1
ATP5A1
TUBB4B
SQOR
MYH9
EHHADH
TUBA1B
4931406C07RIK
ACTG2
GM10639
ASS1
CNNM2
0
0.5
1.0
1.5
2.0
2.5
emPAI value
C
Zinc ion transport
Sodium ion transport
Potassium ion homeostasis
Magnesium ion homeostasis
Iron ion transport
Calcium ion transport
Metal ion transport
Retrograde transport, endosome to Golgi
Protein N-linked glycosylation via asparagine
post-Golgi vesicle-mediated transport
Amino acid transport
Other
5
10
15
20
25
30
Fold enrichment
Count
4
8
12
abs(log2(FDR))
7.5
10.0
12.5
D
kDa
IP
TCL
IgG
CNNM3
25
75
48
ARL15
CNNM3
Actin
E
EV
CNNM1-FLAG
CNNM2-FLAG
CNNM3-FLAG
CNNM4-FLAG
TCL
IP
kDa
ARL15-V5
25
17
48
ARL15
FLAG
PRL-1/2
Total protein

◂ **Figure 2.1: ARL15 interacts with CNNMs.**

A. Immunoblot of GST-mCNNM2 c-tail pGex and empty pGex was used as control. The C-tail of mCNNM2 is purified and bind to glutathione beads. The DCT enriched fraction from 8 parvalbumin GFP mice were added to the bead. B. List of binding proteins to mCnnm2 C-tail (emPAI value). C. Representative pathways related to metal ion transport and Golgi-trafficking identified using gene ontology biological process overrepresentation analysis with ARL15 interacting partners. D. Endogenous CNNM3 was immunoprecipitated from HEK293 lysates and endogenous ARL15 co-immunoprecipitated with it. IgG antibody of the same subclass as CNNM3 antibody was used as negative control. E. Anti-FLAG beads were used to immunoprecipitate overexpressed FLAG-tagged CNNM1-4 proteins. The blot shows that ARL15 interacts with CNNM1-4, as well as endogenous PRL-1 and PRL-2.

emPAI, Exponentially modified protein abundance index; TCL, Total cell lysate; IP, Immunoprecipitation; GST, Glutathione-S-transferase; ARL15, ADP ribosylation factor like GTPase 15; CNNM, Cyclin M.

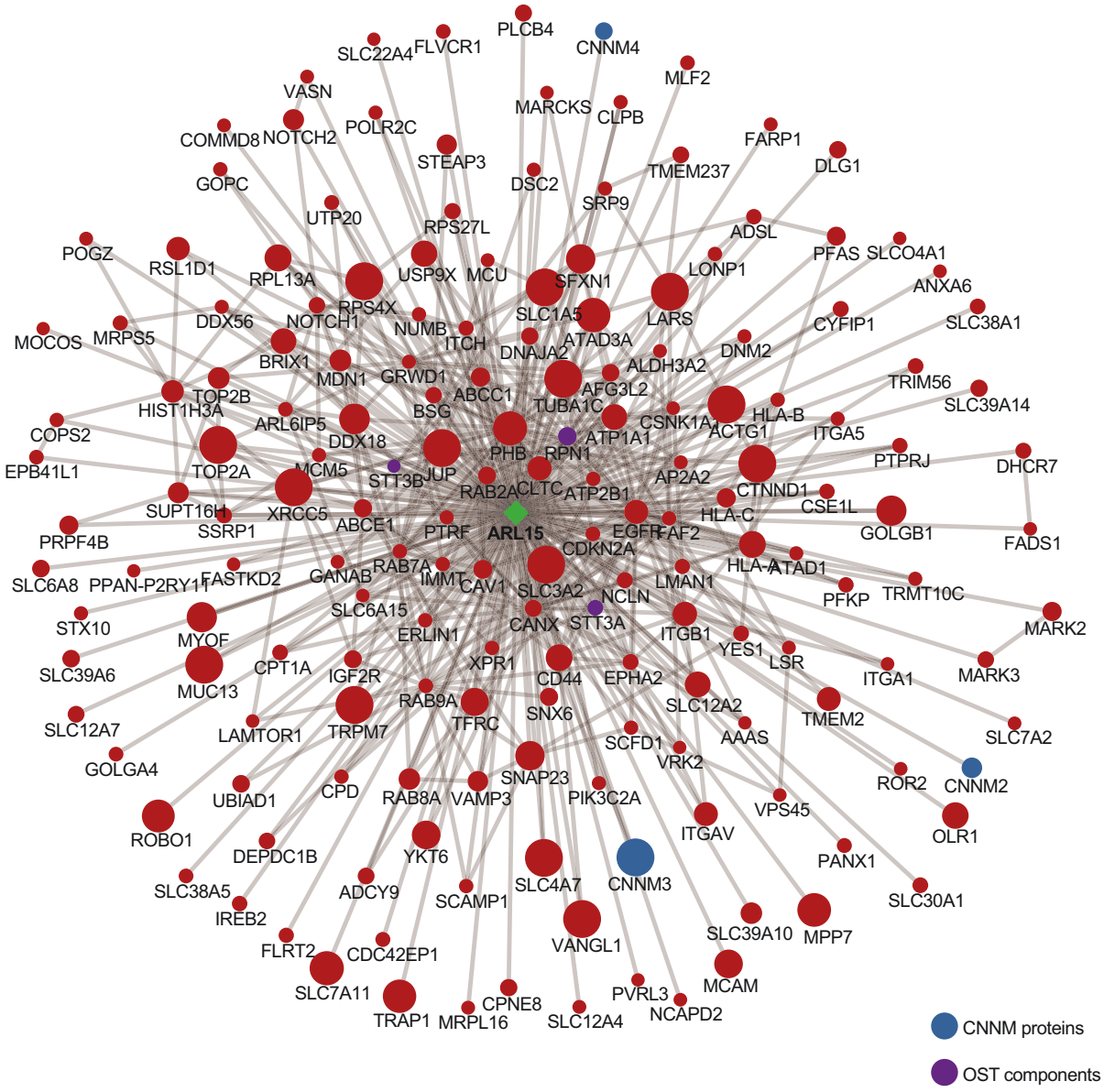

Supplementary Figure 2.1: ARL15 interacting partners identified through BioID
ARL15 interacting partners are presented with the size of the circle corresponding to the average spectral count and the edges between ARL15 and preys were obtained by augmenting the network using 3 different databases: BioGRID, IntAct and iRefIndex.

ARL15 interacts with CNNM2 cytoplasmic region

The topology for CNNMs consists of a signal peptide, three transmembrane domains (TM) and an intracellular C-terminus containing the Bateman module (which in turn is formed by two consecutive CBS domains, CBS1 and CBS2) and a cyclic nucleotide monophosphate-binding homology domain (CNBH) domain) [257]. To determine which domain of CNNM2 is important for the interaction with ARL15, truncated CNNM2 proteins were co-immunoprecipitated with ARL15 (Fig. 2.2A). The presence of the CBS domains is essential for the binding of ARL15 to CNNM2. The interaction of the proteins decreased by 36% when the CBS2 domain is removed (Fig. 2.2B and 2.2C). No interaction with the transmembrane domain was observed. The interaction between ARL15 and the Bateman module of CNNM2 was confirmed by gel filtration chromatography (Fig. 2.2D and 2.2E). Pure ARL15 and $CNNM2_{BAT}$ eluted as homodimers when they were independently loaded into a size exclusion chromatography column ($V_{e(ARL15)}$≈15.02 mL, $M_{exp(ARL15)}$≈ 36.03kDa; $V_{e(CNNM2BAT)}$≈14.67mL, $M_{exp(CNNM2BAT)}$≈ 43.98 kDa, respectively, where V_e indicates the elution volume and M_{exp} indicates the experimental molecular weight). The corresponding $CNNM2_{BAT}$·ARL15 complex (peak marked with *black asterisk*) eluted as a heterotetramer 2xARL15+2x$CNNM2_{BAT}$ (V_e≈13.77 mL, M_{th}= 74.58 kDa, M_{exp}≈ 73.41 kDa). To determine whether the interaction between ARL15 and CNNMs is dependent on Mg^{2+}, ARL15 and CNNM were immunoprecipitated in the presence or absence of Mg^{2+}. Results showed that the presence of 1 mM Mg^{2+} in the lysis buffer does not affect the association between ARL15 and CNNM2 compared to the condition of the lysis buffer without Mg^{2+} (Supp. Fig. 2.2A). In line with this, ARL15 and CNNM3 binding was similar in both conditions (Supp. Fig. 2.2B).

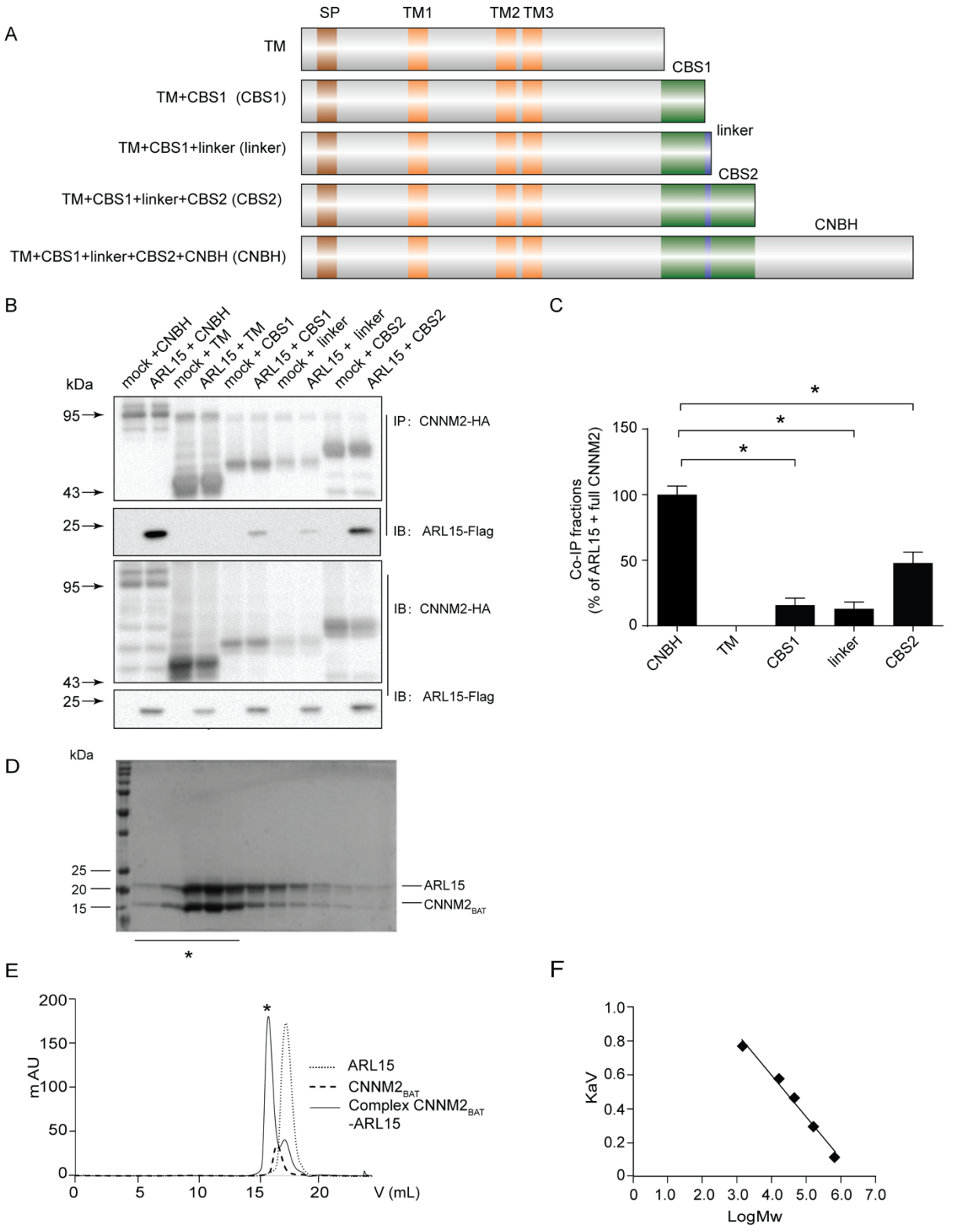
A
SP
TM1
TM2 TM3
TM
CBS1
TM+CBS1 (CBS1)
linker
TM+CBS1+linker (linker)
CBS2
TM+CBS1+linker+CBS2 (CBS2)
CNBH
TM+CBS1+linker+CBS2+CNBH (CNBH)
B
mock +CNBH
ARL15 + CNBH
mock + TM
ARL15 + TM
mock + CBS1
ARL15 + CBS1
mock + linker
ARL15 + linker
mock + CBS2
ARL15 + CBS2
kDa
95
43
25
IP: CNNM2-HA
IB: ARL15-Flag
IB: CNNM2-HA
C
Co-IP fractions
(% of ARL15 + full CNNM2)
150
100
50
0
CNBH
TM
CBS1
linker
CBS2
D
kDa
25
20
15
ARL15
CNNM2BAT
E
200
150
100
50
0
mAU
0
5
10
15
20
V (mL)
ARL15
CNNM2BAT
Complex CNNM2BAT
-ARL15
F
1.0
0.8
0.6
0.4
0.2
0
KaV
0
1.0
2.0
3.0
4.0
5.0
6.0
7.0
LogMw

◂ Figure 2.2: ARL15 interacts with CNNM2 cytoplasmic region.

A. Schematic overview of CNNM2 constructs including the predicted protein domains and truncations. B. HEK293 cells were co-transfected with truncated CNNM2-HA and ARL15-Flag. The upper two blots show the detection of the Flag-tagged proteins in anti-HA precipitated cell lysates. The lower two blots show input controls of HA-tagged and Flag-tagged proteins respectively. C. Quantification of ARL15/CNNM2 binding between the different truncated CNNM2 proteins. Results are the mean ± SEM of 3 independent experiments. * indicate significant differences compared to CNNM2 + ARL15 transfected cells ($P<0.05$). SP, Signal peptide; TM, Transmembrane; CBS, Cytosolic cystathionine β-synthase; CNBH, Cyclic nucleotide monophosphate-binding homology domain ; ARL15, ADP ribosylation factor like GTPase 15; CNNM, Cyclin M. D. SDS-polyacrylamide gel run with the isolated fractions of the $CNNM2_{BAT}$·ARL15 complex. Bands correspond to the isolated peak (marked with *black asterisk* in E) of the chromatographic run of the $CNNM2_{BAT}$·ARL15 complex ($M_{th(ARL15monomer)}$=19.57 kDa and $M_{th(CNNM2BATmonomer)}$= 17.72 kDa, where M_{th} indicates the theoretical molecular weight of each subunit). E. Gel filtration of the $CNNM2_{BAT}$.ARL15 complex and of its individual components. Bands correspond to the peak (marked with *black asterisk*) of the chromatographic run of the complex $CNNM2_{BAT}$·ARL15 ($M_{th(ARL15monomer)}$=19.57 kDa and $M_{th(CNNM2BATmonomer)}$= 17.72 kDa, where M_{th} indicates the theoretical molecular weight of each subunit). F. The calibration trendline calculated from protein standards is y= -0.2451x + 1.5726 ($y = K_{av}$; $x = \log M$).

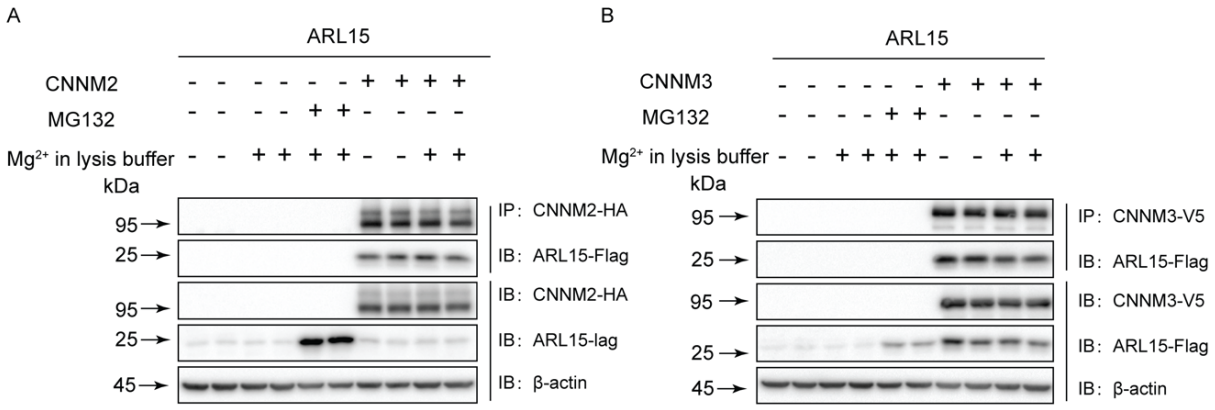

Supplementary Figure 2.2. Binding of ARL15 and CNNM2/3 is independent of magnesium

A. Co-immunoprecipitation of HEK293 cells transfected with ARL15-FLAG and HA-CNNM2 treated with or without 1mM Mg^{2+} in lysis buffer. The upper two blots show the detection of the FLAG-tagged proteins in anti-HA precipitated cell lysates. The lower two blots show input controls of HA-tagged and Flag-tagged proteins respectively. B. Co-immunoprecipitation of HEK293 cells transfected with ARL15-FLAG and V5-CNNM3 treated with or without 1mM Mg^{2+} in lysis buffer. The upper two blots show the detection of the FLAG-tagged proteins in anti-V5 precipitated cell lysates. The lower two blots show input controls of V5-tagged and FLAG-tagged proteins respectively. The figure shows a representative blot of 3 independent experiments.

Docking models of the CNNM-ARL15 interaction

To assess the role of the various cytoplasmic CNNM2 cytosolic domains as targets, ARL15 docking computations were carried out. The coordinates of the flexible linker joining the Bateman module with the CNBH domain were modelled onto the available X-ray diffraction data of the CNNM2 cytosolic domains. Figure 2.3 displays the domain arrangement of CNNM2 cytosolic domains (Fig. 2.3A) as well as the electrostatic potential on their surface (Fig. 2.3B). Notably, the linkers joining the Bateman domain to the CNBH display a stretch of basic residues. Best score solutions displayed ARL15 interacting with both CNNM2 monomers (Supp. Movie 1). ARL15 was partly inserted into the cleft between the Bateman and the CNBH domains (Fig. 2.3C-D). In each of the two symmetric solutions, the total buried solvent accessible surface per partner was 2,175.7 $Å^2$—1,830.8 $Å^2$ (932.6 $Å^2$, from CBS1, 262.3 $Å^2$ from the linker and 344.9 $Å^2$ from the CNBH domain) with one of the two CNNM2 monomers and 344.9 $Å^2$ (190.6 $Å^2$ from CBS1* and 154.3 $Å^2$ from CNBH*) for the interaction with the second CNNM2 monomer. Such values are typical of rather stable complexes, and in the upper limit of non-obligate interactions [261]. In addition, the complex displays complementarity of charges at the rim of the interface, as shown in Fig. 2.3D.

As pointed out, the CBS1 domains from complementary Bateman modules in the CNNM2 dimer contacted with ARL15, in particular that of the first monomer with a surface region defined between α–helix A, the β1-β2 hairpin loop and α-helix H1 in one of them, but also contacting the second monomer. Figure 2.3C shows the lowest energy solution found in different simulations. Other solutions with low energies corresponded to the hydrophobic surface of H0 helix pair, which interacts with the lipid bilayer, and

spots of the CNBH domains in which the absence of coordinates from the nearby unstructured regions disclosed an artifactual interaction site, otherwise concealed. Notably, Brownian Dynamics computations (Supp. Fig. 2.3A, Supp. Table 2.1) yielded results very similar to those displayed herein (Supp. Fig. 2.3). Thus, the interaction model herein is compatible with a 1:1 CNNM2:ARL15 stoichiometry. Other sets of solutions targeted the same region, but displayed different orientations of ARL15 towards CNNM2 surface, and were not found in all simulations. The result in Fig. 2.3, however, was hardly dependent on the modelled conformation of the linker residues 525 to 546 (Fig. 2.3D). Nevertheless, in most simulations several positive residues of the linker mapped near the interface. As CNNM3 has been reported to bind ARL15 with an affinity higher than that for CNNM2, HEX docking simulations were also performed using a CNNM3 model (Supp. Fig. 2.3). Notably, ARL15 targeted the same site in CNNM3 as does in CNNM2, though the orientation differs by a slight rotation of ARL15.

Recently, ARL15 was modelled used two different methods: template-based threading and *ab initio* modelling, while we applied template-driven simulated annealing [262]. Our ARL15 model is in line with this publication.

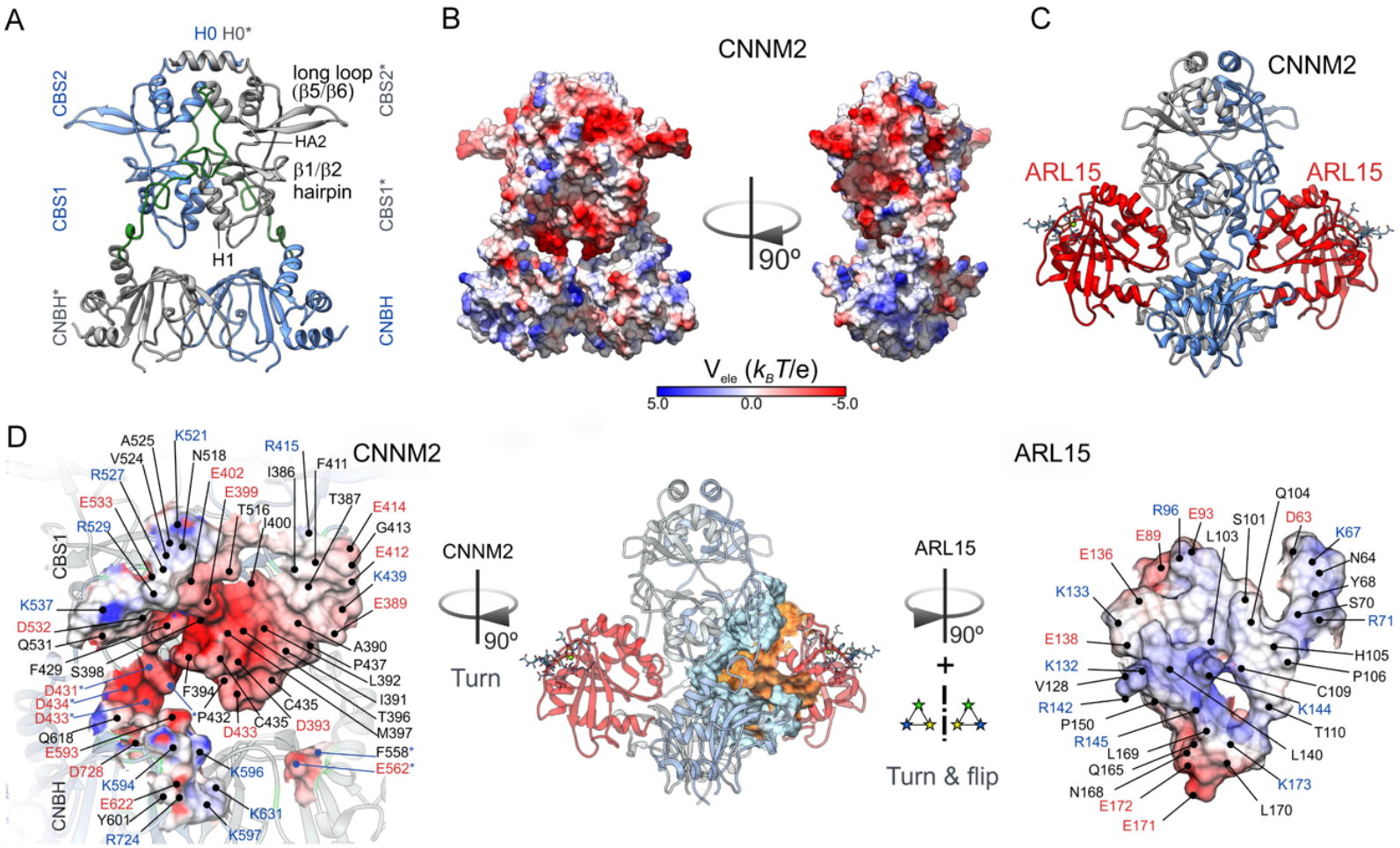

Figure 2.3: Computational structural model of the interaction between the CNNM2 cytosolic domains and ARL15. A. Richardson (ribbon) diagram of the cytosolic CNNM2 dimer domains. Each monomer is in a different color, and the model of flexible linker joining the Bateman domains to the CNBH ones are in light green. B. Electrostatic potentials at the surface of CNNM2 cytosolic domains. Electrostatic grids were generated with APBS 3.0 [263] at 150 mM ionic strength. Best solution of ARL15 (red ribbons) docking to CNNM2 computations. D. Dissection of the interface between ARL15 and CNNM2 (middle) illustrating both the surface and charge complementarity between the two partners.

Supplementary Table 2.1: Brownian Dynamics data

No	Size	Repr	ReprE	ClAE	CLAED	EIE	ElDesE	HyDesE	spread	stddev	max
1	61257	141	-25.858	-25.609	0.743	-7.640	3.766	-21.984	28.666	15.109	44.108
2	63258	277	-25.069	-26.597	1.261	-7.960	6.939	-24.048	19.155	7.041	32.403
3	13185	200	-25.504	-26.276	0.600	-4.104	2.758	-24.158	9.718	16.588	46.429
4	32649	363	-24.803	-26.204	1.889	-1.591	4.212	-27.424	17.866	11.585	29.227
5	9200	484	-24.473	-25.335	0.439	-3.661	3.750	-24.562	4.455	8.879	28.354

No: Cluster Number
Size: Number of representative entries for the cluster
Repr: Representative chosen
ReprE: Total interaction energy of the chosen Representative
ClAE: Average total energy of all cluster members weighted with number of representatives.
CLAED: Weighted standard deviation of total energy of cluster entries in the complexes (f55) file
Ele: Electrostatic energy of the representative complex
ElDesE: Electrostatic desolvation energy of the representative complex
HyDesE: Hydrophobic desolvation energy of the representative complex
spread: arithmetic average of rmsd's of each cluster member from the representative, weighted by occupancy
stddev: Stddev of the rmsd's for a given cluster, weighted by occupancy
max: Maximum rmsd within one cluster from the representative

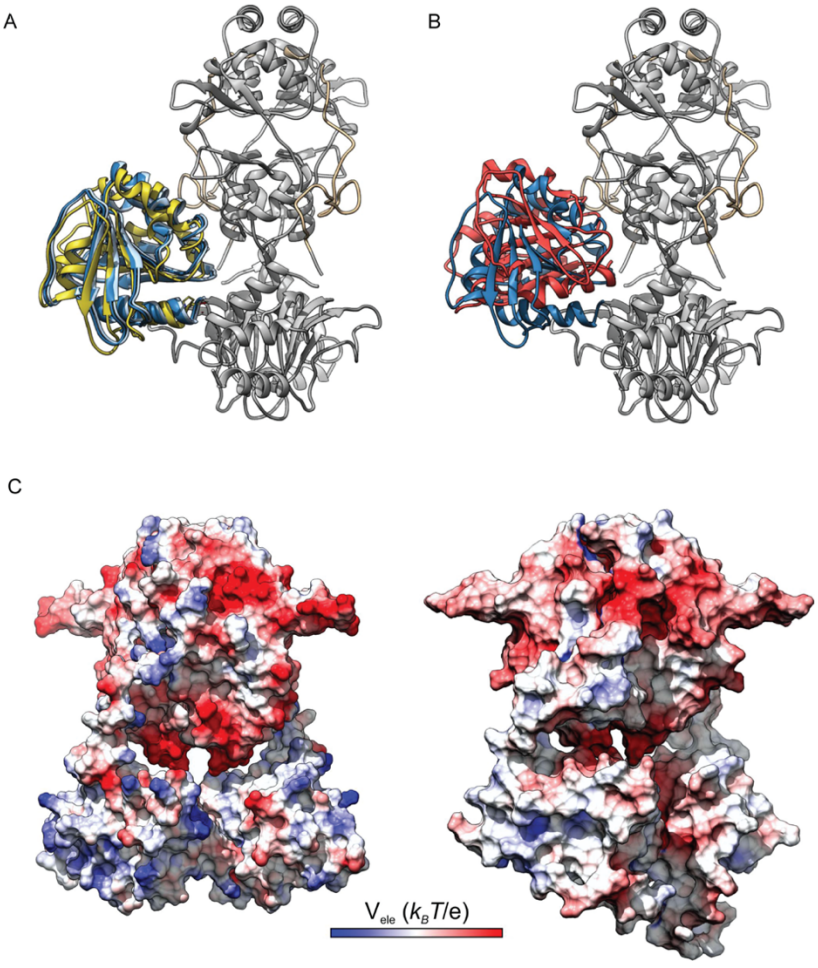

Supplementary Figure 2.3: Overlay of different CNNM2 and CNNM3 docking models A. Overlay of two solutions (dark and light cyan) from different HEX docking computations with the representative structure of the most populated cluster (yellow) from Brownian dynamics computations. B. Overlay of the results from HEX docking computations between Arl15 and CNNM2 and CNNM3. CNNM3 was aligned to CNNM2—which is shown. The ARL15 bound to CNNM3 is in red ribbons. C. Comparison of CNNM2 and CNNM3 electrostatic potentials at the surface level. Positive potentials are in blue, and negative in red. Color scales as in Fig. 3B. The CNNM3 model includes long disordered loops in the CNBH domain loops at the bottom of the structure.

ARL15 and CNNM co-localize in the perinuclear region and in kidney DCTs

The subcellular localization for the ARL15-CNNM complex was determined by immunocytochemistry in HEK293 cells. Overexpression of the mCherry-tagged Golgi-marker Beta-1,4-Galactosyltransferase 1 (B4GALT1) showed co-localization with ARL15 and CNNM2 in HEK293 cells, suggesting that the function of ARL15 is exerted within the perinuclear region containing the endoplasmic reticulum (ER) and the Golgi apparatus (Fig. 2.4A). Similar results were obtained with ARL15 and CNNM3, confirming that the proteins predominantly co-localize in the Golgi-apparatus (Fig. 2.4B). Since CNNM2 has been implicated in Mg^{2+} transport in the DCT segment of the kidney [257], we investigated whether ARL15 co-localizes with CNNM2 in this segment of the nephron (Fig. 2.4C). CNNM2 staining was concomitant with ARL15 staining in mouse kidney sections. In SK-RC-39 kidney cancer cells, similarly to HEK293, wild-type CNNM3 was co-localized with ARL15, however the co-localization with CNNM3 N-glycosylation mutant (N73A) was significantly decreased (Fig. 2.4D, Supp. Fig. 2.4A). Wild-type CNNM3 and ARL15 co-localize partially with ER (Pearson correlation of 0.72 and 0.46, respectively) and Golgi (Pearson correlation of 0.65 and 0.61, respectively) and also showed co-localization at the plasma membrane (Fig. 2.4D, Supp. Fig. 2.4B). CNNM3 N73A mutant was mostly trapped in the perinuclear region and did not localize to plasma membrane (Fig. 2.4D, Supp. Fig. 2.4B). N-glycosylation of CNNM2 has been shown to regulate CNNM2 membrane trafficking [257] and it appears that it plays a similar role with CNNM3. One of the ARL15-interacting partners identified using BioID was ribophorin I protein (RPN1) (Supp. Fig. 2.1). RPN1 is part of the oligosaccharyltransferase complex that is involved in N-glycosylation and is found in the ER [264]. To confirm the

interaction, co-immunoprecipitation assays with overexpressed CNNM3, ARL15 and RPN1 were performed (Supp. Fig. 2.5). CNNM3 interacted with RPN1 and ARL15, corroborating the localization of the three proteins to the ER as well (Fig. 2.4D). Our results demonstrate that ARL15 is localized in the ER and the Golgi-system and one of the enriched GO biological processes identified in ARL15 BioID was “Protein N-linked glycosylation via asparagine” (Fig. 2.1A), which suggests that ARL15 is involved in the N-glycosylation of CNNMs.

Figure 2.4: ARL15 and CNNMs co-localize in the Golgi system. ▸
A. Immunocytochemistry of HEK293 overexpressing ARL15, CNNM2 and mCherry-tagged Golgi-apparatus marker, B4GALT1. Nuclei are stained with DAPI. B. Immunocytochemistry of HEK293 overexpressing ARL15, CNNM3 and mCherry-tagged Golgi-apparatus marker, B4GALT1. Nuclei are stained with DAPI. C. Mouse kidneys were permeabilized and co-immunostained with anti-ARL15 and anti-CNNM2. Merged pictures stained for ARL15 in green, CNNM2 in red and DAPI (nuclei) in blue. Bar in figure A and B represents 5 µm, bar in figure C represents 50 µm. Representative image presented of three independent experiments with three replicates. G, Glomerulus, PT, Proximal tubule, DCT, Distal convoluted tubule. D. SK-RC-39 cells were co-transfected with ARL15-mClover3, CNNM3-mCherry (WT or N73A N-glycosylation mutant) and pmTurquoise2-ER or -Golgi. Plasma membrane localization is indicated with arrows, co-localization in the Golgi with triangles and co-localization in the ER with asterisks.

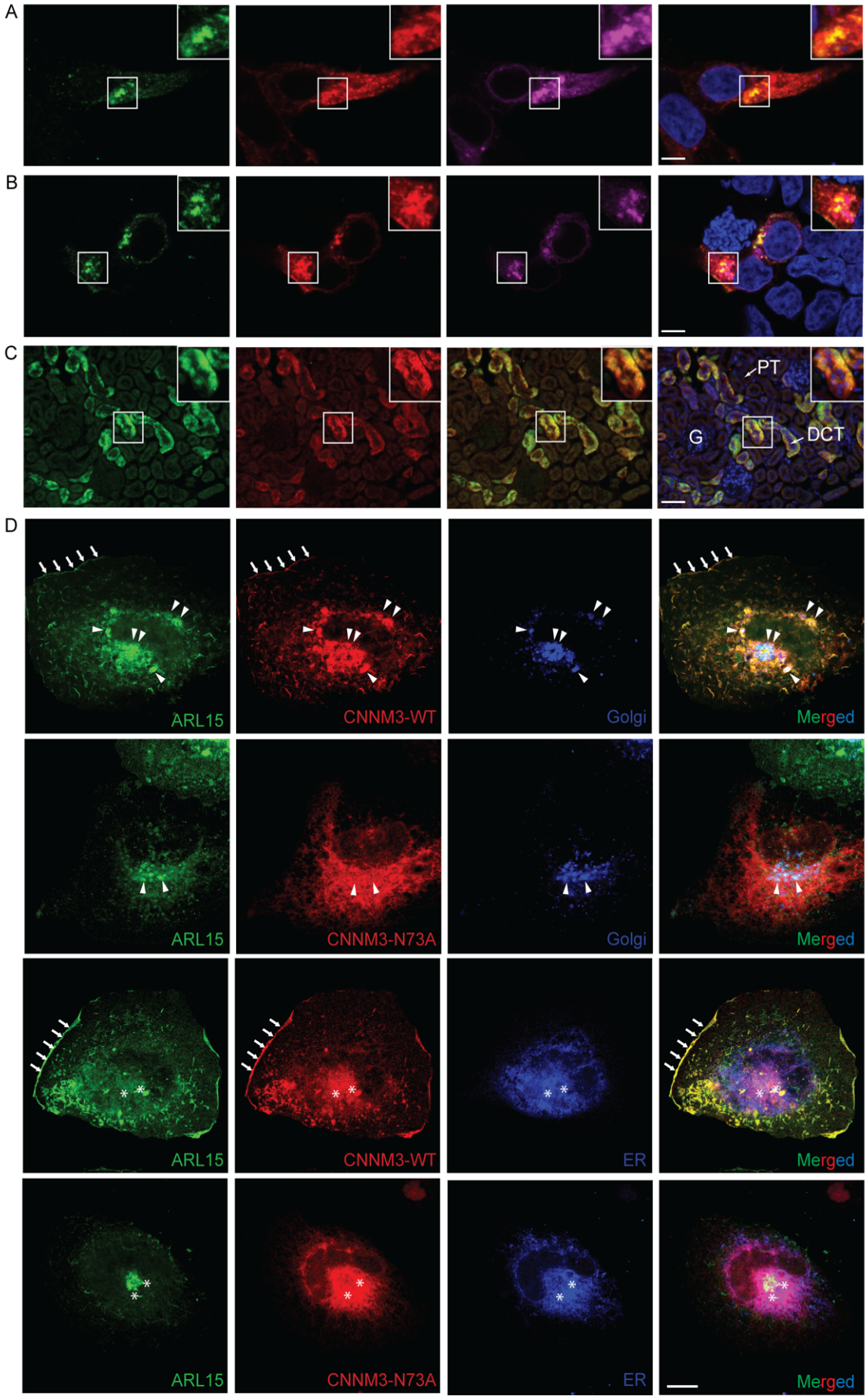
A
B
C
PT
G
DCT
D
ARL15
CNNM3-WT
Golgi
Merged
ARL15
CNNM3-N73A
Golgi
Merged
ARL15
CNNM3-WT
ER
Merged
ARL15
CNNM3-N73A
ER
Merged

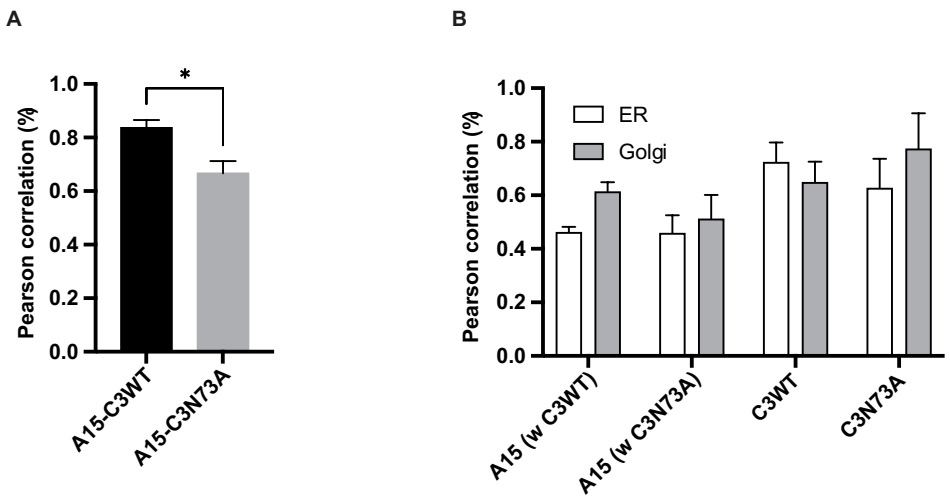

Supplementary Figure 2.4: Co-localization analysis of ARL15 and CNNM3 with Golgi and ER

A. Pearson correlation between ARL15 and either wild-type (A15-C3WT) or N-glycosylation CNNM3 mutant (A15-C3N73A).

B. Pearson correlation between ARL15, CNNM3 and Golgi and ER markers. The correlation was measured in samples with overexpression of ARL15 and either wild-type (A15 (w C3WT) for ARL15 and C3WT for CNNM3) or N-glycosylation CNNM3 mutant (A15 (w C3N73A) for ARL15 and C3N73A for CNNM3 mutant).

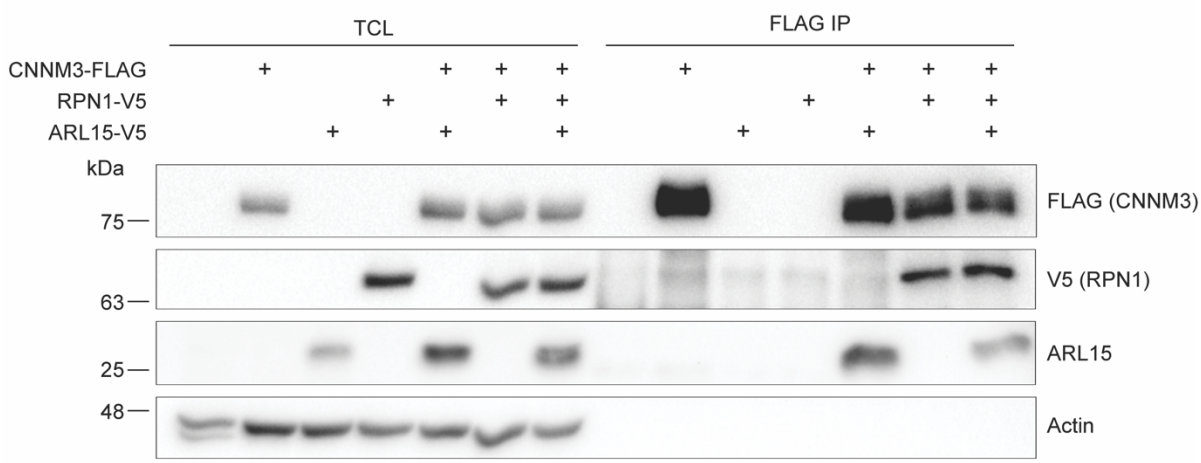

Supplementary Figure 2.5: Co-immunoprecipitation of CNNM3, ARL15 and RPN1

HeLa cells were co-transfected with CNMM3-FLAG, ARL15 and RPN1-V5 and immunoprecipitation was performed using magnetic FLAG beads. CNNM3 co-immunoprecipitated with ARL15 and RPN1.

TCL, Total cell lysate; IP, Immunoprecipitation; ARL15, ADP ribosylation factor like GTPase 15; CNNM, Cyclin M; RPN1, Ribophorin I.

CNNM3 N-glycosylation is modulated by ARL15 and Mg^{2+}

As common post-translational protein modification, N-glycosylation plays important roles to regulate protein functions. Indeed, CNNM2 has been previously shown to have an N-glycosylation site close to its amino (N)-terminus, and it is necessary to stabilize CNNM2 on plasma membrane [257]. Using NetNGlyc [265], N-glycosylation sites were predicted in CNNM1, CNNM3 and CNNM4. The confirmed site in CNNM2 and the predicted sites in the three remaining CNNM family members were analogous (Supp. Fig. 2.6), all located in the extracellular N-terminal domain. The only other predicted CNNM3 N-glycosylation site was asparagine 395, which is located in the cytoplasmic CBS2 domain, which cannot be glycosylated due to its cytoplasmic localization. To confirm that CNNM3 does indeed have an N-glycosylation site similar to CNNM2, the predicted asparagine 73 (N73) was mutated to alanine (N73A mutant). Compared to wild-type (WT) CNNM3, the N73A mutant migrated faster, which is indicative for the loss of N-glycosylation [266] (Fig. 2.5A). Endo H and PNGase F were used to characterize the type of glycans attached to CNNM3 (Fig. 2.5B). When WT CNNM3 was treated with Endo H, which cleaves high mannose and hybrid oligosaccharides from N-linked glycoproteins, the lower band of the doublet shifted further. Cleavage with PNGase F shifted all bands of CNNM3 to a lower molecular mass, indicating that the top band represents the hybrid/complex glycoform (Fig. 2.5A). To verify that N73 is the only site of N-glycosylation, a lectin gel-shift assay was performed, where concanavalin A lectin is added to the top part of the resolving gel and results in a retardation of N-glycosylated proteins during migration [267]. Wild-type CNNM3 resulted in a smear, indicating a retardation of N-glycosylated protein, whereas the N-glycosylation mutant N73A ran

without a smear, indicating that this is the only site of N-glycosylation (Fig. 2.5C). To assess the effect of ARL15 on CNNM3 N-glycosylation, four different kidney cancer cell lines were used: Caki-1 and RCC4 as well as ACHN and SK-RC-39, belonging to renal clear cell carcinoma and papillary renal cell carcinoma, respectively. ARL15 was stably overexpressed in these four cell lines and the pattern of endogenous CNNM3 bands was evaluated. In all four cell lines, overexpression of ARL15 resulted in the increase of hybrid/complex glycoform and a decrease in oligomannose glycoform of CNNM3 (Fig. 2.5D). Interestingly, the effect of ARL15 expression on CNNM3 glycosylation could be modulated by the Mg^{2+} concentration in the growth media (Fig. 5E). When overexpressing ARL15 in SK-RC-39 cells, Mg^{2+} deficient medium resulted in an increase of the oligomannose CNNM3 glycoform. Additionally, CRISPR knockout of ARL15 resulted in a decrease of complex glycoform of CNNM3 as can be seen in the last two lanes (Fig. 2.5E). Neither overexpression nor knockout of ARL15 resulted in changes to overall protein N-glycosylation (Supp. Fig. 2.7), indicating that the effect is specific to CNNMs.

```
CNNM1 88  PSPTLNSGENGTGDWAPRLV 107
CNNM2 103 LRVYGQNINNETWSRIAFTE 122
CNNM3 64  LRLFGPGFANSSWSWVAPEG 83
CNNM4 76  LRLYGYSLGNISSNLISFTE 95
                  .  *  :  .  .
```

Supplementary Figure 2.6: N-glycosylation sequon is conserved in CNNMs
The location of the predicted N-glycosylation residue is indicated. The glycosylated asparagine is highlighted by a box. Amino-acid conservation is indicated below the alignment.

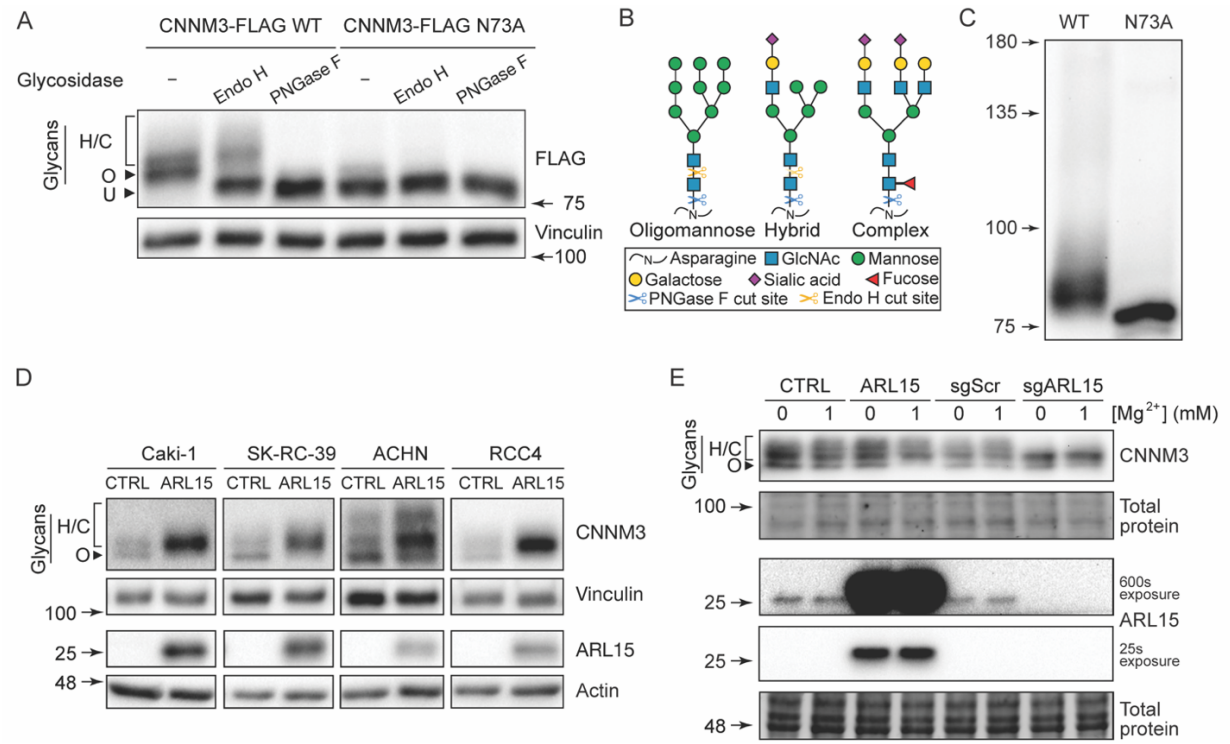

Figure 2.5: CNNM3 N-glycosylation is modulated by ARL15 and Mg^{2+}
A. Wild-type and N-glycosylation mutant CNNM3 were treated with PNGase F and Endo H glycosidases to assess the presence of different glycoforms of CNNM3 and to confirm asparagine 73 as the site of glycosylation. B. Schematic representation of different types of glycans. C. Lectin gel-shift assay of CNNM3 indicates that N73 is the only site of N-glycosylation D. Overexpression of ARL15 increases complex CNNM3 N-glycosylation in kidney cancer cells. E. SK-RC-39 cells were grown in the presence of absence of magnesium in the media and the status of CNNM3 glycoforms was assessed using western blotting. CTRL, Control; sg, Guide RNA; Scr, Scramble; ARL15, ADP ribosylation factor like GTPase 15; CNNM, Cyclin M; PNGase F, Peptide:N-glycosidase F; Endo H, Endoglycosidase

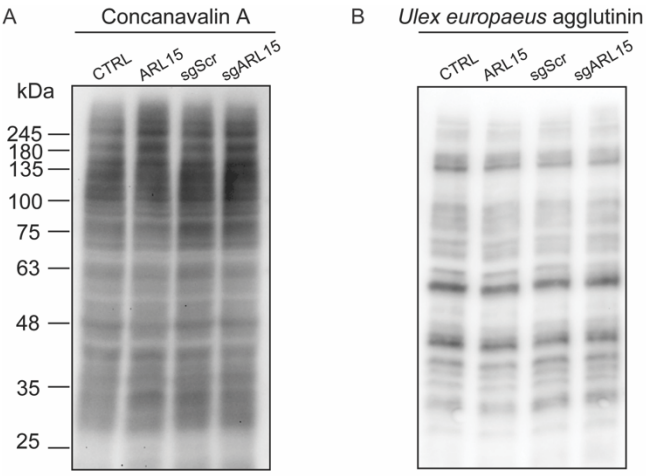

Supplementary Figure 2.7: ARL15 does not affect overall protein N-glycosylation
A. Concanavalin A lectin blot which indicates levels of oligomannose N-glycosylation
B. *Ulex europaeus* agglutinin lectin blot which indicates levels of fucose found only on complex N-glycans

ARL15 affects Mg^{2+} flux and ATP production

To determine whether ARL15 regulates CNNM-dependent Mg^{2+} transport, $^{25}Mg^{2+}$ uptake was studied. Kidney cancer cells were stably transduced to either overexpress or produce a CRISPR knockout of ARL15. ARL15 overexpression decreased $^{25}Mg^{2+}$uptake, while ARL15 knockout significantly increased $^{25}Mg^{2+}$ uptake more than 3-fold in RCC4 and SK-RC-39 cells (Fig. 2.6A). Since multiple enzymes involved in ATP production use Mg^{2+} as a co-factor and ATP is bound to intracellular Mg^{2+} to form Mg-ATP [3], we next assessed the impact of ARL15 expression on ATP production. In RCC4 and SK-RC-39 cells, overexpressing ARL15 resulted in a significant decrease in ATP production (Fig. 2.6B).

Endogenous cell surface expression of CNNM3 was further confirmed using cell surface biotinylation assay in SK-RC-39 cells with overexpression or CRISPR-mediated knockout of ARL15. The complex N-glycosylated CNNM3 glycoform migrates at approximately 90kDa, whereas oligomannose glycoform of CNNM3 migrates at around 75kDa. Although the plasma membrane expression of CNNM3 was not altered in the

presence or absence of ARL15 (Supp. Fig. 2.8), mainly the oligomannose CNNM3 glycoform was observed at the plasma membrane in the ARL15 knockout cells.

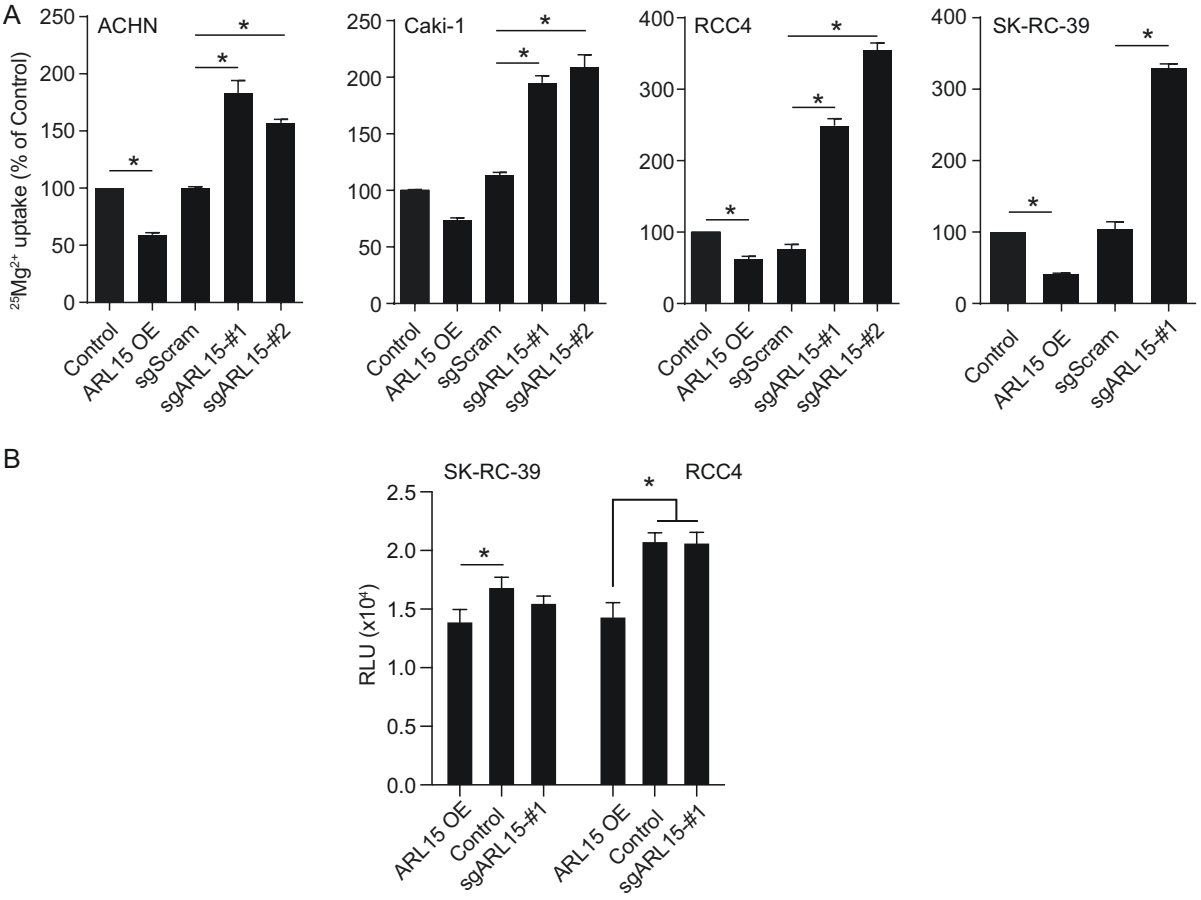

Figure 2.6: ARL15 affects Mg^{2+} flux and ATP production.
A. $^{25}Mg^{2+}$ uptake in stably overexpressed and knockdown ARL15 ACHN, Caki-1, RCC4, and SK-RC-39 cells. These various types of renal carcinoma cell lines were incubated with $^{25}Mg^{2+}$ for 15 minutes and results were normalized to 0 minute. Each data represents the mean of 3 independent experiments ± SEM. * indicates significant difference compared to control cells. B. ATP production in stably overexpressed and knockdown ARL15 SK-RC-39 and RCC4 cells. Results are the mean ± SEM of 3 independent experiments.
sg, Guide RNA; Scr, Scramble; OE, Overexpression; ARL15, ADP ribosylation factor like GTPase 15; CNNM, Cyclin M.

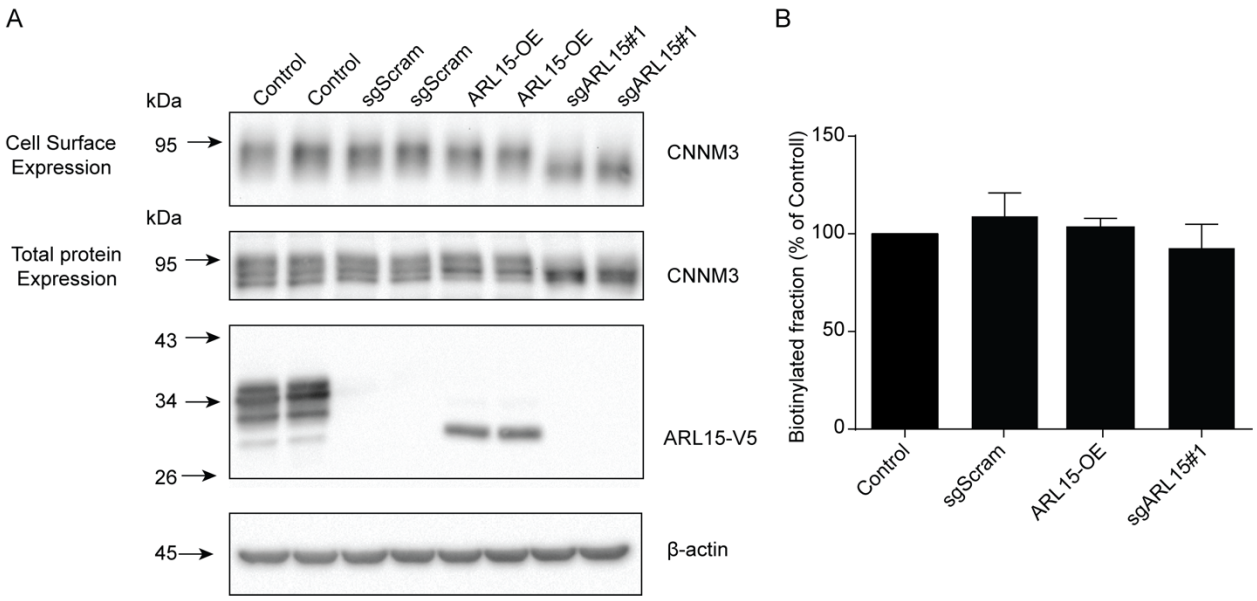

Supplementary Figure 2.8: ARL15 knockdown does not affect CNNM3 cell surface expression.

Endogenous cell surface expression of CNNM3 was detected in SK-RC-39 cells by biotinylation. A. The upper immunoblots show CNNM3 cell membrane expression and the lower blot shows the total CNNM3 expression. B. The diagram shows the quantification of cell surface CNNM3 expression corrected for total CNNM3 protein expression. Results are the mean ± SEM of 3 independent experiments.

Materials and Methods

DNA constructs

Human *CNNM2* cDNA with an in-frame HA tag before CNNM2 stop codon and an *XhoI* restriction site after *CNNM2* stop codon was amplified using Phusion polymerase (New England Biolabs, Ipswich, MA, USA) and then the product was cloned into the pCINeo-IRES-GFP vector using *NheI* and *XhoI* (New England Biolabs). To obtain truncated *CNNM2* plasmids, primers (Forward : 5'-CGGCTAGCGCCACCATGATTGGCTGTGGCGCTTG-3' and Reverse 1 (full-length *CNNM2*: 5'-CCCTCGAGCTATGCGTAGTCTGGCACGT CGTATGGGTAACCGGTGATGGCGCCTTCGTTG-3'), Reverse 2 (*CNNM2* transmembrane region: 5'-CCACCGGTCACGTCCTCCACCGTC-3'), Reverse 3 (*CNNM2* transmembrane+CBS1 region: 5'-CCACCGGTGTCATCGGGATCCAC-3'), Reverse 4 (*CNNM2* transmembrane+CBS1+link region: 5'-CCACCGGTGTGGTTATAAAAT TTGGTGATG-3') or Reverse 5 (*CNNM2* transmembrane+CBS1+link+CBS2 region: 5'-CGGCTAGCGCCACCATGATTGGCTGTGGCGCTTG-3') were synthesized. All primers were purchased from Biolegio BV (Nijmegen, Netherlands). The PCR product was purified using a NucleoSpin® Gel and PCR Clean up kit (Macherey Nagel, Düren, Germany). Subsequently, the truncated *CNNM2* PCR products were cloned into the pCINE-IRES-GFP vector by digestion with restriction enzymes *NheI* (New England Biolabs) and *XhoI* (New England Biolabs).

To obtain C-terminal FLAG-tagged ARL15 and CNNM constructs, human coding sequences were amplified with appropriate primers containing attB1 and attB2 recombination site overhangs. Amplification was carried out with KAPA HiFi polymerase

using GC buffer (Kapa Biosystems, Wilmington, MA, USA). Amplicons were gel purified and Gateway cloning was used to first recombine the amplicon into pDONR221 vector and then, pDEST26-C-FLAG (Addgene #79275) [268] vector, using Gateway BP or LR Clonase II enzyme mix, respectively (Thermo Fisher Scientific, Waltham, MA, US). Chemically competent DH5α *E. coli* were transformed with pDONR221 and pDEST26-C-FLAG vectors. To obtain C-terminal mClover3-tagged ARL15, mClover3 was amplified from pKanCMV-mClover3-18aa-actin vector (Addgene #74259) [269] and at the C-terminal of ARL15 vector using SLiCE cloning [270]. For fluorescence imaging of ER and Golgi pmTurquoise2-ER (Addgene #36204) and pmTurquoise2-Golgi (Addgene #36205) were used, respectively [271]. All constructs were verified by sequence analysis.

Cell culture, transfection and transduction

HEK293 cells were grown in Dulbecco's Modified Eagle Medium (DMEM) (Biowhittaker Europe, Vervier, Belgium) supplemented with 10% (v/v) fetal calf serum (PAA Laboratories, Linz, Austria), non-essential amino acids, and 2 mM L-glutamine at 37 °C in a humidified incubator with 5% (v/v) CO_2 (New Brunswick Galaxy 170s). Cells were seeded 6 hours before transient transfection with Lipofectamine 2,000 (Invitrogen, Breda, The Netherlands), the ratio of DNA: Lipofectamine 2,000 was 1:2.

ACHN, Caki-1, HeLa, RCC4 and SK-RC-39 cells were grown in DMEM, high glucose (Thermo Fisher Scientific) supplemented with 10% fetal bovine serum (FBS) (Thermo Fisher Scientific) and 2 mM GlutaMAX at 37 °C in a humidified incubator with 5% (v/v) CO_2.

For lentivirus production, HEK293T/17 cells were transfected with a 4:2:1 ratio of lentiviral construct of interest:PAX2:VSV-G. 24 hours later, the media was changed. 48 hours later, the media was collected and filtered through a 0.45 µm filter. To infect the cells, media was substituted with HEK293T/17 supernatant containing virus with 8 µg/ml polybrene. 48 hours later, the media was changed to fresh media containing a selection reagent and the selection was carried out for 7 days.

Cell lines used for experiments were obtained from ATCC.

Site-directed mutagenesis

To mutate asparagine 73 (N73) that was predicted to be the site of N-glycosylation of CNNM3 into alanine (A), pcDNA3.1-CNNM3-mCherry or pDONR221-CNNM3 carrying the wild-type sequence without a stop codon was amplified using a single primer PCR. Amplification was carried out with KAPA HiFi polymerase using GC buffer (Kapa Biosystems, Wilmington, MA, USA). The following primer was used: 5'-GGCCCGGGCTTCGCCgcCAGCTCTTGGTCCTGGGTGG-3', indicating the nucleotides necessary to introduce the mutation in lower-case letters. After amplification, the original plasmid was digested with *DpnI* (New England Biolabs) for 2 hours at 37 °C, which was followed by transformation of chemically competent DH5α E. coli. The construct was verified by sequencing.

Pull-down assay

A pull-down assay was performed to determine which proteins of mice DCT interact with CNNM2. pGEX-mCNNM2 c-tail-GST was inserted in bacteria to be able to multiply the protein. Afterwards bacteria were lysed with lysis buffer (150mM NaCl, 5mM EGTA, Triton 1% (v/v), 1mg/ml pepstatin, 1mM PMSF, 5mg/ml leupeptin, 5mg/ml aproptin, 50mM Tris/HCl, pH 7.5). Glutathione beads (Thermo Fisher, Rockford, IL, USA) were used to purify the samples to obtain only Cnnm2 c-tail. The beads were washed with pull down buffer (20mM Tris-HCL pH 7.4, 140mM NaCl, 1 mM $CaCl_2$, 0.2% (v/v) triton-x-100, 0.2% (v/v) NP-40, 1:1000 pepstatin, 1:1000 Aprotin, 1:400 Leupeptin, 1:100 PMSF) and bacterial lysate was added to the beads followed by an incubation of 3 hours at 4 °C. After incubation, beads were transferred into a new tube and washed with pull down buffer. For kidney tissue, kidneys of 8 PV-GFP mice were dissected and minced in small pieces. The DCT was selected and dissolved in pull down buffer followed by homogenizing of the mixture using ultra turrax. After 30 minutes of incubation on ice, aliquots were taken and centrifuged. Supernatant was added to the beads followed by an incubation overnight rotating at 4 °C. After incubation, beads were washed with pull down buffer, Laemmli and DTT were added, and Western blot was performed. Migration was stopped when the sample was 1 cm in the running gel. Then samples were cut out and measured with mass spectrometry.

BioID

BioID was performed as previously described [272]. Briefly, cleared lysates from ARL15^{A86L} expressing Flp-In™ T-REx™ HeLa cells were incubated with streptavidin beads (17-5113-01, 5 ml, GE Healthcare). Trypsin digestion on beads was performed and peptides were collected in water, dried in a SpeedVac and pellets were resuspended in 5% formic acid prior to their injection into the mass spectrometers. Digested peptides from HEK293 and HeLa cells were respectively injected into LTQ-Orbitrap Velos and Q Exactive (Thermo Fisher) onto a 75 µm i.d. × 150 mm Self-Pack C18 column installed in the Easy-nLC 1000 system (Proxeon Biosystems) coupled to a Nanospray Flex Ion Source, at the IRCM Proteomics core facility.

Raw mass spectrometry files were analyzed, as previously described [272], using the Human RefSeq database (version 57) supplemented with ''common contaminants'' from Max Planck Institute (https://maxquant.org/), Global Proteome Machine (http://www.thegpm.org/crap/index.html) and decoy sequences with the Mascot search engine through the iProphet pipeline integrated in ProHits. Significance Analysis of INTeractome (SAINT; version 3.6.1) files generated with ProHits using iProphet protein probability ≥ 0.9 and unique peptides ≥ 2, comparing samples against negative controls, were used to estimate interactions statistics with ProHits-viz [273]. (https://prohits-viz.lunenfeld.ca/). An average probability (AvgP) ≥ 0.95 was used as a cutoff to consider statistically significant and of high confidence interactions. Gene ontology overrepresentation analysis was performed using PANTHER 15.0 [274].

Gel filtration

Gel filtration chromatography of the $CNNM2_{BAT}$.ARL15 complex was performed using 1 mg/mL protein at 0.5 ml/min using a Superdex 200 Increase 10/300 GL column in 50 mM Hepes, pH 8.5, 200 mM NaCl, 1 mM $MgCl_2$, 1 mM TCEP buffer. The following values were used: V_o=8.61 mL,void volume; V_t=24 mL, total column volume. The calibration trendline is y= -0.2451x + 1.5726 ($y = K_{av}$; x = log$M$). The standard proteins used to calibrate the column were: 1, thyroglobulin; 2, gamma-globulin; 3, ovoalbumin; 4, myoglobin; 6, Vitamin B12.

ARL15 model

A model of the structure of ARL15 was generated by simulated annealing as implemented in MODELLER [275] using as templates the X-ray diffraction coordinates of the complex between human ARL2 and BART (pdb code 3DOE chain A; 36.3 identity) complex between murine ARL2 and PDEδ (pdb code 1KSG chain A; 36.3 identity) murine ARF6 (pdb code 6BBQ; 35.67% identity) human ARF6 (pdb code 2A5G; 35.67% identity). Results were monitored in UCSF Chimera [276]. A single structure—displaying the lowest zDOPE [277] score (-0.58) and an RMSD value of 3.54 Å with respect to the closest template—out of 100 results was selected. This structure was subjected energy minimization using the Amber 14SB force field [278]. A final check was performed with Coot [279] before deposition and the ModelArchive server.

CNNM2 models

To generate alternative linker conformations, in addition to completing sidechains from a SAXS model, simulated annealing computations were carried out using MODELLER [275]. 100 conformations were generated, arranged according to their zDOPE [277] scores and tested for collisions with other subunits with UCSF Chimera [276]. At the end, three different conformations were tested. A model of the cytosolic domains of CNNM3 was also generated using the full precursor sequence (NCBI accession code 060093.3) and the XRD coordinates of the CNNM2 and CNNM4 cytosolic domains, obtained from corresponding crystals of the independent cytosolic domains and from SAXS data of the entire cytosolic region of CNNM4 [280]. The dimeric assembly of the complementary Bateman modules used in the model corresponds to the flat (ATP-bound and/or PRL-bound like) conformation of the CBS module (association of two Bateman domains) [191, 280]. The modeled region showed a 53.6 % sequence identity with respect to the template. Best model showed 6.1 Å RMSD with respect to the template, and a zDOPE value of 0.39. This positive value is mainly due to the model including flexible loop and linker regions.

Docking models

Docking computations were carried out with benchtop HEX [281] and compared with Brownian dynamics (BD) computations (see Supplemental methods). Hex computations included shape evaluation, in vacuo electrostatics and Decoys As a Reference State (DARS) potentials [282]. In every simulation, 20000 structures were generated, clustered using a RMSD cut-off value of 3 Å and arranged according to their energies. First 100

were selected for analysis. Post-processing consisted in a short OPLS energy minimization as implemented in the software.

Brownian dynamics

Docking modeling was complemented with Brownian Dynamics computations using the WebSDA server [283] to test if results could be reproduced by other methods. The force-field grids used in BD included all electrostatics and desolvation [284, 285] grids. Charges were added with PDB2PQR [286].

200 trajectories of BD computations were run in docking mode. A total of 500 non-redundant complexes were recorded along the computations. Supplemental table 2.1 displays the summary of the clustering analysis of the distinct complexes found. First cluster corresponds to binding to CNBH domains at regions nearby missing structure, so they are considered artefactual. Cluster 2, however, showed the highest population and—on average— displayed lowest energies, and the lowest dispersion of conformations, according to RMSD values with respect to the representative structure. Supplemental figure 2.3 illustrates the consistency between the BD computations and docking simulations performed with Hex (see main text).

Glycosidase and tunicamycin treatment

20 μg of protein from SK-RC-39 cells were treated with N-glycosidase F (PNGase F) and Endoglycosidase H (Endo H) (New England Biolabs) according to the manufacturer's instructions. Briefly: protein was denatured at 100 ℃ for 10 minutes, 1 unit/μl of a glycosidase was added with appropriate buffers and digested at 37 ℃ for 1 hour. SK-

RC-39 cells grown in DMEM were treated with tunicamycin (Sigma-Aldrich) at 1 ug/ml for 8 hours to inhibit N-glycosylation.

Immunohistochemistry

5 µm kidney frozen sections were fixed with formalin and washed with TN buffer (0.1 M Tris/HCl (pH 7.6) 0.15 M NaCl). Then, the sections were permeabilized in TN-Triton (TN with 0.1% (v/v) Triton X-100) for 30 minutes. After incubation, the sections were washed and blocked with TN with 0.5% (w/v) Blocking Reagent TSA fluorescein system (Perkin Elmer, Waltham, MA, USA) for 30 minutes. The sections were incubated overnight at 4 ℃ with the following primary antibodies: guinea pig anti-CNNM2 (1:100), rabbit anti-ARL15 (Sigma-Aldrich, St. Louis, MO, USA, 1:50). For detection, kidney sections were incubated with Alexa Fluor 488 conjugated goat anti-rabbit and Alexa Fluor 596 conjugated goat anti-Guinea pig IgG secondary antibodies (Thermo Fisher, Rockford, IL, USA, 1:300). Images were visualized using AxioCam cameras (Zeiss, Oberkochen, Germany) and AxioVision software (Zeiss).

Immunocytochemistry

HEK293 cells were seeded at a low density on 0.01% (w/v) poly-L-lysine (Sigma, St Louis, MO, USA) coated coverslips and were transfected the subsequent day using Lipofectamine 2000 (Invitrogen, Breda, The Netherlands). Cells were transfected with the following constructs: pLenti6-CNNM3-V5, pDEST26-ARL15-FLAG, and mCherry-Golgi-7. After 24 hours, cells were washed with PBS, followed by fixation for 10 minutes using 4% (w/v) methanol-free formaldehyde (ThermoFisher, Waltham, MA, USA) in PBS. Afterwards, cells were permeabilized for 10 minutes in 0.1% (v/v) Triton-X100 and 0.3%

(w/v) bovine serum albumin solution. Subsequently, cells were treated with 50 mM NH_4Cl in PBS to reduce background. Thereafter, cells were washed 3x in PBS followed by blocking in 16% (v/v) normal goat serum (Merck Milipore, Burlington, MA, USA) supplemented with 0.1% (v/v) Triton-X100 for 30 minutes. Cells were then probed with primary antibody diluted in blocking buffer overnight at 4 ℃. Cells were washed three times and incubated in secondary antibodies for 45 minutes at room temperature in the dark. Cells were washed three times with PBS and subsequently mounted using mounting medium supplemented with 4′, 6-diamidino-2-phenylindole (DAPI; Southern Biotech, Birmingham, AL, USA). Images were made using the Zeiss LSM880 (Oberkochen, Germany) and analyzed using the freely available Fiji software [287]. The following antibodies were used: mouse monoclonal anti-V5 (Thermo Fisher, Rockford, IL, USA, 1:1,000) and rabbit polyclonal anti-FLAG (Sigma-Aldrich, St. Louis, MO, USA, 1:1,000), Alexa Fluor 488 conjugated goat anti-rabbit and Alexa Fluor 647 conjugated goat anti-mouse (Thermo Fisher, Rockford, IL, USA, 1:300).

Fluorescence imaging

SK-RC-39 cells were transfected with pcDNA3.1-CNNM3-WT-mCherry WT, pcDNA3.1-CNNM3-N73A-mCherry, ARL15-mClover3, pmTurquoise2-ER and pmTurquoise2-Golgi using Lipofectamine 2000 (Invitrogen, Breda, The Netherlands) for 24H and then transferred to an 8-chamber slide (ibidi GmbH, Fitchburg, WI, USA). Cells were fixed with 4%PFA for 10 min, briefly rinsed with PBS, then coverslips were mounted with Mowiol mounting medium (Millipore Sigma, Darmstadt, Germany). Slides were cured for 24 hrs

and pictures were taken by using the Zeiss LSM880 with Airyscan processing (Zeiss, Oberkochen, Germany).

Western blot

Cells were lysed with lysis buffer added 1 mg/ml pepstatin, 1 mM PMSF, 5 mg/ml leupeptin, 5 mg/ml aproptin protease inhibitors. The lysis buffer contained 50 mM Tris-HCl (pH 7.5), 1 mM EDTA, 1 mM EGTA, 150 mM NaCl, 1 mM sodium-orthovanadate, 10 mM sodium-glycerophosphate, 50 mM sodium fluoride, 0.27 M sucrose, 10 mM sodium pyrophosphate, 1% (v/v) Triton X-100. Protein concentrations were measured by performing a Bicinchoninic Acid protein assay (BCA) (Fisher Scientific, Hampton, NH, USA) and 20 µg protein was used for western blot. Blots were then incubated in primary antibody overnight rolling at 4 °C. Primary antibodies were diluted in 1% (w/v) milk diluted in TBST as following; anti-HA (Cell Signaling technology, Leiden, The Netherlands) diluted 1:5,000, anti-FLAG (Sigma-Aldrich, St. Louis, MO, USA) diluted 1:5,000, anti-V5 (Thermo Fisher, Rockford, IL, USA) diluted 1:5,000, anti-β-actin (Sigma-Aldrich, St. Louis, MO, USA) diluted 1:10,000, all are raised in mice. After washing with Tris-Buffered Saline and Tween 20 (TBST), blots were incubated for 1 hour rolling at RT in secondary antibody which was anti-mouse antibody raised in sheep (Sigma-Aldrich, St. Louis, MO, USA) diluted 1:10,000. Then, proteins were visualized with were made with ChemiDoc (Bio-Rad Laboratories Inc, Hercules, CA, USA). Subsequent analysis was done using ImageJ [287]. Lectin gel-shift assay was performed as described previously [267]. Briefly, upon polymerization of a standard 6% SDS-PAGE gel, 5 mm of

6% SDS-PAGE containing 10 mg/ml concanavalin A (Sigma-Aldrich, St. Louis, MO, USA) was poured on top and allowed to polymerize.

Co-Immunoprecipitation

HEK293 or HeLa cells were seeded and transfected in petri dishes, 24 to 48 hours after transfection cells were lysed with lysis buffer. 12 hours before collecting the transfected HEK293 cells, carbobenzoxy-Leu-Leu-leucinal (MG132) (Sigma-Aldrich, St. Louis, MO, USA) dissolved in Dimethyl sulfoxide (DMSO) were treated to the HEK293 cells. BCA assay was performed to determine the protein concentration of the lysates. Input samples were taken to be able to check transfection efficiency by performing western blot. For co-immunoprecipitation samples, 30 µl/sample protein A/G plus agarose beads (Santa Cruz Biotechnology, CA, USA) were washed with PBS. And 1.5 µl/sample in mouse raised antibody for human HA (Sigma-Aldrich, St. Louis, MO, USA) was added to the beads. For negative control, no antibody was added to the beads. Samples were then incubated for 2 hours rotated at 4 °C. Unbound antibodies were removed by washing with lysis buffer. Then lysates with the same amount of proteins (as calculated with the BCA test) were added to the beads and incubated overnight rotated at 4 °C. After incubation, lysates and beads were washed with PBS, Laemmli and DTT were added, and western blot was performed. For FLAG-tagged protein immunoprecipitation, for each sample 20 µg of ANTI-FLAG® M2 affinity agarose gel (Sigma-Aldrich, St. Louis, MO, US) were pre-blocked with 5% (w/v) BSA and 300 ug of total cell lysate (TCL) was pre-cleared with 20 µg of Protein A/G agarose mix, for 2H at 4°C on a rotator. TCL

supernatant was collected and incubated with pre-blocked FLAG beads for 2 hours at 4°C on a rotator.

CRISPR-Cas9 experiments

sgRNAs targeting ARL15 were cloned into lentiCRISPRv2 plasmid (Addgene #52961) [288] using Golden-Gate Assembly with the Esp3I endonuclease following the standard protocol [289]. For lentivirus production, HEK293T/17 were transfected using Lipofectamine 2000 (Invitrogen, Breda, The Netherlands) with 4:2:1 ratio of lentiCRISPRv2:PAX2:VSV-G. 24H later the media was changed. 48H later the media was collected and filtered through a 0.45 µm filter. To transduce the cells, media was substituted with HEK293T/17 supernatant containing virus with 8 µg/ml polybrene. 48H later the media was changed to fresh media containing puromycin and the selection was carried out for 7 days.

ATP production

5,000 kidney cancer cells were plated per well in a 96-well plate and ATP production was measured after growing overnight. CellTiter-Glo 2 kit (Promega) using manufacturer's instructions.

$^{25}Mg^{2+}$ uptake

Cells were seeded in petri dishes and 24 hours after transfection cells were reseeded into 12-well plates. Two days after transfection, cells were washed once with basic uptake buffer without Mg^{2+} (125 mM NaCl, 5 mM KCl, 0.5 mM $CaCl_2$, 0.5 mM Na_2HPO_4, 0.5 mM Na_2SO_4, 15 mM HEPES/NaOH, pH 7.5), followed by an incubation for 0 or 15

minutes at 37°C with basic uptake buffer containing 1 mM $^{25}Mg^{2+}$ (Cortecnet, Voisins Le Bretonneux, France). After incubation, the basic uptake buffer containing $^{25}Mg^{2+}$ was removed and cells were washed with ice cold PBS. Then cells were lysed with 1 ml nitric acid which was then diluted in Milli-Q until a nitric acid (Sigma Aldrich, St. Louis, MO, USA) concentration of 10%. Samples were analysed with ICP-MS (inductively coupled plasma mass spectrometry).

Cell surface biotinylation

Petri dishes were coated with poly-L-lysine before seeding and transfection. Two days after transfection the cells were washed with PBS-CM (100 ml 10x PBS, 1 mM $MgCl_2$, 0.5 mM $CaCl_2$, pH 8.0 adjusted with NaOH, Milli-Q until total volume of 1,000 ml) followed by adding 0.5 mg/ml Sulfo-NHS-LC-LC-biotin (Thermo fisher scientific, Rockford, USA). After 30 minutes incubation, cells were washed with 0.1% (w/v) PBS-CM BSA and PBS. Cells were then lysed with lysis buffer, and protein concentration was measured with a BCA test. Input samples were taken to be able to check transfection efficiency by performing Western blot. Then, lysates with the same amount of proteins (as calculated with the BCA test) were added with the neutravidin agarose beads (Thermo fisher scientific, Rockford, USA) and incubated overnight rotated at 4°C. After incubation, protein lysates were washed with lysis buffer and Laemmli and DTT buffer were added and incubated at 37°C for 30 minutes before loading the protein samples on SDS-PAGE.

Statistical analysis

Results are expressed as mean ± standard error of the mean (SEM). Biotinylation results of experiments are statistically analyzed by performing one-way ANOVA followed by Tukey as post-test. $^{25}Mg^{2+}$ uptake results with CNNM2 and ARL15 are statistically analyzed by performing a two-way ANOVA followed by Tukey as post-test. Differences with $p<0.05$ were regarded as statistically significant.

Discussion

In this study, we identified ARL15 as a novel interacting partner of CNNMs. ARL15 binds to CNNMs in the ER and regulates their complex N-glycosylation in the Golgi system (Fig. 2.7). Our data suggest that the complex N-glycosylation of CNNMs reduces their activity at the plasma membrane, as reflected in a reduced $^{25}Mg^{2+}$ uptake in renal carcinoma cells. As such, ARL15 may affect cellular Mg^{2+} homeostasis and energy metabolism.

ARL15 is a member of the superfamily of ARF-like (ARL) proteins, which have been functionally characterized as small GTPases. Although ARL15 has been relatively scarcely studied to date, many studies have demonstrated that other ARL and ARF proteins are involved in vesicle trafficking [290]. Our immunocytochemistry in HEK293 cells demonstrated that ARL15 is predominantly localized in the plasma membrane and the perinuclear region (Fig. 2.4), which is in line with previous reports of ARL15 in 3T3-L1 pre-adipocytes [92]. Moreover, proximity labeling of ARL15 identified many Golgi-specific proteins (Supp. Fig. 2.1), such as golgins (GOLGA3, GOLGA4, GOLGB1), Golgi SNAP receptor complex member 1 (GOSR1), and Golgi scaffolding protein GOPC, that also interacts with another member of the ARF family ARFRP1 [291]. However, the localization with RPN1, a protein of the oligosaccharyltransferase complex, suggests that the interaction between ARL15 and CNNMs is already formed in the ER. Indeed, several ARF proteins, e.g. ARF1 and ARF3, have been shown to regulate ER-to-Golgi trafficking [292].

The main finding of our study is that ARL15 binds CNNMs and modulates their activity via N-glycosylation. Biosynthesis of glycoproteins commences in the ER, where a pre-assembled oligosaccharide is bound onto the nascent protein by oligosaccharyl-transferases. After passing the ER, a series of reactions further assemble the glycan in the medial-Golgi and maturation takes place in the trans-Golgi. Three different types of N-glycans are commonly present on proteins; oligomannose, hybrid and complex N-glycans. Our results demonstrate that ARL15 stimulates the formation of complex N-glycans on CNNMs. Although ARL15 does not possess the enzymatic capacity to change the glycosylation *per se*, we have identified several proteins of the oligosaccharyltransferase complex in our BioID experiments (e.g. RPN1, STT3A and STT3B) (Fig. 2.1). Moreover, protein N-glycosylation was among the enriched GO-terms in our analysis. Additionally, LMAN1 was identified in the BioID experiments. LMAN1 is located in the ER-Golgi intermediate compartment (ERGIC) and it participates in ER-to-Golgi trafficking of proteins by binding oligomannose N-glycan moieties of N-glycosylated cargo [293]. We hypothesize that trans-Golgi trafficking via ARL15 is an essential step in the complex glycosylation of CNNMs. A similar mechanism has been postulated for ARFGEF1, which regulates the N-glycosylation and trafficking of integrins [294].

Multiple solute carrier proteins were identified in the ARL15 BioID. These are transmembrane proteins which are N-glycosylated. For example, the importance of N-glycan glycoforms in its localization has been shown for mouse Slc12a2 [295]. N-glycosylation of another putative ARL15 interacting partner SLC26A3 has been implicated in its plasma membrane expression and activity [296].

The N-glycosylation of CNNMs is essential for their plasma membrane expression. CNNMs contain a single N-glycosylation site in the extracellular N-terminal region [257]. Mutation of the Asn73 residue to Ala in CNNM3 completely abrogated its N-glycosylation (Fig. 2.5A) and its membrane expression (Fig. 2.4D). Similar results were previously obtained for Asn112 residue in CNNM2 [257]. In this study, we demonstrated that not only the presence of, but also the composition of the glycan is essential for the protein function. ARL15 overexpression resulted in a complex glycosylation of CNNM3, which was accompanied by a significant reduction of $^{25}Mg^{2+}$ uptake. *Vice versa*, ARL15 downregulation resulted in oligomannose glycoform and increased $^{25}Mg^{2+}$ uptake. Altogether, we propose a model in which the composition of the N-glycan affects CNNM activity (Summarized in Figure 2.7).

Multiple roles for N-glycosylation of plasma membrane proteins have been described, ranging from effects on membrane trafficking, membrane stability and protein degradation [297, 298]. In our experiments, neither ARL15 overexpression nor ARL15 downregulation affected the plasma membrane localization of CNNM3 (Supp. Fig. 2.7), suggesting that membrane trafficking of CNNM3 is not affected by ARL15. Consequently, changes in N-glycosylation may directly affect the activity of CNNM3 at the plasma membrane. It has been extensively described that N-glycans interact with glycan-binding proteins in the extracellular spaces, such as lectins. Lectin-glycan interactions are involved in many biological cellular processes such as apoptosis, differentiation as well as regulation of membrane transport [299]. Indeed, binding of lectins and other glycan-binding proteins has been shown to regulate TRPV5-mediated

Ca^{2+} transport [300, 301]. Whether the binding of lectins explains the changes in CNNM3 activity remains to be defined.

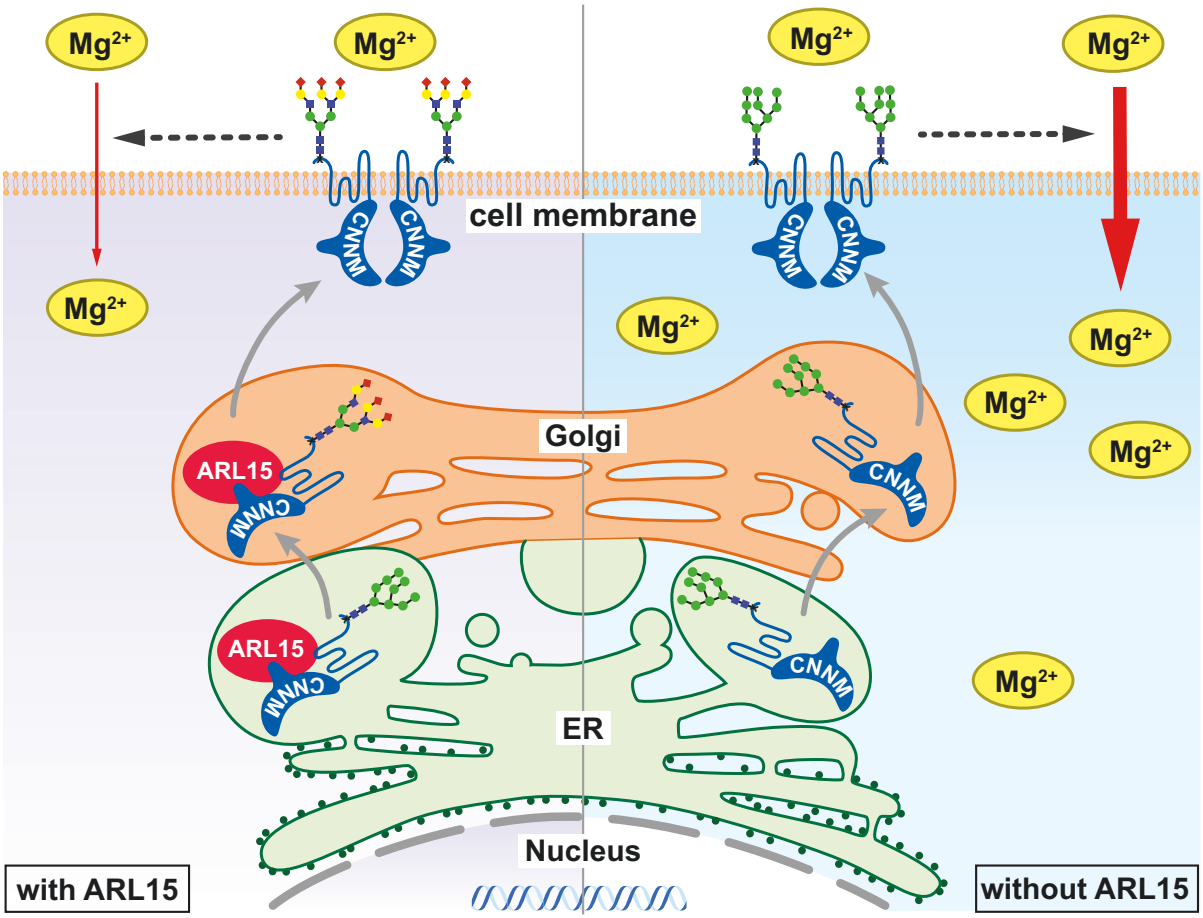

Figure 2.7: Summary of the effect of ARL15·CNNM complex on Mg^{2+} flux.
In the presence of ARL15, it interacts with CNNMs in the ER and Golgi, resulting in their complex N-glycosylation, which in turn decreases Mg^{2+} uptake. In the absence of ARL15, CNNMs are found in less complex glycoforms and that results in increased Mg^{2+} uptake. ER, Endoplasmic reticulum; ARL15, ADP ribosylation factor like GTPase 15; CNNM, Cyclin M.

The interaction model that we developed is compatible with a 1:1 CNNM2:ARL15 stoichiometry. ARL15 interacts with the Bateman CBS1 domains, in particular with a surface region defined between α–helix A, the β1-β2 hairpin loop and α-helix H1. Indeed, co-immunoprecipitation experiments confirmed that the CBS domains are essential for ARL15 binding (Fig. 2.2B). The interaction also involves the CNBH domains 3C, thereby explaining the larger affinity observed with the full-length constructs. Overall, the interaction displays high surface complementarity and presents a core of hydrophobic and polar residues surrounded by charged ones. Interestingly, the negative-charged residues present in the CNNM2 docking site is complementarity to the positive-charged surface of ARL15 (Fig. 2.3D). The interaction of ARL15 with CNNM3 cytosolic domain seems to use the same region. The more negative charge as compared to CNNM2 may explain the larger affinity toward positively charged ARL15. Notably, no overlap is observed between the binding site of ARL15 and PRL, which mostly binds CBS2 by its long loop region comprising β5 and β6 [191] (Supp. Movie 1).

The identification of ARL15 as a novel regulator of CNNM Mg^{2+} transport activity is of particular interest in the DCT segment of the kidney. In the DCT, transient receptor potential cation channel subfamily M member 6 (TRPM6) facilitates apical Mg^{2+} transport [302]. Basolateral Mg^{2+} extrusion in the DCT is regulated by CNNM2. Consequently, mutations in CNNM2 and TRPM6 have been shown to cause renal Mg^{2+} wasting in patients [156, 157, 303]. Interestingly, the ARL15 locus was recently associated with urinary Mg^{2+} wasting in a GWAS [96]. In the same study, TRPM6 channel activity was shown to be significantly increased in the presence of ARL15 [96]. Our results demonstrate that ARL15 also binds CNNM2, suggesting that both the apical and

basolateral Mg^{2+} transport mechanisms are simultaneously regulated. These findings explain how ARL15 determines urinary Mg^{2+} excretion. Interestingly, overexpression of ARL15 resulted in decreased ATP levels (Fig. 2.6B). Intracellular Mg^{2+} and ATP levels are closely associated, as ATP must be bound to this cation to be biologically active [3]. Indeed, previous studies have shown that PRL-2 knockdown and decreased intracellular Mg^{2+} levels, reduce intracellular ATP levels and regulate cellular metabolism [18, 304]. Given that ARL15 overexpression reduced CNNM-mediated Mg^{2+} uptake, the expression of ARL15 may indirectly regulate cellular metabolism. Indeed, ARL15 has been associated with a wide range of metabolic parameters and diseases in GWAS, including adiponectin, HDL, diabetes mellitus and body shape [82–84, 305–307]. As these studies did not analyze Mg^{2+} status as a modifying factor, it cannot be excluded that ARL15 has additional functions that explain these associations. Indeed, ARL15 has been demonstrated to modify the insulin-signaling pathway in myotubes [308].

Overall, our work establishes complex N-glycosylation of CNNMs as an essential process to regulate their activity. This crucial post-translational modification promoted by ARL15 on CNNMs adds to recent mechanisms of CNNMs modulation such as their circadian rhythm expression [309] and their interactions with the PRL family by a magnesium-sensitive mechanism [18, 192]. The increasing complexity of CNNMs regulation provides a dynamic system to ensure the correct levels of intracellular Mg^{2+} during metabolic changes and cell requirements.

Declarations

Funding

This work was financially supported by grants from the European Joint Program for Rare Diseases (EJPRD2019-40), the Netherlands Organization for Scientific Research (NWO Veni 016.186.012. Vici 016.130.668), the Dutch Diabetes Research Foundation (2017.81.014), the Spanish Ministry of Science and Innovation and Universities (PGC2018-096049-B-I00), European Regional Development Fund (FEDER), and the Andalusian Government (BIO-198, US-1254317 and US-1257019). This project “FIGHT-CNNM2” was supported by a grant from Fonds de recherche du Québec - Santé (FRQS) FRQ-S #294027 and by a grant from the CIHR ERT-168503, under the frame of E-Rare-3, the ERA-Net for Research on Rare Diseases. In addition, this project has received funding from the European Union's Horizon 2020 research and innovation programme under the EJP RD COFUND-EJP N° 825575.

In addition, it was also supported by Canadian Institutes of Health Research Grants MOP-142497 and FDN-159923. M.L.T. is a Jeanne and Jean-Louis Lévesque Chair in Cancer Research and holds a Distinguished James McGill Chair from McGill University. Y.Z. was supported by a scholarship from the Fonds de recherche du Québec – Santé (FRQS) and by a travel award from the Canderel Foundation at the Goodman Cancer Research Centre.

Conflicts of interest

The authors declare that they have no conflict of interest.

Authors' contributions

Y.Z., C.M., S.H., J.H., M.L.T. and J.d.B. designed the research studies, Y.Z., C.M., I.D.M., A.D.Q., G.A.C.F., I.G.R., E.K., F.L., J.B., M.-P.T., L.A.M.C., J.F.C., N.U., S.H., J.H., M.L.T. and J.d.B. conducted experiments and/or analyzed data, Y.Z., C.M., S.H., M.L.T. and J.d.B. wrote the manuscript. All authors corrected the manuscript and approved the final version.

Availability of data and material

ARL15 model is available at ModelArchive server DOI: 10.5452/ma-c4ded.

CNNM3 model is available at ModelArchive server DOI 10.5452/ma-v6la8. The ARL15 BioID proteomics data is deposited to MassIVE under accession number MSV000087061 and the BirA* control dataset is deposited under accession number MSV000084477.

Ethics approval

The animals were housed at the Radboud Institute for Molecular Life Sciences, Nijmegen, the Netherlands, according to the institutional guidelines. The study was ethically approved by the Local Ethical Committee of the Radboud University Nijmegen (RU DEC 2015-0112) and by the Dutch Central Commission for Animal Experiments (CCD, AVD103002016382).

Acknowledgements

We thank Caro Bos, Milou Smits and Shirin Mostert for excellent technical support. We thank Dr. Arnim Pause for generously providing the kidney cancer cell lines.

Connecting the post-translational modification of CNNMs and the regulation of TRPM7

We identified the involvement of the small GTPase ARL15 in the modulation of CNNM glycoforms and subsequent changes in magnesium flux and ATP production. Nevertheless, the direct mechanism of Mg^{2+} regulation was not uncovered. Additionally, the role of the interplay between ARL15 and PRLs, which strongly interact with CNNMs, has not been studied. Since the BioID experiment unveiled not only the interaction between ARL15 and CNNMs, but also its interaction with TRPM7, the canonical magnesium channel. We sought to understand the function of this interaction in the following chapter. We have found that ARL15 is indeed involved in the interaction between CNNMs and TRPM7. CNNMs were found to be inhibitory regulators of TRPM7. Furthermore, a cascade of dynamic changes in response to magnesium levels was unraveled which showed that the interactions between ARL15, PRL-1/2 and CNNM3 regulate the activity of TRPM7.

Chapter 3

CNNMs and their interacting partners regulate TRPM7

Yevgen Zolotarov*, Serge Hardy*, Noriko Uetani, Jacob A.C. Coleman, Simon Roitman, Michel L. Tremblay

* These authors contributed equally to the preparation of the manuscript
In preparation

Abstract

Transient receptor potential melastatin 7 (TRPM7) is a ubiquitously expressed magnesium channel that is required for the maintenance of magnesium homeostasis through its activity in the intestine and the kidneys. We have identified ADP-ribosylation factor-like protein 15 (ARL15) to interact with cyclin and CBS domain divalent metal cation transport mediator (CNNM) proteins and to enhance their interaction with TRPM7. TRPM7 influences cells morphology and the presence of CNNMs reverses that effect. Using a novel genetically encoded magnesium reporter we demonstrate that CNNMs inhibit the activity of TRPM7. Presence of ARL15 increases the inhibitory effect of CNNMs, whereas PRL-1/2 decreases that effect. Overexpression PRL-2 modulated subcellular localization of CNNM3 away from the plasma membrane to cytoplasm. We found that magnesium itself regulates the interaction between TRPM7 and CNNM3, PRLs and ARL15. Absence of magnesium reduces the interaction between TRPM7 and CNNM3, reduces the interaction between ARL15 and CNNM3 and increases the interaction between CNNM3 and PRL-1/2. Knockdown of PRL-1/2 without magnesium increased the interaction between TRPM7 and CNNM3. Our results reveal a novel dynamic regulation of TRPM7 through CNNMs and their interacting partners – PRLs and ARL15.

Introduction

TRPM7 is a ubiquitously expressed divalent cation channel which is predominantly involved in the influx of magnesium, calcium and trace metals [197, 199, 310]. It is required for proper development [311, 312] and magnesium homeostasis [198, 255]. TRPM7 and its homologue, TRPM6, are unique among the TRP family of channels in that they contain a serine/threonine kinase in the C-terminal region of the protein [210, 313]. TRPM7 is involved in cellular proliferation [314–317], migration [316, 318–320], growth of primary tumours [321, 322] and metastases [320, 323]. TRPM7 regulates cell morphology and adhesion by affecting filopodia, lamellipodia and focal adhesion formation [211, 316, 319, 324, 325]. TRPM7 regulates cell intravasation by affecting shear sensitivity of tumour cells [326]. TRPM7 is itself regulated by intracellular magnesium ($[Mg^{2+}]_i$) and the native form of ATP bound to magnesium (Mg•ATP), where low magnesium increases and high magnesium suppresses the channel activity [197, 322]. However, this mechanism is not well understood.

Magnesium transport mediators CNNMs modulate Mg^{2+} homeostasis and they are regulated by their interactions with PRLs and ARL15 [192, 327]. PRLs (phosphatases of regenerating liver) have been associated with progression of multiple cancer types, such as breast cancer and colon cancer [102]. Some of PRLs' proto-oncogenic activity is linked with their interaction with CNNMs, which affects Mg^{2+} flux and growth, as well as progression of different cancers [182, 192, 194].

We have recently identified a novel CNNM interacting partner, ARL15 (ARF-like protein 15) that regulates magnesium homeostasis [327], and that has been previously

shown to affect urinary magnesium handling through its regulation of TRPM6-mediated currents [96]. However, it is not understood if and how ARL15 regulates TRPM7 and what function do CNNMs and PRLs play in that regulation.

In this study we show that all 4 members of the CNNM family interact with TRPM7, and that this interaction is significantly strengthened in the presence of ARL15. Using a novel genetically encoded magnesium reporter we demonstrate that CNNMs inhibit TRPM7 activity. TRPM7-mediated changes in cell morphology are abrogated by CNNMs. A dynamic interplay between TRPM7 and CNNM3 is affected by PRL-2 and ARL15 and mediated by magnesium concentration. Furthermore, TRPM7-mediated signaling is suppressed by CNNM3 and the localization of CNNM3 is affected by PRL-2. Our study has uncovered a novel layer of regulation of TRPM7 that responds to changes in magnesium levels.

Results

ARL15 interacts with TRPM7 and strengthens its interaction with CNNMs

The BioID experiment performed in our previous paper indicated that ARL15 not only interacts with CNNMs but with TRPM7 as well [327]. To confirm the interaction between CNNM3, ARL15 and TRPM7 we performed co-immunoprecipitation (co-IP) experiments with these overexpressed proteins (Fig. 3.1A). CNNM3 interacted with TRPM7 and the presence of ARL15 significantly strengthened the interaction. To test whether this effect extends to all four members of the CNNM family we performed co-IPs of TRPM7, ARL15 and CNNM1-4. ARL15 strengthened the interaction between all four CNNMs and TRPM7 (Fig. 3.1B). We have previously shown that a single mutation (D426A) in the extended loop of the CNNM3 Bateman domain abolishes its interactions with PRLs [182]. To verify whether this interaction is necessary to interact with TRPM7, co-IPs of TRPM7 and a CNNM3-WT or CNNM3-D/A mutant were performed in the absence and presence of ARL15. The CNNM3 D426A mutation did not abolish the interaction with TRPM7 (Fig. 3.1C, lanes 3 and 6). As described previously, wild-type ARL15 affected TRPM6 channel activity when both proteins were overexpressed together, while a dominant negative mutant of ARL15 (T46N) did not have an effect [96]. To test whether the ARL15 T46N mutant would affect the interaction between CNNM3 and TRPM7, co-IPs were performed. ARL15 mutant acted in a similar way to wild-type, and it still strengthened the interaction between CNNM3 and TRPM7 (Fig. 3.1C, lane 8). We noticed that ARL15 was not detected when it was overexpressed without CNNM3 (Fig. 3.1C, lanes 4 and 7). To test whether CNNM3 was required for its expression, we overexpressed ARL15 in the

absence and presence of CNNM3 or MG132, a proteasomal degradation inhibitor. Without CNNM3 or MG132, ARL15 was not detected. However, the presence of either proteasome inhibitor or CNNM3 prevented ARL15 degradation (Supp. Fig. 3.1).

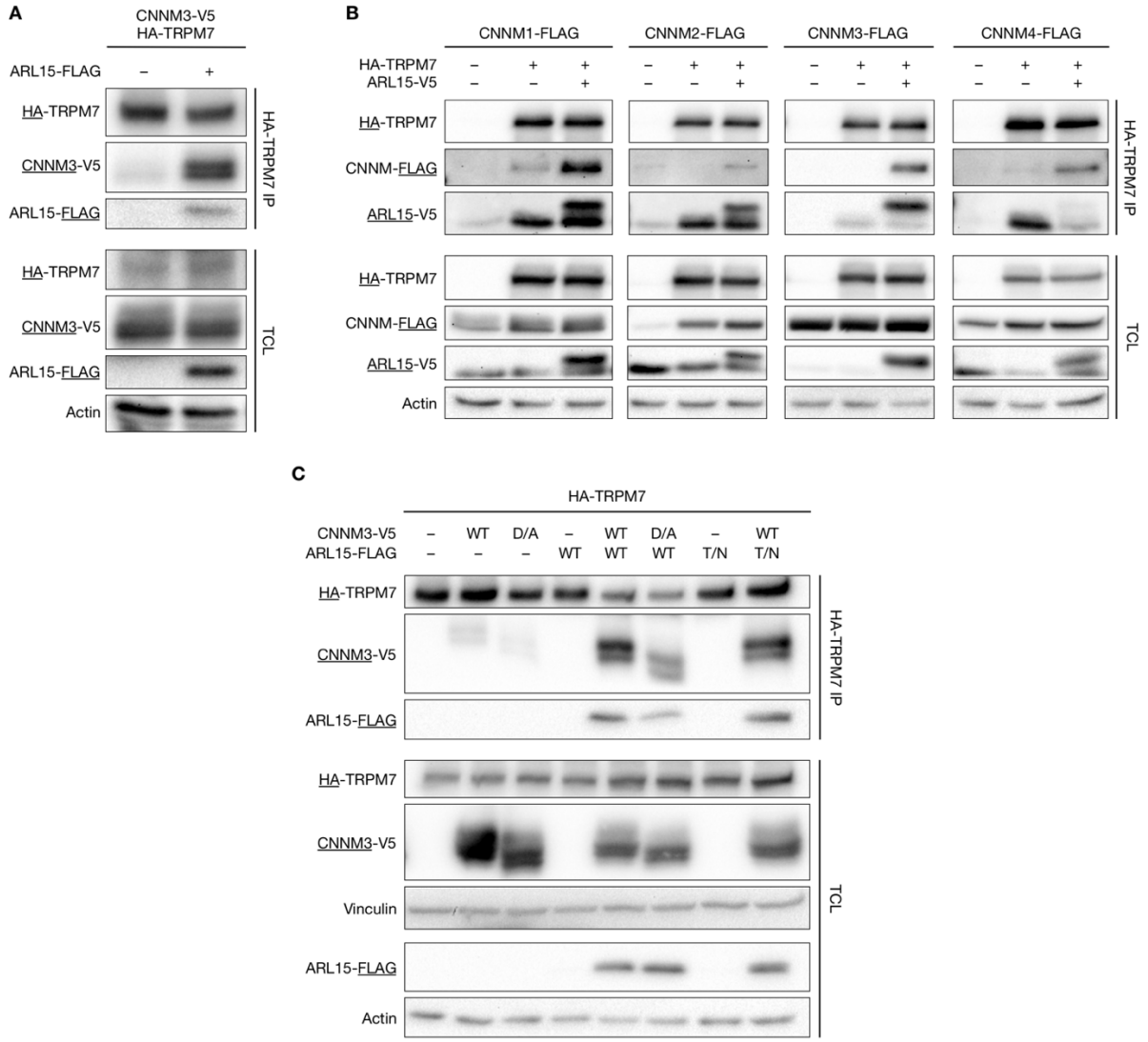

Figure 3.1: Interaction between TRPM7, ARL15 and CNNMs
A. HA-TRPM7 was immunoprecipitated from HEK293 cells with doxycycline inducible TRPM7 expression with overexpression of CNNM3-V5 with and without ARL15-FLAG. CNNM3 interacted with TRPM7 and the presence of ARL15 increased the interaction. B. HA-TRPM7 was co-expressed with FLAG-tagged CNNM1-4 and ARL15-V5. Immunoprecipitation of TRPM7 showed that it interacted with all four CNNMs and that ARL15 increased that interaction. C. HA-TRPM7 was co-overexpressed and immunoprecipitated with WT and mutants of ARL15 and CNNM3, which did not affect the interactions.

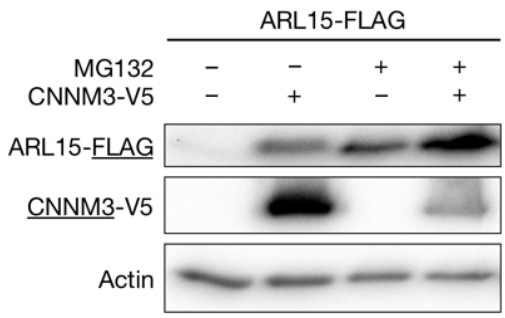

Supplementary Figure 3.1: Degradation of ARL15 is inhibited by CNNM3.
ARL15-FLAG was overexpressed in HEK293 cells with or without CNNM3-V5. The cells were treated for 24H with either vehicle or MG132. Overexpression of CNNM3 and MG132 treatment prevented ARL15 degradation.

Genetically encoded magnesium reporter

We have recently shown that PRL-1/2 translation is regulated specifically by intracellular magnesium levels due to ribosome stalling at the upstream open reading frame (uORF) [18]. Based on this work, we fused the 5′ UTR of PTP4A2 to a destabilized firefly luciferase (Fig. 3.2A) to create a reporter that has an inverse response to the intracellular magnesium concentration: the lower is the $[Mg^{2+}]_i$ the stronger is the luciferase signal. We confirmed that it responds specifically to changes in extracellular magnesium (Fig. 3.2B), but not to other divalent cations transported by TRPM6/7, calcium, and zinc (Fig. 3.2C, D). A reporter without the PTP4A2 5′ UTR did not respond to changes in magnesium (Supp. Fig. 3.2A). To further assess the specificity of the reporter, cells were treated with FCCP, which is known to induce magnesium release from mitochondria to cytosol [328]. In the condition of depleted cytosolic magnesium, we observed a significant decrease in the activity of the reporter upon treatment with FCCP, due to the release of mitochondrial magnesium (Supp. Fig. 3.2B). Since the reporter responded

specifically to changes in magnesium but not to other divalent cations transported by TRPM7, we assessed the effect of TRPM7 overexpression on its activity. Similarly to the lack of magnesium in the media, cells expressing low endogenous levels of TRPM7 produced in a significantly higher reporter signal, indicating lower $[Mg^{2+}]_i$, compared to cells overexpressing TRPM7 (Fig. 3.2E). The reporter without the PTP4A2 5′ UTR did not respond to changes in TRPM7 expression (Supp. Fig. 3.2C). We confirmed that overexpression of TRPM7 results in an increase in $[Mg^{2+}]_i$ using Magnesium Green, a magnesium-specific fluorescent indicator (Supp. Fig. 3.2D).

Next, we tested the effect of NS8593, a magnesium-dependent TRPM7 channel inhibitor [329]. Treatment of cells with endogenous TRPM7 levels with the inhibitor resulted in a slight (1.1-fold) but significant increase in the reporter activity (Fig. 3.2F). Application of NS8593 to cells overexpressing TRPM7 resulted in a larger increase in reporter activity (1.7-fold), indicating that there was a relatively larger inhibition of magnesium uptake (Fig. 3.2F).

These results demonstrate that the novel magnesium reporter is specific to $[Mg^{2+}]_i$ and it responds to changes in TRPM7 expression levels.

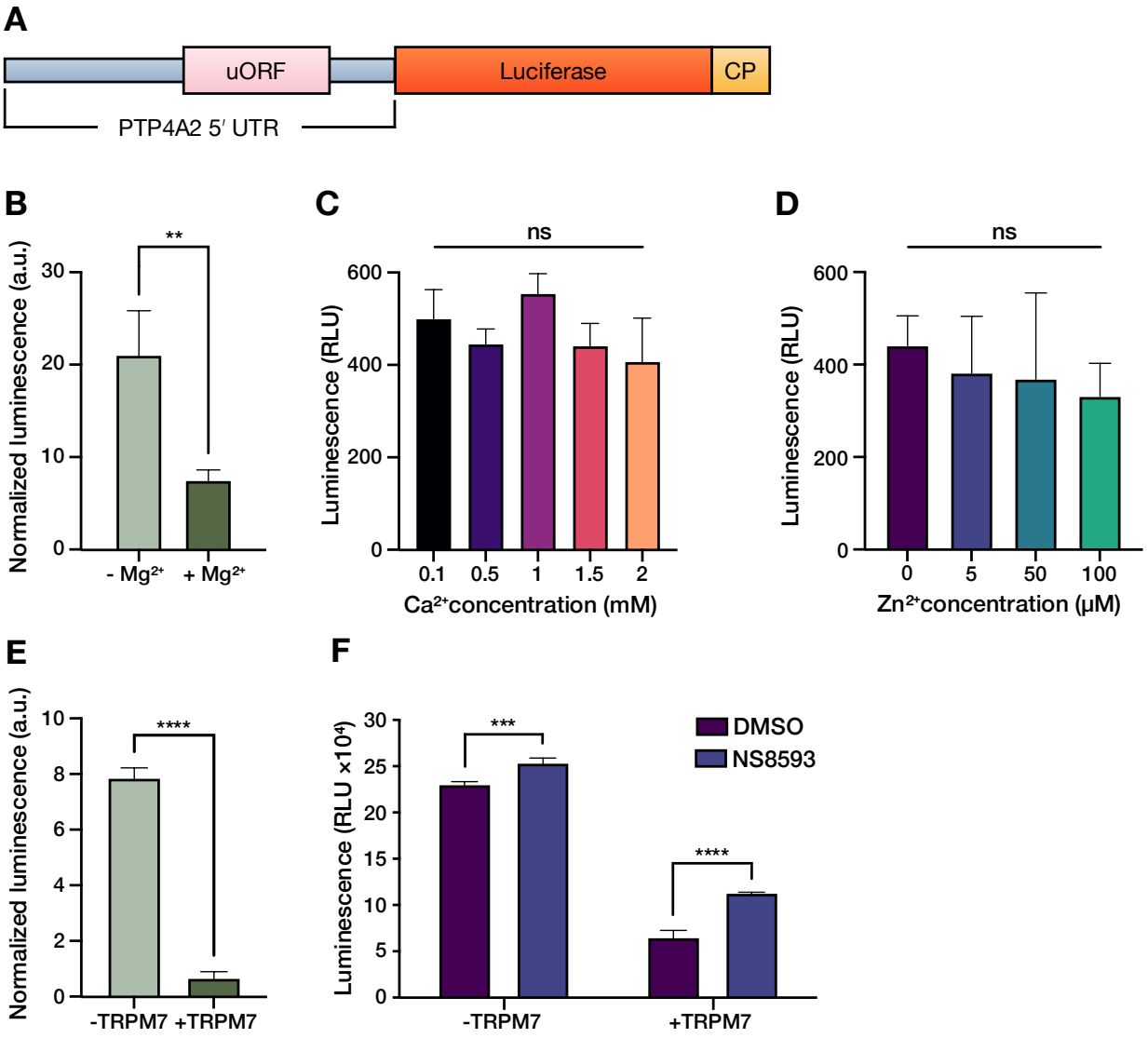

Figure 3.2: Genetically encoded luciferase reporter is specific to magnesium.
A. A schematic of the reporter design – firefly luciferase with a destabilizing sequence CP fused at the C-terminus and PTP4A2 5′ UTR containing the ribosome stalling uORF upstream of the start codon. B. HEK293 cells transiently transformed with the reporter and renilla luciferase control constructs were grown with and without magnesium for 24H and lytic luciferase assay was performed at the endpoint. C, D. HEK293 cells with stable expression of the construct were grown in a media with different calcium (C) and zinc (D) concentrations and live time course luciferase assay was performed, the 6H signal peak is presented. E. HEK293 cells with inducible TRPM7 expression were transfected as in A and the reporter signal was recorded 24H after treating the cells with DMSO or doxycycline. F. HEK293 cells with inducible TRPM7 expression and stable expression of the reporter were treated with either DMSO of doxycycline, with and without NS8593. T-test (B, E), one-way ANOVA (C, D) and two-way ANOVA followed by Tukey's multiple comparison test were performed.

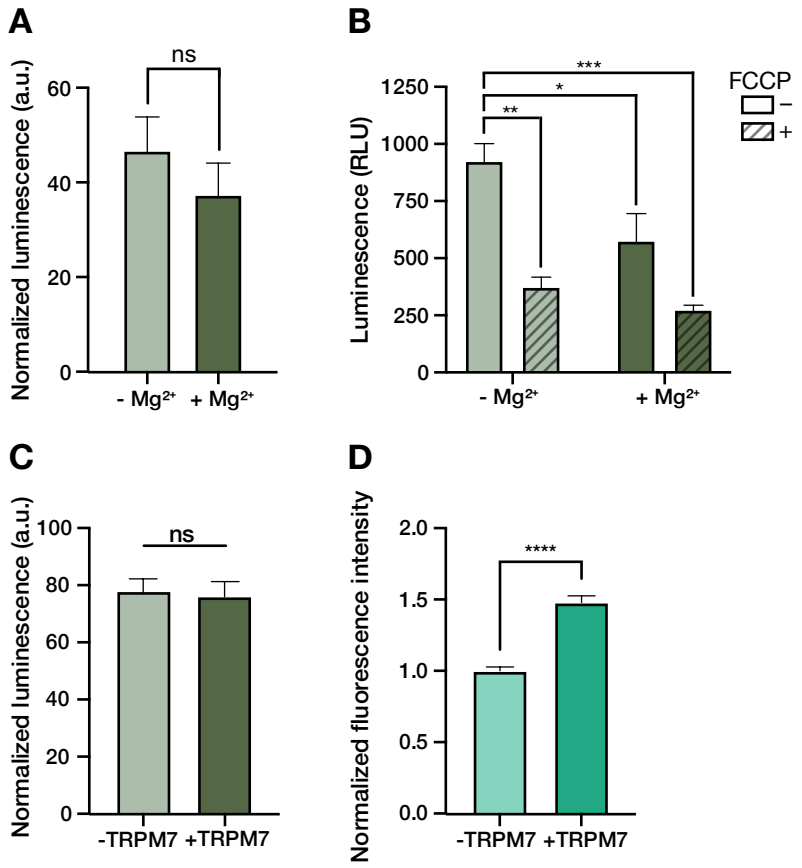

Supplementary Figure 3.2: Activity of the reporter and Magnesium Green
A. Same as Fig 3.2B except a reporter without PTP4A2 5' UTR was used B. HEK293 cells with stable expression of the reporter were grown with or without magnesium in the media and were treated with either FCCP or DMSO and 6H time point was recorded C: Same as Fig 3.2E except a reporter without PTP4A2 5' UTR was used. D. Magnesium Green probe was used in HEK293 cells with inducible expression of TRPM7, which were treated with either DMSO or doxycycline. T-test or two-way ANOVA followed by Tukey's multiple comparison were used.

CNNMs inhibit TRPM7

Since all four members of the CNNM family interacted with TRPM7 (Fig. 3.1B), we tested the effect of their overexpression on TRPM7 activity. It was previously shown that TRPM7 plays a role in cell morphology and cytoskeletal rearrangement, with overexpression of TRPM7 resulting in rounding of cells and decreased lamellipodia formation [197, 324]. Knockdown of TRPM7 decreased cell surface area and magnesium

was necessary to counteract this effect [319]. To confirm previous observations, we overexpressed TRPM7 in HEK293 cells and observed cell rounding (Fig. 3.3A) and decreased confluency (Fig. 3.3B), compared to cells with endogenous TRPM7 expression Overexpression of CNNMs without inducing TRPM7 did not have a significant effect on cell morphology (Fig. 3.3A). However, overexpression of either member of the CNNM family restored TRPM7-mediated changes in cell morphology and cell confluency (Fig. 3.3A, B). Only TRPM7-expressing control cells without CNNM overexpression were unable to reach complete confluency (Supp. Fig. 3.3). Overexpression of CNNMs in TRPM7-induced cells allowed them to become confluent at the same rate as control cells without induction of TRPM7 expression (Supp. Fig. 3.3). When CNNMs were overexpressed in cells with endogenous TRPM7 levels, the activity of the Mg^{2+} reporter increased slightly (1.2-1.3-fold), indicating a decrease in intracellular magnesium (Fig. 3.3C). A larger increase (1.6-2.2-fold) in reporter activity was observed upon overexpression of CNNMs in the context of TRPM7 induction, indicating that overexpression of TRPM7 augmented magnesium uptake and $[Mg^{2+}]_i$, which was significantly inhibited by CNNM overexpression (Fig. 3.3C).

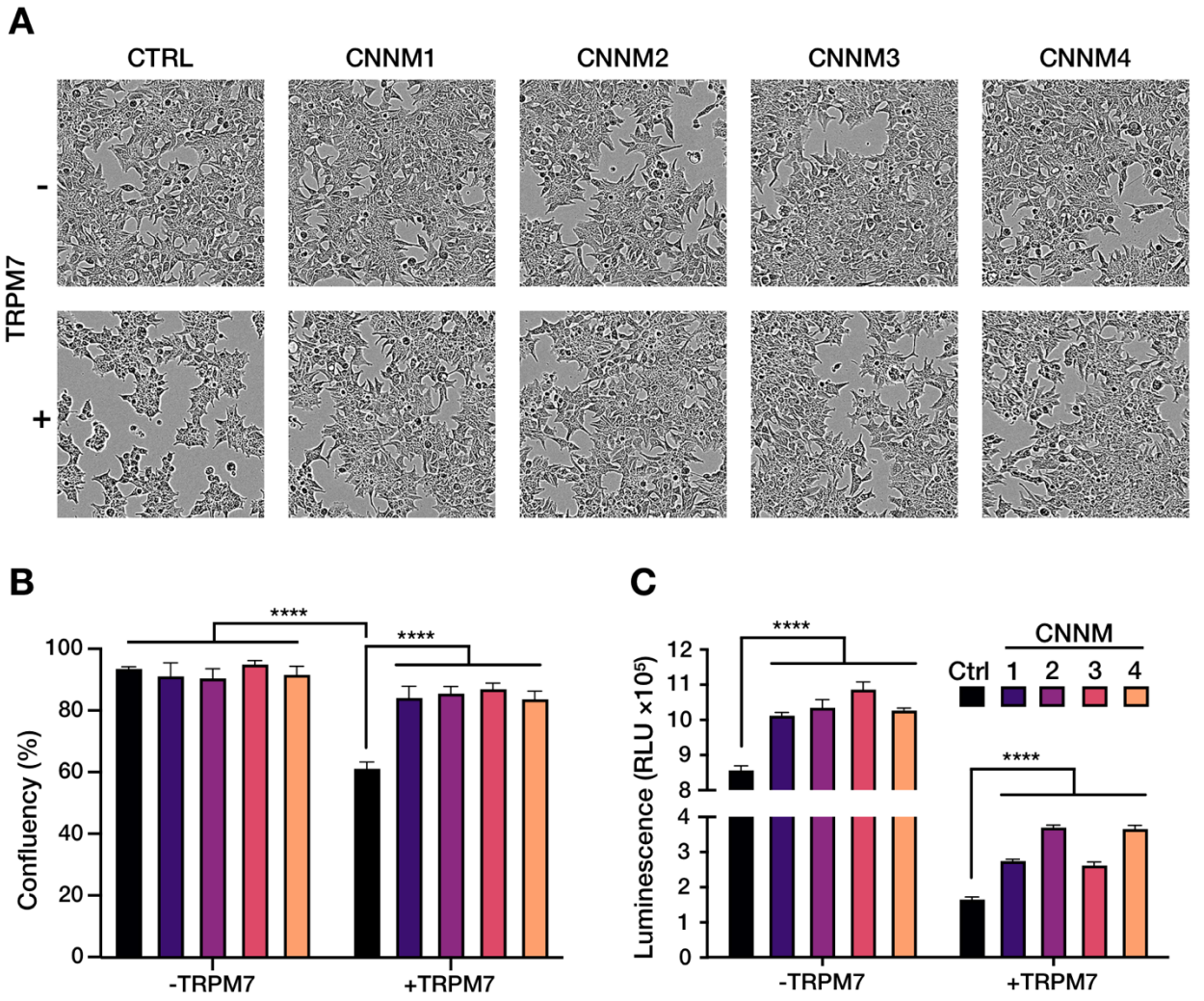

Figure 3.3: CNNMs inhibit TRPM7

A. HEK293 cells with doxycycline inducible expression of TRPM7 were transfected with control (GFP) plasmid or CNNM1-4 expressing plasmids for 24H, then TRPM7 was induced, and cell confluency was measured over time. The pictures show cell morphology at 38H post TRPM7 induction. B. Confluency of the cells from A. Overexpression of either of the four CNNMs counteracted the effect of TRPM7 on confluency C. HEK293 cells with doxycycline inducible expression of TRPM7 and stable expression of the magnesium luciferase reporter were transfected as in A. Luminescence was recorded 24H after induction of TRPM7. Two-way ANOVA followed by Tukey's multiple comparison was used for statistical comparisons.

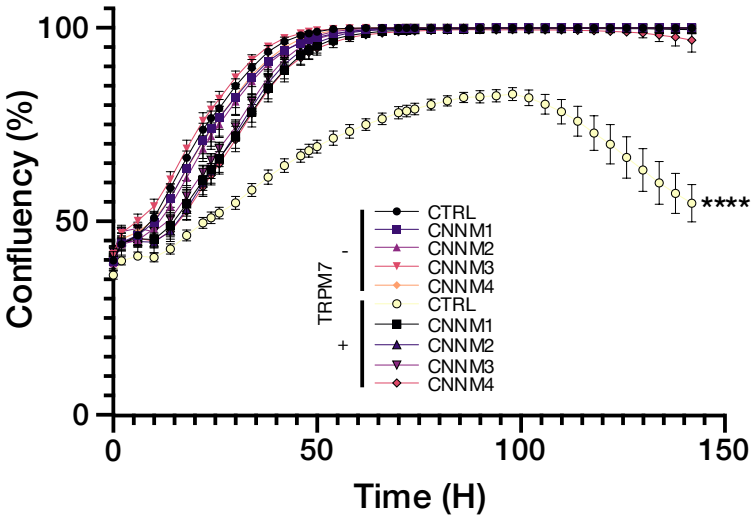

Supplementary Figure 3.3: CNNMs rescue TRPM7-induced growth phenotype
Confluency of the cells in a 148H experiment associated with Fig. 3.3A, showing that cells with TRPM7 and CTRL overexpression fail to reach maximum confluency. This phenotype is rescued by overexpression of CNNMs.

PRL-2 affects CNNM3 localization

We have previously shown that PRLs interact with CNNMs and affect magnesium transport, where knockdown of PRL-2 decreased magnesium uptake [192]. Additionally, magnesium and TRPM7 expression influence PRL-1/2 translation itself [18]. To understand the role of PRLs in the inhibitory effects of CNNMs on TRPM7 activity, we performed co-localization studies of PRL-2 and CNNM3. We saw that wild-type CNNM3 was localized at the plasma membrane and cytoplasm (Fig. 3.4, row 1). However, overexpression of PRL-2 resulted in a change in CNNM3 localization since it was no longer found at the plasma membrane and was concentrated in the cytoplasm, whereas PRL-2 itself was still found at the plasma membrane (Fig. 3.4, row 2). The localization pattern of CNNM3-D426A mutant, which cannot interact with PRLs [182], was similar to that of wild-type CNNM3 (Fig. 3.4, row 3). Importantly, both wild-type and mutant

CNNM3 interacted with ARL15 and TRPM7 (Fig. 3.1C). As expected, overexpression of PRL-2 had no effect on the localization of CNNM3-D426A mutant (Fig. 3.4, row 4).

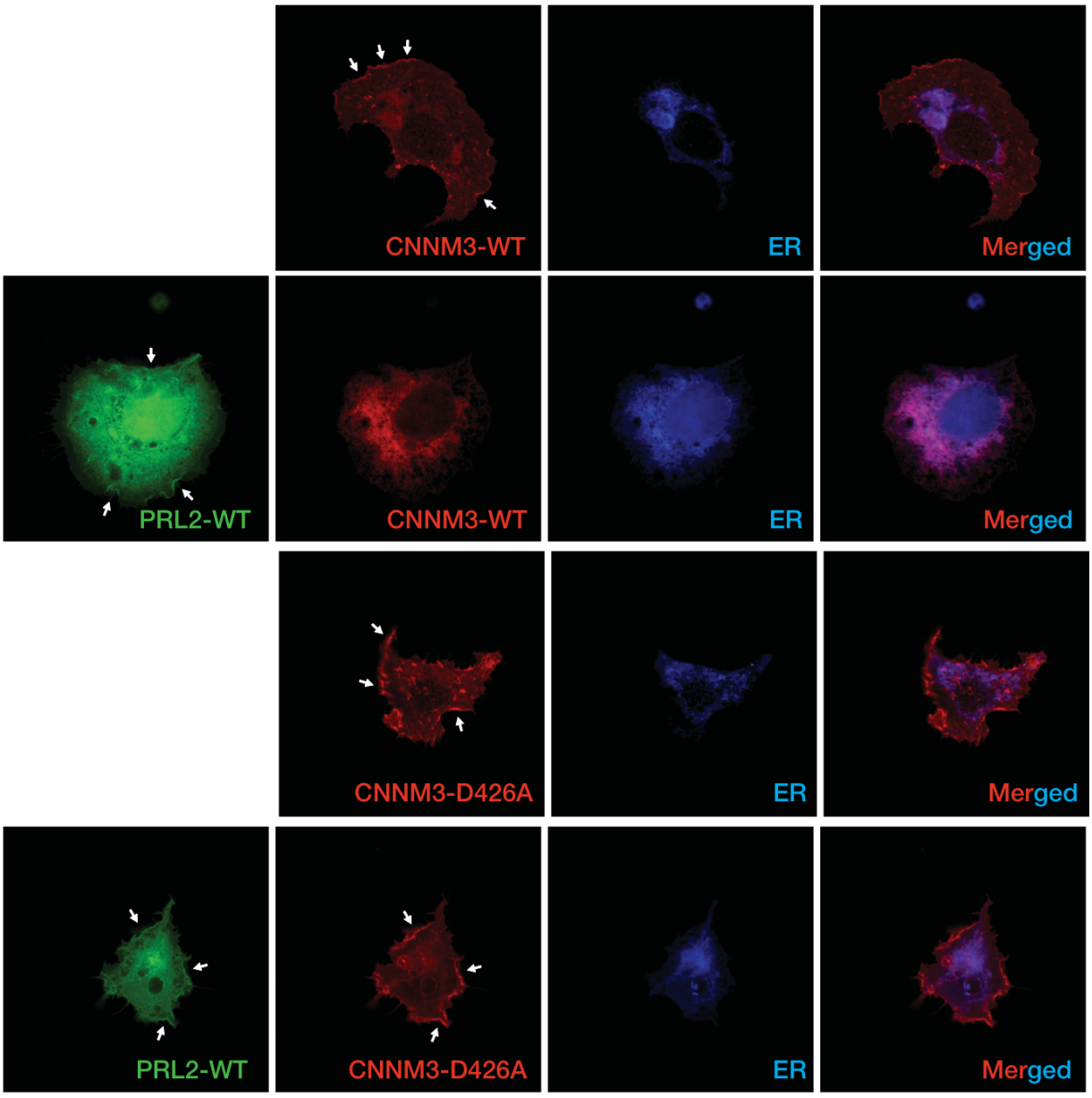

Figure 3.4: PRL-2 affects CNNM3 localization
moxGFP-PRL-2, CNNM3-mCherry (WT and D426A mutant) and pmTurquoise2-ER were overexpressed in HEK293 cells. Confocal microscopy images indicate that WT CNNM3 is relocalized from the plasma membrane to the cytoplasm upon PRL-2 overexpression. White arrows indicate plasma membrane localization.

Signaling interplay between CNNM3, PRL-1/2 and TRPM7

To further understand the effect of CNNMs on TRPM7 inhibition, we looked at how CNNM3 affects TRPM7-mediated downstream signaling. We have previously shown that expression of PRL-1/2 is sensitive to intracellular magnesium levels [18]. Overexpression of TRPM7 increases $[Mg^{2+}]_i$ and results in downregulation of PRL-1/2 [18]. On the other hand, overexpression of CNNM3 increases PRL-1/2 levels [182]. Here, we show that CNNM3 counteracts the TRPM7-induced downregulation of PRL-1/2 (Fig. 3.4A), presumably through inhibition of TRPM7-mediated magnesium uptake. TRPM7 has been linked with mTORC1 activation in lymphocytes, where knockout of TRPM7 resulted in delayed mTORC1 signaling observed by phosphorylation of S6K and 4E-BP1 [315]. Upon overexpression of TRPM7, we observe that S6 is hyperphosphorylated at S6K/RSK-dependent serines 234/236 and at S6K-dependent serines 240/244 [330] (Fig. 3.4A). Overexpression of CNNM3 alone does not affect S6 phosphorylation, but it does counteract the hyperphosphorylation induced by TRPM7 when both proteins are overexpressed. ERK-1/2 follows a pattern of phosphorylation similar to S6.

CNNM3 and TRPM7 have an antagonistic effect on S6 phosphorylation, PRL-1/2 expression (Fig 3.4A) and intracellular magnesium (Fig 3.3C). PRL-1/2 affect magnesium uptake [192, 194] and respond to $[Mg^{2+}]_I$ [18]. We sought to understand the effect of PRL-1/2 on TRPM7 signaling by modulating their expression and observing the effect on S6 phosphorylation. When both PRL-1 and PRL-2 were knocked down using siRNA, the effect of TRPM7 on S6 phosphorylation was dampened (Fig. 3.5B). When PRL-2 was overexpressed, the opposite effect was observed, with increased S6 phosphorylation compared to endogenous PRL expression (Fig. 3.5B). This could be understood in the

light of inhibition of TRPM7 by CNNM3 as we have shown above. Overexpression of PRL-2 changes localization of CNNM3 from plasma membrane to the cytoplasm (Fig. 3.4), thus preventing alleviating the inhibition of TRPM7 at the cell surface. Knockdown of PRL-1/2 would have the opposite effect and would enhance the inhibition of TRPM7 by CNNM3 at the cell surface.

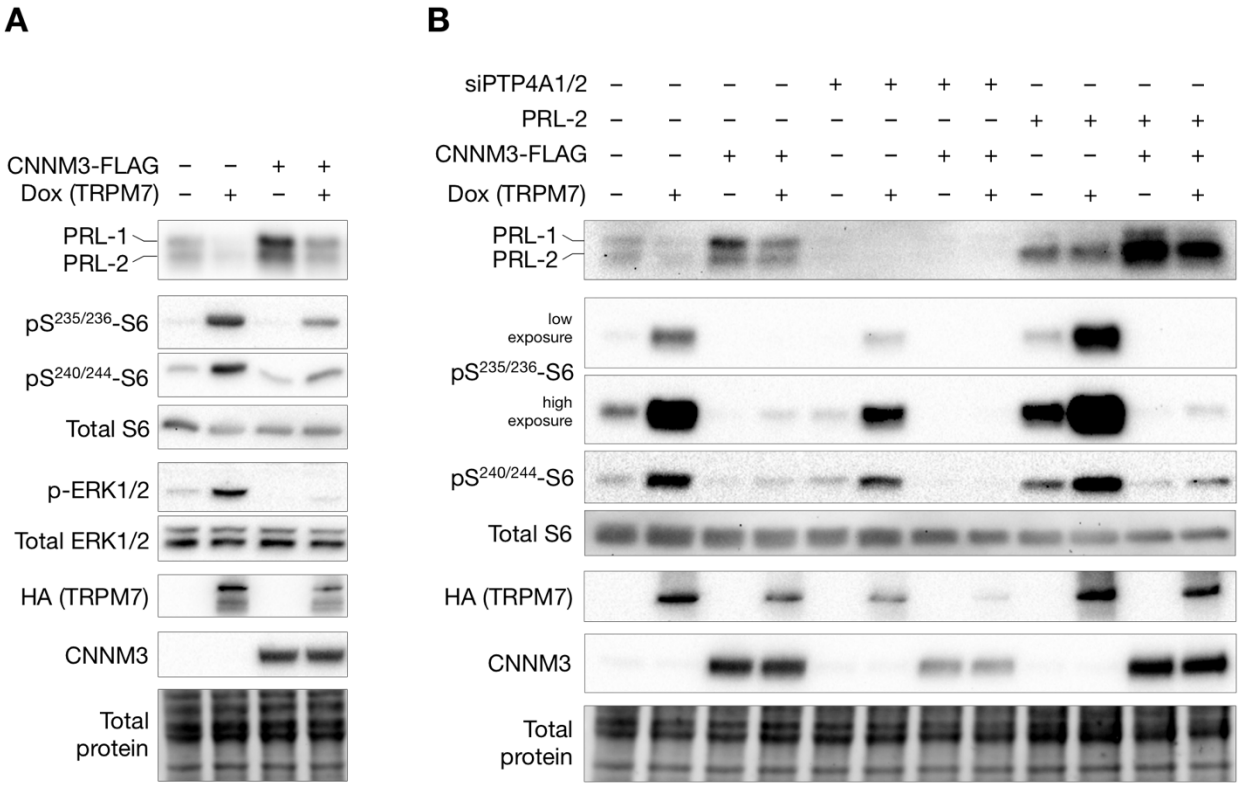

Figure 3.5: Interplay between CNNM3, PRL-1/2 and TRPM7
A. HEK293 cells with doxycycline inducible expression of TRPM7 were transfected with control (GFP) or CNNM3 plasmid for 24H, TRPM7 was then induced for 24H. B. Same as A except cells were first transfected with control or PTP4A1/2-targetting siRNA for 24H, then with control (GFP), CNNM3 or PRL-2 plasmid for 24H and finally TRPM7 was then induced for 24H.

Magnesium regulates interactions between TRPM7 and the CNNM3/PRL-2/ARL15 complex

The activity of TRPM7 is regulated by intracellular magnesium [197, 322], but this mechanism of action is not well understood. To better understand how magnesium itself affects TRPM7, we performed co-immunoprecipitation experiments in low and physiological magnesium concentrations. When TRPM7 was immunoprecipitated, less CNNM3 was observed to interact with it in low magnesium conditions compared to physiologically relevant levels (Fig. 3.6A). Similarly, when IP of CNNM3 was performed, its interaction with TRPM7 was reduced in low Mg^{2+} (Fig. 3.6B). Considering that CNNM3 plays an inhibitory role in magnesium uptake, decreasing the interaction between TRPM7 and CNNM3 in low Mg^{2+} conditions would allow increased magnesium influx. PRL-2 expression is increased under low magnesium conditions [18], it interacts with CNNM3 and alters its localization from cell surface to the cytoplasm, thus preventing TRPM7 inhibition. We observe that in a low $[Mg^{2+}]_e$ condition, when CNNM3 is immunoprecipitated, its interaction with PRL-1/2 is increased, while less TRPM7 was found to interact with it (Fig. 3.6C). To understand the role of PRL-1/2 in this interaction, we used siRNAs targeting both phosphatases and found that when CNNM3 is immunoprecipitated, depletion of PRLs increases the interaction between CNNM3 and TRPM7 in low magnesium condition (Fig. 3.6D). ARL15 which strengthened the interaction between CNNM3 and TRPM7 interacted less with CNNM3 under low $[Mg^{2+}]_e$ condition (Fig. 6E). Thus, a dynamic interplay emerges where the interaction between CNNM3 and TRPM7 is regulated by PRL-1/2 and ARL15 in response to changes in magnesium concentrations.

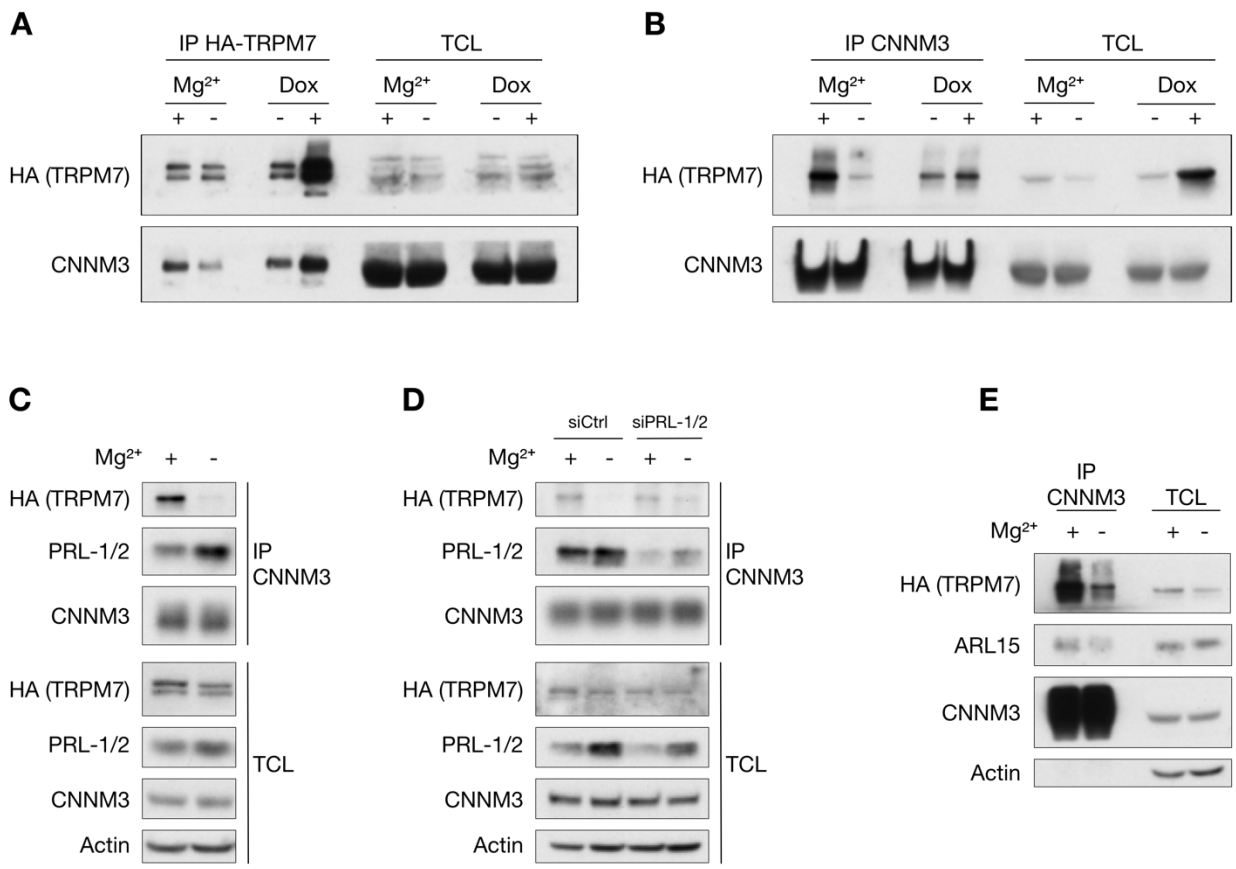

Figure 3.6: Magnesium regulates the interaction between TRPM7 and the CNNM3/PRL-2/ARL15 complex

A. HA-TRPM7 was immunoprecipitated from HEK293 cells with doxycycline inducible TRPM7 expression grown with and without magnesium and Western blotting was performed. B. Same as A, except endogenous CNNM3 was immunoprecipitated. C. Same as B with additional observation of endogenous PRL-1/2. D. Control or PRL-1/2 targeting siRNAs were transfected into HEK293 cells with doxycycline inducible TRPM7 expression grown with and without magnesium and immunoprecipitation of CNNM3 was done followed by Western blotting.

Discussion

In this study we have identified several novel interactions that regulate magnesium homeostasis and the activity of TRPM7 (summarized in Fig. 3.7). First, we observed that the four members of the CNNM family of magnesium modulators interact with the TRPM7 magnesium channel. Second, that interaction is significantly strengthened in the presence of the small GTPase ARL15, which we have recently identified as an interacting partner of CNNMs that affects magnesium flux [327]. Third, CNNMs appear to have an inhibitory effect on the activity of TRPM7 as a magnesium channel, on its ability to affect cytoskeletal rearrangements and on its downstream signaling. Finally, magnesium itself regulates the interaction between members of the CNNM/PRL-1/2/ARL15 complex and TRPM7. Under normal magnesium conditions, CNNMs interact with TRPM7 at the plasma membrane, where ARL15 enhanced the interaction to inhibit magnesium uptake since cells contain enough magnesium. Once extracellular magnesium concentration decreases, intracellular concentration follows. To alleviate this reduction in magnesium the cells respond in following ways: expression of PRL-1/2 goes up [18], their interaction with CNNMs increases, that changes their localization to endosomes, which have been previously shown to harbor CNNMs [331] and PRLs [104], the interaction between ARL15 and CNNMs decreases. All these steps result in derepression of TRPM7, which increases magnesium influx.

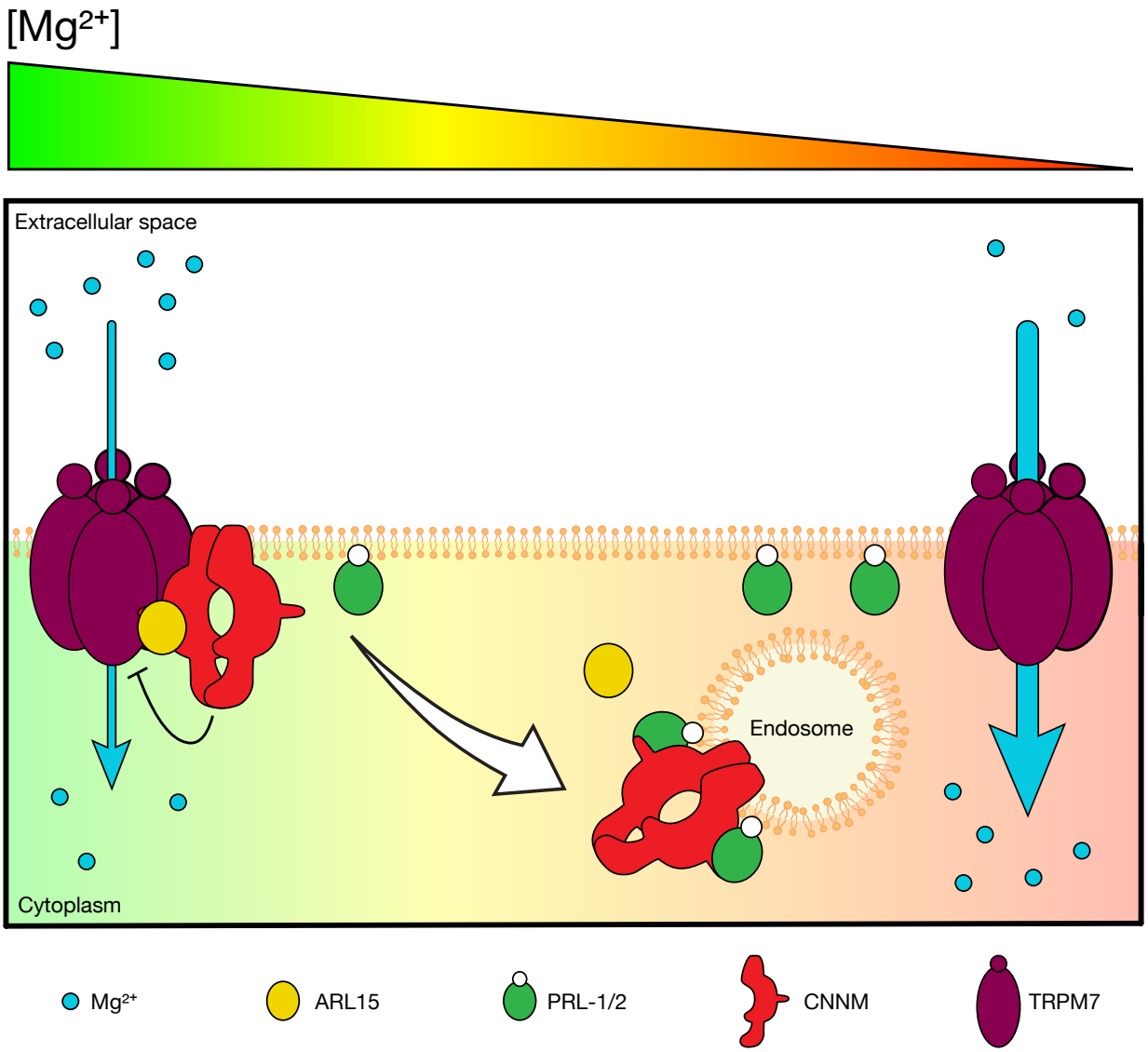

Figure 3.7: Summary of the interactions between CNNMs/PRL-1/2/ARL15 and TRPM7 and their effect on magnesium flux

Ubiquitously expressed TRPM7, as well as its homologue expressed mostly in the kidney and intestine, TRPM6, are well studied magnesium channels that regulate magnesium homeostasis. TRPM6 and TRPM7 are in turn regulated by intracellular magnesium and Mg•ATP levels [197, 302, 332–334]. It was suggested that the kinase domain of TRPM7 is involved in the regulation of the channel's activity by intracellular

free magnesium [334]. However, mice expressing kinase-dead TRPM7 do not show changes in homeostasis of magnesium and other divalent cations [198], nor was the sensitivity of the channel to $[Mg^{2+}]_i$ affected by autophosphorylation or a kinase-dead mutant [217]. Therefore, the precise mechanism of the channel's regulation by intracellular magnesium is still not well understood. We propose here that CNNMs act as inhibitors of TRPM7 function, and that the interaction between CNNMs and TRPM7 is regulated by PRL-1/2 and ARL15 and is dependent on magnesium concentration. This dynamic change in interactions between CNNMs, PRL-1/2 and ARL15 in response to intracellular magnesium levels allows to regulate the activity of TRPM7.

PRLs have been demonstrated to be involved in the progression of multiple cancer types (reviewed in [102]). We were first to show that PRLs interact with CNNMs and that this interaction is involved in magnesium transport [192]. The importance of this interaction in cancer development was also demonstrated [182, 192, 194], which highlighted the potential role of magnesium in cancer growth. Likewise, TRPM7 is overexpressed in multiple cancers and is involved in their progression, which is dependent on magnesium in multiple cases (reviewed in [335] and [336]). In addition, TRPM7 is involved in the regulation of cellular morphology [319, 324] and cytoskeletal dynamics, which alters the proliferation and migration of cancer cells [335, 337, 338]. A recent paper demonstrated that TRPM7 regulates intravasation and formation of metastatic lesions by sensing shear stress [326]. Thus, it would be important to better understand the effect of CNNMs, PRL-1/2 and ARL15 on cancer progression as a consequence of TRPM7 regulation.

Mutations in CNNM2 and TRPM6 result in hypomagnesemia (OMIM: 613882, 616418, 602014) due to dysfunction in renal magnesium reabsorption and intestinal absorption. Regulation of magnesium homeostasis occurs in the intestine and kidneys and TRPM6 is expressed in both organs [339], while CNNM2 is expressed in the kidneys, and more specifically both proteins are expressed in the distal convoluted tubule (DCT) of the nephron [3]. ARL15 is also localized in the DCT [327] and PRL-2 was shown to be expressed in the kidney [340]. A recent paper linked CNNM4 with the development of non-alcoholic steatohepatitis due to magnesium dysregulation [184]. Inhibition of TRPM7 with 2-APB resulted in decreased magnesium import and lipid accumulation which was reversed by reducing CNNM4 levels [184], perhaps due to reversal of its effect on TRPM7. Better understanding and targeting of the dynamic interactions between CNNMs, PRLs, ARL15 and TRPM6/7 could help alleviate multiple human diseases related to dysregulation of magnesium homeostasis.

Materials and methods

DNA constructs

The following constructs were previously described: human FLAG-tagged pDEST26-CNNM1-4, pcDNA3.1-CNNM3-mCherry and FLAG-tagged ARL15 [327], V5-tagged wild-type CNNM3 and D426A mutant [182]. V5-tagged ARL15 was obtained from the McGill Platform for Cellular Perturbation (MPCP) cloned into pLX317 plasmid. pmTurquoise2-ER (Addgene #36204) [271] and moxGFP (Addgene #68070) [341] were obtained from Addgene. PRL-2 was cloned into moxGFP plasmid using SLiCE cloning [270].

Magnesium reporter construct was created by cloning PRL-2 5′ UTR upstream of firefly luciferase was as previously described [18]. Firefly luciferase with destabilizing sequence was amplified from CMV-LUC2CP/ARE plasmid (Addgene #62857) [342]. PRL-2 5′ UTR firefly luciferase was cloned into pZDonor-AAVS1-poromycin vector using SLiCE cloning. sgRNAs targeting the AAVS1 locus were cloned into pSpCas9(BB)-2A-GFP (PX458) (Addgene #48138) [343]. The sequences forward and reverse sgRNA oligos are below:

Forward: 5′-CACCGGGGCCACTAGGGACAGGAT-3′

Reverse: 5′-AAACATCCTGTCCCTAGTGGCCCC-3′

Cloned plasmids were transformed into chemically competent DH5α *Escherichia coli* bacteria by heat shock, plated on agar plates containing the appropriate antibiotic and grown overnight at 37 °C. Single colonies were selected, expanded in liquid media and plasmids were extracted using a Presto Mini Plasmid kit (Geneaid #PDH100).

Degradation of ARL15

1.5 µg of each pDEST26-ARL15-FLAG and pLenti6-CNNM3-V5 or pcDNA3.1-GFP as control were transfected into HEK293 cells using Lipofectamine 2000 (Invitrogen #11668019). Cells were treated 5 µM of MG132 proteasome inhibitor (Cayman Chemical #10012628) or DMSO overnight. Cells were lysed and Western blotting was performed.

Site-directed mutagenesis

To introduce the T46N mutation into ARL15, pDONR221-ARL15 without a stop codon was amplified using a single primer PCR using KAPA HiFi polymerase (Roche #07958846001). The following primer was used: 5′-ACAGGTTCTGGCAAA

aacAGTCTGTTGTCCAAAC-3′, with the codon introducing the mutation indicated in lower case. After PCR, the original plasmid was digested with *DpnI* for 2H at 37 °C, followed by the transformation of chemically competent DH5α.

Cell culture and transfection

HEK293 and HeLa cells were grown in high glucose DMEM (Fisher Scientific, #SH30081.01) supplemented with 2 mM GlutaMAX (Life Technologies, #35050061), 1% gentamicin (Wisent Bioproducts, #450-135-XL) and 10% FBS Life Technologies, #12483020) at 37 °C in a humidified incubator with 5% (v/v) CO_2. Transfection was performed with Lipofectamine 2000 (Invitrogen #11668019) for protein overexpression at 1:2 (μg DNA:μL Lipofectamine) or Lipofectamine RNAiMAX (Fisher Scientific #13-778-150) for siRNA at 4:1 (nM siRNA:μl Lipofectamine). Dharmacon siRNA were purchased from Horizon for knockdown of PRL-1 (L-006333-00-0005), PRL-2 (M-009078-01-0005) and non-targeting control (D-001810-10-05). Nucleotides and Lipofectamine were mixed in 1X OptiMEM and incubated at room temperature for 25 min (Life Technologies #31985070).

HEK293 cells with doxycycline inducible N-terminal HA-tagged TRPM7 expression [333] were a gift from Drs. Carsten Schmitz and Anne-Laure Perraud (Integrated Department of Immunology, National Jewish Health and University of Colorado) and were grown and transfected in the same manner as HEK293 cells. TRPM7 expression was induced with 1 μg/mL doxycycline (Sigma-Aldrich, #D3072).

For experiments with cation exclusion, custom high glucose DMEM without magnesium, calcium, phenol red and L-glutamine was used (Wisent Bioproducts, #319-129-CL). It was supplemented with $MgSO_4$, $CaCl_2$ and $ZnCl_2$ as needed.

Generation of stable cell lines

pZDonor-AAVS1-UTR-fLuc and lentiCRISPR v2 (Addgene #52961) containing sgRNA targeting the AAVS1 locus were transfected in HEK293 and HeLa cells us Lipofectamine 2000. Puromycin antibiotic selection was performed followed by single clone expansion. Luciferase activity assays were performed to identify the most active clones. Integration into the AAVS1 locus was confirmed by PCR.

Proliferation analysis

Reverse transfection was used with 50 ng of DNA and 0.1 µL of Lipofectamine 2000 in 10 µL of OptiMEM per well in a 96-well plate. 5000-20000 HEK293-TRPM7 cells in 90 µL of DMEM were added to each well. 12 hours later, doxycycline was added to the well to induce TRPM7 expression. The plate was then placed inside IncuCyte ZOOM system with a 4X objective. Photos of wells were taken every 2 hours for 6 days and then analyzed in the IncuCyte software to measure cell confluence.

Luciferase activity assay

Luciferase assays were performed as described previously [18]. Briefly, for firefly and Renilla luciferase lytic assay Dual-Glo luciferase assay system (Promega #2920) was used. For live luciferase measurements, original media was aspirated and replaced with MFM media with 100 µM D-luciferin, the plate was sealed with clear adhesive tape and

the readings were collected every 10 minutes for 25-48H. SpectraMax i3 (Molecular Devices) plate reader was used for luminescence measurements.

Fluorescence imaging

HEK293 cells were transfected with moxGFP-PRL-2 with either pcDNA3.1-CNNM3-mCherry WT or D426A mutant, and pmTurquoise2-ER. The cells were transferred into a chamber slide (ibidi #80841). 4% PFA was used to fix cells for 10 min, washed with PBS and mounted with Mowiol mounting medium (Sigma-Aldrich #81381). Zeiss LSM880 confocal microscope with Airyscan processing was used to take pictures.

Western blot

Western blotting was done as described previously [327]. The following antibodies were used: PRL-1/2 (Sigma-Aldrich #05-1583), CNNM3 (Proteintech #13976-1-AP), HA (Cell Signaling #3724), FLAG (Cell Signaling #14793), pS235/236 S6 (Cell Signaling #4858), pS240/244 S6 (Cell Signaling #2215), S6 (Cell Signaling #2317), pERK1/2 (Cell Signaling #4376S), ERK1/2 (Cell Signaling #4695), Actin (Sigma-Aldrich #A3853), V5 (Life Technologies #R96025)

Co-Immunoprecipitation

HEK293 cells were transfected for 24h, TRPM7 expression was induced for another 24h and the cells were lysed in a mild IP lysis buffer containing 150 mM NaCl, 20 mM Tris, 1% Triton X-100 at pH 7.5. BCA assay was performed to measure protein concentrations (Fisher Scientific #PI23225). Anti-FLAG (Sigma-Aldrich #M8823) and anti-HA (Fisher Scientific #88836) magnetic beads were used to immunoprecipitate tagged proteins. The

beads were washed and pre-blocked with 5% BSA for 1h on a rotator at 4°C. Protein lysates were pre-cleared with washed plain agarose beads (Agarose Bead Technologies #A-1040S-500) for 1h on a rotator at 4°C. The lysates and beads were mixed and incubated on a rotator for 2H at 4°C. After incubation, lysates were aspirated away from beads on a magnetic rack and the beads were washed 5 times with the IP lysis buffer. 2X Laemmli buffer with 2-mercaptoethanol (Life Technologies #21985023) was added to the beads after washing and incubated at 100°C for 5 min. The buffer was cooled down, separated from the beads, and subjected to Western blotting.

Statistical analysis

GraphPad Prism 9 was used for statistical analysis. T-test, one-way or two-way ANOVA followed by Tukey multiple comparison test was used depending on the experimental design. At least 3 replicates were used for analysis.

Acknowledgements

The authors are thankful to Mehdi Amiri for his deep insight on the regulation of S6 phosphorylation and for providing research materials.

Chapter 4

Discussion and conclusion

Magnesium is vital for the proper functioning of our cells and for our health [3]. As a cofactor magnesium is involved in hundreds of enzymatic reactions and numerous metabolic pathways. Due to poor diet and type 2 diabetes, among other issues, rates of hypomagnesemia are high in many countries [41, 81, 344]. Multiple genetic mutations result in hypomagnesemia and carry an associated health burden [345, 346]. Additionally, progression of multiple cancers has been linked with genes involved in the regulation of magnesium transport [102, 182, 192, 316, 322].

Our laboratory was the first to discover the involvement of PRLs in magnesium regulation through their interactions with CNNMs [192]. Since then multiple studies have expanded on the effect of this interaction on magnesium flux and cancer progression [108, 109, 182, 194]. As an additional layer of regulation, Hardy *et al.* showed in 2019 that PRL-1/2 expression is regulated by intracellular magnesium through ribosome stalling at PTP4A1/2 uORFs. Given the importance of magnesium in a large number of metabolic pathways, it is not surprising that multiple proteins are involved in a complex regulatory network that tightly regulates magnesium flux.

This thesis explores the role of ARL15 in magnesium homeostasis through post-translational modification of the CNNM family of magnesium modulators. It also uncovers a dynamic complex composed of CNNMs and either PRL-1/2 or ARL15 and its function in the regulation of the canonical magnesium channel TRPM7.

A poorly studied small GTPase ARL15 was previously linked with renal magnesium handling and regulation of TRPM6 magnesium flux [96]. However, the mechanism by which ARL15 affects magnesium uptake or regulates TRPM6 was not uncovered in that study.

To understand the role of ARL15 in magnesium regulation, we performed BioID experiments and identified multiple potential interacting partners, many of which grouped into gene ontology categories related to metal ion transport. The magnesium ion homeostasis category containing the CNNMs was significantly enriched. We have chosen renal cancer cells lines to carry out our studies for two reasons: kidneys are the organs involved in magnesium reabsorption and ARL15 was significantly downregulated in TCGA renal cancer datasets compared to normal tissue. We confirmed the interaction of ARL15 with CNNMs by co-immunoprecipitation experiments. Modulation of ARL15 expression resulted in the change in post-translational N-glycosylation forms of CNNM3. The interaction between CNNM3 and ARL15 was computationally modelled, and it indicated that while PRLs and ARL15 interact with different domains of CNNMs, there is a potential for competition. Changes in extracellular magnesium concentration had an effect on N-glycosylation as well. Overexpression of ARL15 resulted in decrease in magnesium uptake and ATP production, while its knockout significantly increased magnesium uptake. The activity of ARL15 reinforces the link between N-glycosylation and magnesium transport. Several proteins involved in post-translation modifications of proteins, such as N-glycosylation (MAGT1 and MMGT1) and S-palmitoylation (HIP14 and HIP14L), were misclassified as magnesium transporters in the past [241, 248, 253]. This was probably due to the fact that they affect the activity and localization of actual magnesium transporters or transport modulators, similar to how ARL15 affects CNNMs. A recent paper showed that ARL15 is S-palmitoylated [94] and according to our BioID data ARL15 interacts with ZDHHC5, while BioGRID [347] shows an interaction with ZDHHC11. These palmitoyltransferases belong to the same family as HIP14 (official gene

name: ZDHHC17) and HIP14L (ZDHHC13). This potential link between S-palmitoylation and magnesium flux could be an interesting avenue to explore in the future.

We have shown that ARL15 influences magnesium homeostasis, but the mechanism of action was not completely understood. One of the interacting partners identified in the BioID study was TRPM7 – the canonical magnesium transporter. To further explore the link between ARL15, CNNMs and TRPM7 we performed co-immunoprecipitation experiments with these proteins. We observed that TRPM7 interacted with CNNMs, and that this interaction was highly strengthened in the presence of ARL15. To assess changes in magnesium flux we have developed a genetically encoded magnesium sensor based on the 5′ UTR of PTP4A2 [18]. We have shown that it specifically responds to changes in magnesium levels but not to other cations. Using this sensor and other methods, we were able to show that CNNMs play an inhibitory role on multiple aspects of TRPM7 activity: magnesium influx, cell morphology and downstream signaling. Our lab has previously shown that PRL-1/2 increase magnesium influx through their interactions with CNNMs [192]. In this paper we further uncovered this mechanism: PRL-2 interaction with CNNM3 modulates its localization from the plasma membrane to the cytoplasm and reduces CNNMs' interaction with TRPM7. This in turn disinhibits TRPM7 and increases magnesium influx. Furthermore, upregulation of PRL-2 expression increases TRPM7 downstream signaling, while knockdown of PRL-1/2 dampens it. It has been previously shown that high intracellular magnesium and Mg•ATP inhibit the channel activity of TRPM7 [197, 322]. To better understand the regulation of TRPM7 by Mg^{2+} we modulated extracellular magnesium levels and performed co-immunoprecipitation experiments. Lack of

magnesium decreased the interaction between TRPM7 and CNNM3 when either protein was immunoprecipitated, while increasing the interaction between PRL-1/2 and CNNM3. Meanwhile, ARL15 interaction with CNNM3 decreased. While TRPM7 is directly regulated by intracellular magnesium [348], these changes in its interactions with CNNMs/ARL15/PRL-1/2 in response to Mg^{2+} levels could partly explain how TRPM7 is regulated by magnesium. Low magnesium decreases TRPM7 inhibitory ARL15•CNNM3 interaction and increases activating PRL-1/2•CNNM3 interaction. This could also explain how ARL15 decreases magnesium uptake and PRL-1/2 increase it – not by direct regulation of Mg^{2+} flux through CNNMs but via modulation of TRPM7 activity.

We have shown that ARL15 and magnesium affect N-glycosylation of CNNM3. We then demonstrated that ARL15 strengthens the interaction between CNNM3 and TRPM7. What remains to be seen is whether changes in CNNM3 N-glycosylation affect its interaction with TRPM7. Additionally, TRPM7 has been shown to be N-glycosylated [202, 349] and yet it is unknown whether magnesium or ARL15 can affect TRPM7 glycoforms and what roles, if any, these glycoforms might play.

Prior to this work, ARL15 was identified as having a role in adiponectin secretion [92] and renal magnesium handling [96]. We have found a link between ARL15 and N-glycosylation. Whereas in **Chapter 2** we show that general N-glycosylation is not affected by ARL15, these studies were done in cells with long-term modulation of ARL15 expression. The acute effect of ARL15 was not studied and could be important in understanding its activity on post-translational modification of proteins. A large proportion of targets identified in the ARL15 BioID are transmembrane proteins which are involved in the transport of small molecules and cations. Other members of the ARF

and ARL family of proteins are involved in trafficking [290, 292]. It is possible that ARL15 exerts its effects through modulation of trafficking of its interacting partners through the ER and Golgi. The effect of ARL15 on the activity of these proteins and the molecules they transport should be elucidated in future studies.

Expression of CNNMs and PRLs has been linked with progression of various cancers, [102, 109, 194], specifically breast cancer [182, 192]. The expression of PRLs is upregulated in multiple malignancies and this was shown to increase their growth and metastatic rates [102, 117, 182]. More and more evidence is accumulating that this effect is not independent from their involvement in magnesium transport though the interaction with CNNMs [109, 182, 192]. Our data indicates that PRLs oppose the inhibitory effect of CNNMs on TRPM7. This would increase magnesium uptake and ATP production and would allow to satisfy cancer cells' hunger for energy required during growth and metastasis. On the other hand, ARL15 increases the inhibitory effect of CNNMs on TRPM7 and decreases magnesium uptake, which makes sense given that ARL15 expression is significantly reduced in colon, breast, lung and two subtypes of kidney cancers (TCGA Research Network: https://www.cancer.gov/tcga). This decrease in ARL15 expression would allow for increased magnesium uptake and proliferation. In addition, N-glycosylation is modulated in many cancers [231-233] and the effect of ARL15 on cancer N-glycome should be further explored. TRPM7 has been linked with breast cancer metastasis [337] and its expression regulates cell shear sensitivity and intravasation [326]. Since we have shown that TRPM7 is regulated by CNNMs, PRLs and ARL15, their involvement in the progression of breast and other cancers and metastasis formation should be examined.

During the writing of this thesis, two papers [97, 350] were published that uncovered the interaction between TRPM7 and the members of the CNNM family. The paper by Kollewe *et al.* showed that TRPM7 interacts with CNNMs, ARL15 and PRL-1/3 and that ARL15 but not CNNMs, inhibits TRPM7 activity. The paper by Bai *et al.* confirmed the interactions between TRPM7, CNNMs, ARL15 and PRL-1. However, they showed that CNNMs have a dual function: they activate, rather than inhibit, TRPM7 divalent cation influx activity while themselves directly increase Mg^{2+} efflux activity. They also showed that overexpression of ALR15 decreases TRPM7-mediated Zn^{2+} influx, while its knockdown had an opposite effect. Additionally, they demonstrate that PRL-2 stimulates TRPM7 activity, even in the absence of CNNM3 and CNNM4. The results of these two papers are difficult to reconcile: they disagree on the effects of CNNMs on TRPM7 activity while agreeing on the effect of ARL15. Our data also does not correspond perfectly with these publications: we show that CNNMs and ARL15 inhibit TRPM7, while PRL-1/2 indirectly activate it. These disagreements reinforce the complexity of studying magnesium regulation. While two recent papers on the structure of archaeal and bacterial homologues of CNNMs [154, 155] point towards their ability to transport magnesium, they do not invalidate the possibility of mammalian CNNMs to act as Mg^{2+} sensors. CNNM3 lacks the residues necessary for magnesium coordination that were found in prokaryotic homologues and yet it is able to regulate magnesium flux through TRPM7. As suggested by Bai *et al.*, CNNMs could act as both TRPM7 regulators and genuine magnesium transporters. The tools available to study intracellular magnesium concentration, such as magnesium indicators, are not perfect and we hope

that the genetically encoded sensor that we developed can further advance the study of magnesium regulation.

In conclusion, first, we have uncovered the role of a poorly described small GTPase ARL15 in the regulation of magnesium homeostasis through post-translational modification of CNNM magnesium transport mediators. Second, we described a novel layer of magnesium homeostasis regulation by dynamic interactions between the magnesium channel TRPM7 and CNNM magnesium mediators, fine-tuned by ARL15 and PRL-1/2, in response to changes in magnesium levels. As such, we have uncovered numerous interactions and novel regulatory mechanisms that modulate magnesium homeostasis.

References

1. Sreedhara A, Cowan JA (2002) Structural and catalytic roles for divalent magnesium in nucleic acid biochemistry. BioMetals 15:211–223. https://doi.org/10.1023/A:1016070614042

2. Wishart DS, Feunang YD, Marcu A, et al (2018) HMDB 4.0: the human metabolome database for 2018. Nucleic Acids Research 46:D608–D617. https://doi.org/10.1093/nar/gkx1089

3. de Baaij JHF, Hoenderop JGJ, Bindels RJM (2015) Magnesium in Man: Implications for Health and Disease. Physiological Reviews 95:1–46. https://doi.org/10.1152/physrev.00012.2014

4. Briggs KT, Giulian GG, Li G, et al (2016) A Molecular Model for Lithium's Bioactive Form. Biophysical Journal 111:294–300. https://doi.org/10.1016/j.bpj.2016.06.015

5. Buelens FP, Leonov H, de Groot BL, Grubmüller H (2021) ATP–Magnesium Coordination: Protein Structure-Based Force Field Evaluation and Corrections. J Chem Theory Comput 17:1922–1930. https://doi.org/10.1021/acs.jctc.0c01205

6. Rudack T, Xia F, Schlitter J, et al (2012) The Role of Magnesium for Geometry and Charge in GTP Hydrolysis, Revealed by Quantum Mechanics/Molecular Mechanics Simulations. Biophysical Journal 103:293–302. https://doi.org/10.1016/j.bpj.2012.06.015

7. Williams NH (2000) Magnesium Ion Catalyzed ATP Hydrolysis. J Am Chem Soc 122:12023–12024. https://doi.org/10.1021/ja0013374

8. Lu Q, Nassar N, Wang J (2011) A mechanism of catalyzed GTP hydrolysis by Ras protein through magnesium ion. Chemical Physics Letters 516:233–238. https://doi.org/10.1016/j.cplett.2011.09.071

9. Yamagami R, Sieg JP, Bevilacqua PC (2021) Functional Roles of Chelated Magnesium Ions in RNA Folding and Function. Biochemistry 60:2374–2386. https://doi.org/10.1021/acs.biochem.1c00012

10. Schauss J, Kundu A, Fingerhut BP, Elsaesser T (2021) Magnesium Contact Ions Stabilize the Tertiary Structure of Transfer RNA: Electrostatics Mapped by Two-Dimensional Infrared Spectra and Theoretical Simulations. J Phys Chem B 125:740–747. https://doi.org/10.1021/acs.jpcb.0c08966

11. Klein DJ, Moore PB, Steitz TA (2004) The contribution of metal ions to the structural stability of the large ribosomal subunit. RNA 10:1366–1379. https://doi.org/10.1261/rna.7390804

12. Petrov AS, Bernier CR, Hsiao C, et al (2012) RNA–Magnesium–Protein Interactions in Large Ribosomal Subunit. J Phys Chem B 116:8113–8120. https://doi.org/10.1021/jp304723w

13. Pontes MH, Yeom J, Groisman EA (2016) Reducing Ribosome Biosynthesis Promotes Translation during Low Mg 2+ Stress. Molecular Cell 64:480–492. https://doi.org/10.1016/j.molcel.2016.05.008

14. Arjona FJ, Chen Y-X, Flik G, et al (2013) Tissue-specific expression and in vivo regulation of zebrafish orthologues of mammalian genes related to symptomatic hypomagnesemia. Pflugers Arch - Eur J Physiol 465:1409–1421. https://doi.org/10.1007/s00424-013-1275-3

15. de Baaij JHF, Arjona FJ, van den Brand M, et al (2016) Identification of SLC41A3 as a novel player in magnesium homeostasis. Sci Rep 6:28565. https://doi.org/10.1038/srep28565

16. Arjona FJ, Latta F, Mohammed SG, et al (2019) SLC41A1 is essential for magnesium homeostasis in vivo. Pflugers Arch - Eur J Physiol 471:845–860. https://doi.org/10.1007/s00424-018-2234-9

17. Groenestege WMT, Hoenderop JG, van den Heuvel L, et al (2006) The Epithelial Mg^{2+}Channel Transient Receptor Potential Melastatin 6 Is Regulated by Dietary Mg^{2+} Content and Estrogens. JASN 17:1035–1043. https://doi.org/10.1681/ASN.2005070700

18. Hardy S, Kostantin E, Wang SJ, et al (2019) Magnesium-sensitive upstream ORF controls PRL phosphatase expression to mediate energy metabolism. PNAS 116:2925–2934. https://doi.org/10.1073/pnas.1815361116

19. Sponder G, Mastrototaro L, Kurth K, et al (2016) Human CNNM2 is not a Mg2+ transporter per se. Pflugers Arch - Eur J Physiol 468:1223–1240. https://doi.org/10.1007/s00424-016-1816-7

20. Fleig A, Schweigel-Röntgen M, Kolisek M (2013) Solute carrier family SLC41: what do we really know about it? Wiley Interdisciplinary Reviews: Membrane Transport and Signaling 2:227–239. https://doi.org/10.1002/wmts.95

21. Kolisek M, Nestler A, Vormann J, Schweigel-Röntgen M (2012) Human gene SLC41A1 encodes for the Na^{+}/Mg^{2+} exchanger. American Journal of Physiology-Cell Physiology 302:C318–C326. https://doi.org/10.1152/ajpcell.00289.2011

22. Tatarkova Z, de Baaij JHF, Grendar M, et al (2020) Dietary Mg^{2+} Intake and the Na+/Mg^{2+} Exchanger SLC41A1 Influence Components of Mitochondrial Energetics in Murine Cardiomyocytes. IJMS 21:8221. https://doi.org/10.3390/ijms21218221

23. Goytain A, Quamme GA (2005) Functional characterization of human SLC41A1, a Mg^{2+} transporter with similarity to prokaryotic MgtE Mg^{2+} transporters. Physiological Genomics 21:337–342. https://doi.org/10.1152/physiolgenomics.00261.2004

24. Sahni J, Nelson B, Scharenberg AM (2007) SLC41A2 encodes a plasma-membrane Mg^{2+} transporter. Biochemical Journal 401:505–513. https://doi.org/10.1042/BJ20060673

25. de Baaij JHF, Groot Koerkamp MJ, Lavrijsen M, et al (2013) Elucidation of the distal convoluted tubule transcriptome identifies new candidate genes involved in renal Mg^{2+} handling. American Journal of Physiology-Renal Physiology 305:F1563–F1573. https://doi.org/10.1152/ajprenal.00322.2013

26. Mastrototaro L, Smorodchenko A, Aschenbach JR, et al (2016) Solute carrier 41A3 encodes for a mitochondrial Mg^{2+} efflux system. Sci Rep 6:27999. https://doi.org/10.1038/srep27999

27. Kolisek M, Zsurka G, Samaj J, et al (2003) Mrs2p is an essential component of the major electrophoretic Mg^{2+} influx system in mitochondria. The EMBO Journal 22:1235–1244. https://doi.org/10.1093/emboj/cdg122

28. Zsurka G, Gregáň J, Schweyen RJ (2001) The Human Mitochondrial Mrs2 Protein Functionally Substitutes for Its Yeast Homologue, A Candidate Magnesium Transporter. Genomics 72:158–168. https://doi.org/10.1006/geno.2000.6407

29. Piskacek M, Zotova L, Zsurka G, Schweyen RJ (2009) Conditional knockdown of hMRS2 results in loss of mitochondrial Mg^{2+} uptake and cell death. Journal of Cellular and Molecular Medicine 13:693–700. https://doi.org/10.1111/j.1582-4934.2008.00328.x

30. Daw CC, Ramachandran K, Enslow BT, et al (2020) Lactate Elicits ER-Mitochondrial Mg^{2+} Dynamics to Integrate Cellular Metabolism. Cell 1–16. https://doi.org/10.1016/j.cell.2020.08.049

31. Kolisek M, Sponder G, Pilchova I, et al (2019) Magnesium Extravaganza: A Critical Compendium of Current Research into Cellular Mg2+ Transporters Other than TRPM6/7. In: de Tombe P, Gudermann T, Jahn R, Lill R (eds) Reviews of Physiology, Biochemistry and Pharmacology 176. Springer International Publishing, Cham, pp 65–105

32. Wilde BR, Christofk HR (2020) O-Mg! Lactate Drives Mg^{2+} Mobilization. Molecular Cell 80:762–763. https://doi.org/10.1016/j.molcel.2020.11.023

33. Yamanaka R, Tabata S, Shindo Y, et al (2016) Mitochondrial Mg^{2+} homeostasis decides cellular energy metabolism and vulnerability to stress. Scientific Reports 6:1–12. https://doi.org/10.1038/srep30027

34. Pilchova I, Klacanova K, Tatarkova Z, et al (2017) The Involvement of Mg^{2+} in Regulation of Cellular and Mitochondrial Functions. Oxidative Medicine and Cellular Longevity 2017:1–8. https://doi.org/10.1155/2017/6797460

35. Fiermonte G, De Leonardis F, Todisco S, et al (2004) Identification of the Mitochondrial ATP-Mg/Pi Transporter. Journal of Biological Chemistry 279:30722–30730. https://doi.org/10.1074/jbc.M400445200

36. Schäffers OJM, Hoenderop JGJ, Bindels RJM, de Baaij JHF (2018) The rise and fall of novel renal magnesium transporters. American Journal of Physiology-Renal Physiology 314:F1027–F1033. https://doi.org/10.1152/ajprenal.00634.2017

37. Pleiner T, Tomaleri GP, Januszyk K, et al (2020) Structural basis for membrane insertion by the human ER membrane protein complex. Science 369:433–436. https://doi.org/10.1126/science.abb5008

38. Ramírez AS, Kowal J, Locher KP (2019) Cryo–electron microscopy structures of human oligosaccharyltransferase complexes OST-A and OST-B. Science 366:1372–1375. https://doi.org/10.1126/science.aaz3505

39. Ayuk J, Gittoes NJ (2014) Contemporary view of the clinical relevance of magnesium homeostasis. Ann Clin Biochem 51:179–188. https://doi.org/10.1177/0004563213517628

40. Moore-Schiltz L, Albert JM, Singer ME, et al (2015) Dietary intake of calcium and magnesium and the metabolic syndrome in the National Health and Nutrition Examination (NHANES) 2001–2010 data. Br J Nutr 114:924–935. https://doi.org/10.1017/S0007114515002482

41. Schimatschek HF, Rempis R (2001) Prevalence of hypomagnesemia in an unselected German population of 16,000 individuals. Magnes Res 14:283–290

42. Syedmoradi L, Ghasemi A, Zahediasl S, Azizi F (2011) Prevalence of hypo- and hypermagnesemia in an Iranian urban population. Ann Hum Biol 38:150–155. https://doi.org/10.3109/03014460.2010.500472

43. Razzaque M (2018) Magnesium: Are We Consuming Enough? Nutrients 10:1863. https://doi.org/10.3390/nu10121863

44. Vormann J (2003) Magnesium: nutrition and metabolism. Molecular Aspects of Medicine 24:27–37. https://doi.org/10.1016/S0098-2997(02)00089-4

45. Vormann J, Anke M (2002) Dietary Magnesium: Supply, Requirements and Recommendations - Results From Duplicate and Balance Studies in Man. J Clin Basic Cardiol 5:49–53

46. Grotto D, Zied E (2010) The Standard American Diet and Its Relationship to the Health Status of Americans. Nutr Clin Pract 25:603–612. https://doi.org/10.1177/0884533610386234

47. Jacka FN, Overland S, Stewart R, et al (2009) Association Between Magnesium Intake and Depression and Anxiety in Community-Dwelling Adults: The Hordaland Health Study. Aust N Z J Psychiatry 43:45–52. https://doi.org/10.1080/00048670802534408

48. Anjom-Shoae J, Sadeghi O, Hassanzadeh Keshteli A, et al (2018) The association between dietary intake of magnesium and psychiatric disorders among Iranian adults: a cross-sectional study. Br J Nutr 120:693–702. https://doi.org/10.1017/S0007114518001782

49. Tarleton EK, Littenberg B, MacLean CD, et al (2017) Role of magnesium supplementation in the treatment of depression: A randomized clinical trial. PLoS ONE 12:e0180067. https://doi.org/10.1371/journal.pone.0180067

50. Kieboom BCT, Ligthart S, Dehghan A, et al (2017) Serum magnesium and the risk of prediabetes: a population-based cohort study. Diabetologia 60:843–853. https://doi.org/10.1007/s00125-017-4224-4

51. Nozue T, Kobayashi A, Uemasu F, et al (1995) Magnesium Status, Serum HDL Cholesterol, and Apolipoprotein A-1 Levels. Journal of Pediatric Gastroenterology and Nutrition 20:316–318. https://doi.org/10.1097/00005176-199504000-00009

52. Castellanos-Gutiérrez A, Sánchez-Pimienta TG, Carriquiry A, et al (2018) Higher dietary magnesium intake is associated with lower body mass index, waist circumference and serum glucose in Mexican adults. Nutr J 17:114. https://doi.org/10.1186/s12937-018-0422-2

53. Zhao B, Zeng L, Zhao J, et al (2020) Association of magnesium intake with type 2 diabetes and total stroke: an updated systematic review and meta-analysis. BMJ Open 10:e032240. https://doi.org/10.1136/bmjopen-2019-032240

54. Kass L, Weekes J, Carpenter L (2012) Effect of magnesium supplementation on blood pressure: a meta-analysis. Eur J Clin Nutr 66:411–418. https://doi.org/10.1038/ejcn.2012.4

55. Piuri G, Zocchi M, Della Porta M, et al (2021) Magnesium in Obesity, Metabolic Syndrome, and Type 2 Diabetes. Nutrients 13:320. https://doi.org/10.3390/nu13020320

56. Bouras H, Roig SR, Kurstjens S, et al (2020) Metformin regulates TRPM6, a potential explanation for magnesium imbalance in type 2 diabetes patients. Can J Physiol Pharmacol 98:400–411. https://doi.org/10.1139/cjpp-2019-0570

57. Villa-Bellosta R (2020) Dietary magnesium supplementation improves lifespan in a mouse model of progeria. EMBO Mol Med 12:. https://doi.org/10.15252/emmm.202012423

58. Sharain K, May AM, Gersh BJ (2015) Chronic Alcoholism and the Danger of Profound Hypomagnesemia. The American Journal of Medicine 128:e17–e18. https://doi.org/10.1016/j.amjmed.2015.06.051

59. Chadda KD, Lichstein E, Gupta P (1973) Hypomagnesemia and refractory cardiac arrhythmia in a nondigitalized patient. The American Journal of Cardiology 31:98–100. https://doi.org/10.1016/0002-9149(73)90818-7

60. Shaikh MN, Malapati BR, Gokani R, et al (2016) Serum Magnesium and Vitamin D Levels as Indicators of Asthma Severity. Pulmonary Medicine 2016:1–5. https://doi.org/10.1155/2016/1643717

61. Griffiths B, Kew KM (2016) Intravenous magnesium sulfate for treating children with acute asthma in the emergency department. Cochrane Database of Systematic Reviews 2016:. https://doi.org/10.1002/14651858.CD011050.pub2

62. Boulos MI, Shoamanesh A, Aviv RI, et al (2012) Severe Hypomagnesemia Associated With Reversible Subacute Ataxia and Cerebellar Hyperintensities on MRI. The Neurologist 18:223–225. https://doi.org/10.1097/NRL.0b013e31825bbf07

63. Rouco Axpe I, Almeida Velasco J, Barreiro Garcia JG, et al (2017) Hypomagnesemia: a Treatable Cause of Ataxia with Cerebellar Edema. Cerebellum 16:988–990. https://doi.org/10.1007/s12311-017-0873-6

64. Derom M-L, Sayón-Orea C, Martínez-Ortega JM, Martínez-González MA (2013) Magnesium and depression: a systematic review. Nutritional Neuroscience 16:191–206. https://doi.org/10.1179/1476830512Y.0000000044

65. Bagis S, Karabiber M, As I, et al (2013) Is magnesium citrate treatment effective on pain, clinical parameters and functional status in patients with fibromyalgia? Rheumatol Int 33:167–172. https://doi.org/10.1007/s00296-011-2334-8

66. Choi M-K, Bae YJ (2015) Association of Magnesium Intake with High Blood Pressure in Korean Adults: Korea National Health and Nutrition Examination Survey 2007–2009. PLoS ONE 10:e0130405. https://doi.org/10.1371/journal.pone.0130405

67. Whang R, Chrysant S, Dillard B, et al (1982) Hypomagnesemia and hypokalemia in 1,000 treated ambulatory hypertensive patients. Journal of the American College of Nutrition 1:317–322. https://doi.org/10.1080/07315724.1982.10719001

68. Rodríguez-Ramírez M, Simental-Mendía LE, González-Ortiz M, et al (2015) Prevalence of Prehypertension in Mexico and Its Association With Hypomagnesemia. AJHYPE 28:1024–1030. https://doi.org/10.1093/ajh/hpu293

69. Wang K, Wei H, Zhang W, et al (2018) Severely low serum magnesium is associated with increased risks of positive anti-thyroglobulin antibody and hypothyroidism: A cross-sectional study. Sci Rep 8:9904. https://doi.org/10.1038/s41598-018-28362-5

70. Maier JA, Castiglioni S, Locatelli L, et al (2021) Magnesium and inflammation: Advances and perspectives. Seminars in Cell & Developmental Biology 115:37–44. https://doi.org/10.1016/j.semcdb.2020.11.002

71. Mauskop A, Varughese J (2012) Why all migraine patients should be treated with magnesium. J Neural Transm 119:575–579. https://doi.org/10.1007/s00702-012-0790-2

72. Rodríguez-Hernández H, Gonzalez JL, Rodríguez-Morán M, Guerrero-Romero F (2005) Hypomagnesemia, Insulin Resistance, and Non-Alcoholic Steatohepatitis in Obese Subjects. Archives of Medical Research 36:362–366. https://doi.org/10.1016/j.arcmed.2005.03.008

73. Eshraghian A, Nikeghbalian S, Geramizadeh B, Malek-Hosseini SA (2018) Serum magnesium concentration is independently associated with non-alcoholic fatty liver and non-alcoholic steatohepatitis. United European Gastroenterology Journal 6:97–103. https://doi.org/10.1177/2050640617707863

74. Fang X, Wang H, Liu Z, et al (2020) Posterior reversible encephalopathy syndrome in preeclampsia and eclampsia: The role of hypomagnesemia. Seizure 76:12–16. https://doi.org/10.1016/j.seizure.2020.01.003

75. Nuytten D, Van Hees J, Meulemans A, Carton H (1991) Magnesium deficiency as a cause of acute intractable seizures. J Neurol 238:262–264. https://doi.org/10.1007/BF00319737

76. Chen BB, Prasad C, Kobrzynski M, et al (2016) Seizures Related to Hypomagnesemia: A Case Series and Review of the Literature. Child Neurology Open 3:2329048X1667483. https://doi.org/10.1177/2329048X16674834

77. Weisleder P, Tobin JA, Kerrigan JF, Bodensteiner JB (2002) Hypomagnesemic Seizures: Case Report and Presumed Pathophysiology. J Child Neurol 17:59–61. https://doi.org/10.1177/088307380201700117

78. Gupta SK, Manhas AS, Gupta VK, Bhatt R (1994) Serum magnesium levels in idiopathic epilepsy. J Assoc Physicians India 42:456–457

79. Rosique-Esteban N, Guasch-Ferré M, Hernández-Alonso P, Salas-Salvadó J (2018) Dietary Magnesium and Cardiovascular Disease: A Review with Emphasis in Epidemiological Studies. Nutrients 10:168. https://doi.org/10.3390/nu10020168

80. Fang X, Wang K, Han D, et al (2016) Dietary magnesium intake and the risk of cardiovascular disease, type 2 diabetes, and all-cause mortality: a dose-response meta-analysis of prospective cohort studies. BMC Med 14:210. https://doi.org/10.1186/s12916-016-0742-z

81. Gommers LMM, Hoenderop JGJ, Bindels RJM, de Baaij JHF (2016) Hypomagnesemia in Type 2 Diabetes: A Vicious Circle? Diabetes 65:3–13. https://doi.org/10.2337/db15-1028

82. Richards JB, Waterworth D, O'Rahilly S, et al (2009) A Genome-Wide Association Study Reveals Variants in ARL15 that Influence Adiponectin Levels. PLOS Genetics 5:e1000768. https://doi.org/10.1371/journal.pgen.1000768

83. Dastani Z, Hivert M-F, Timpson N, et al (2012) Novel Loci for Adiponectin Levels and Their Influence on Type 2 Diabetes and Metabolic Traits: A Multi-Ethnic Meta-Analysis of 45,891 Individuals. PLOS Genetics 8:e1002607. https://doi.org/10.1371/journal.pgen.1002607

84. Ried JS, M JJ, Chu AY, et al (2016) A principal component meta-analysis on multiple anthropometric traits identifies novel loci for body shape. Nature Communications 7:13357. https://doi.org/10.1038/ncomms13357

85. Li Y, Yang Y, Yao Y, et al (2014) Association Study of ARL15 and CDH13 with T2DM in a Han Chinese Population. Int J Med Sci 11:522–527. https://doi.org/10.7150/ijms.8206

86. Domínguez-Cruz MG, Muñoz M de L, Totomoch-Serra A, et al (2018) Pilot genome-wide association study identifying novel risk loci for type 2 diabetes in a Maya population. Gene 677:324–331. https://doi.org/10.1016/j.gene.2018.08.041

87. Sun J-Q, Yin R-X, Shi G-Y, et al (2015) Association of the ARL15 rs6450176 SNP and serum lipid levels in the Jing and Han populations. Int J Clin Exp Pathol 8:12977–12994

88. Negi S, Juyal G, Senapati S, et al (2013) A genome-wide association study reveals ARL15, a novel non-HLA susceptibility gene for rheumatoid arthritis in North Indians. Arthritis Rheum 65:3026–3035. https://doi.org/10.1002/art.38110

89. Pandey AK, Saxena A, Dey SK, et al (2021) Correlation between an intronic SNP genotype and ARL15 level in rheumatoid arthritis. J Genet 100:26

90. Li C, He J, Chen J, et al (2017) Genome-Wide Gene–Potassium Interaction Analyses on Blood Pressure: The GenSalt Study (Genetic Epidemiology Network of Salt Sensitivity). Circ Cardiovasc Genet 10:. https://doi.org/10.1161/CIRCGENETICS.117.001811

91. Matsuba R, Imamura M, Tanaka Y, et al (2016) Replication Study in a Japanese Population of Six Susceptibility Loci for Type 2 Diabetes Originally Identified by a Transethnic Meta-Analysis of Genome-Wide Association Studies. PLoS ONE 11:e0154093. https://doi.org/10.1371/journal.pone.0154093

92. Rocha N, Payne F, Huang-Doran I, et al (2017) The metabolic syndrome-associated small G protein ARL15 plays a role in adipocyte differentiation and adiponectin secretion. Scientific Reports 7:17593. https://doi.org/10.1038/s41598-017-17746-8

93. Fisman EZ, Tenenbaum A (2014) Adiponectin: a manifold therapeutic target for metabolic syndrome, diabetes, and coronary disease? Cardiovasc Diabetol 13:103. https://doi.org/10.1186/1475-2840-13-103

94. Wu Y, Bai Y, McEwan DG, et al (2021) Palmitoylated small GTPase ARL15 is translocated within Golgi network during adipogenesis. Biology Open bio.058420. https://doi.org/10.1242/bio.058420

95. Gorski M, van der Most PJ, Teumer A, et al (2017) 1000 Genomes-based meta-analysis identifies 10 novel loci for kidney function. Sci Rep 7:45040. https://doi.org/10.1038/srep45040

96. Corre T, Arjona FJ, Hayward C, et al (2018) Genome-Wide Meta-Analysis Unravels Interactions between Magnesium Homeostasis and Metabolic Phenotypes. JASN 29:335–348. https://doi.org/10.1681/ASN.2017030267

97. Kollewe A, Chubanov V, Tseung FT, et al (2021) The molecular appearance of native TRPM7 channel complexes identified by high-resolution proteomics. eLife 10:e68544. https://doi.org/10.7554/eLife.68544

98. Koscielny G, Yaikhom G, Iyer V, et al (2014) The International Mouse Phenotyping Consortium Web Portal, a unified point of access for knockout mice and related phenotyping data. Nucl Acids Res 42:D802–D809. https://doi.org/10.1093/nar/gkt977

99. Kozlov G, Cheng J, Ziomek E, et al (2004) Structural Insights into Molecular Function of the Metastasis-associated Phosphatase PRL-3. Journal of Biological Chemistry 279:11882–11889. https://doi.org/10.1074/jbc.M312905200

100. Skinner AL, Vartia AA, Williams TD, Laurence JS (2009) Enzyme Activity of Phosphatase of Regenerating Liver Is Controlled by the Redox Environment and

Its C-Terminal Residues. Biochemistry 48:4262–4272. https://doi.org/10.1021/bi900241k

101. Mohn KL, Laz TM, Hsu JC, et al (1991) The immediate-early growth response in regenerating liver and insulin-stimulated H-35 cells: comparison with serum-stimulated 3T3 cells and identification of 41 novel immediate-early genes. Mol Cell Biol 11:381–390. https://doi.org/10.1128/mcb.11.1.381-390.1991

102. Hardy S, Kostantin E, Hatzihristidis T, et al (2018) Physiological and oncogenic roles of the PRL phosphatases. The FEBS Journal 285:3886–3908. https://doi.org/10.1111/febs.14503

103. Manolaridis I, Kulkarni K, Dodd RB, et al (2013) Mechanism of farnesylated CAAX protein processing by the intramembrane protease Rce1. Nature 504:301–305. https://doi.org/10.1038/nature12754

104. Zeng Q, Si X, Horstmann H, et al (2000) Prenylation-dependent Association of Protein-tyrosine Phosphatases PRL-1, -2, and -3 with the Plasma Membrane and the Early Endosome. Journal of Biological Chemistry 275:21444–21452. https://doi.org/10.1074/jbc.M000453200

105. Wang J, Kirby CE, Herbst R (2002) The Tyrosine Phosphatase PRL-1 Localizes to the Endoplasmic Reticulum and the Mitotic Spindle and Is Required for Normal Mitosis. Journal of Biological Chemistry 277:46659–46668. https://doi.org/10.1074/jbc.M206407200

106. Pascaru M, Tanase C, Vacaru AM, et al (2009) Analysis of molecular determinants of PRL-3. Journal of Cellular and Molecular Medicine 13:3141–3150. https://doi.org/10.1111/j.1582-4934.2008.00591.x

107. Sievers F, Higgins DG (2018) Clustal Omega for making accurate alignments of many protein sequences: Clustal Omega for Many Protein Sequences. Protein Science 27:135–145. https://doi.org/10.1002/pro.3290

108. Zhang H, Kozlov G, Li X, et al (2017) PRL3 phosphatase active site is required for binding the putative magnesium transporter CNNM3. Sci Rep 7:48. https://doi.org/10.1038/s41598-017-00147-2

109. Kozlov G, Funato Y, Chen YS, et al (2020) PRL3 pseudophosphatase activity is necessary and sufficient to promote metastatic growth. J Biol Chem jbc.RA120.014464. https://doi.org/10.1074/jbc.RA120.014464

110. Hornbeck PV, Zhang B, Murray B, et al (2015) PhosphoSitePlus, 2014: mutations, PTMs and recalibrations. Nucleic Acids Research 43:D512–D520. https://doi.org/10.1093/nar/gku1267

111. Saha S, Bardelli A, Buckhaults P, et al (2001) A phosphatase associated with metastasis of colorectal cancer. Science 294:1343–1346. https://doi.org/10.1126/science.1065817

112. Wang H, Vardy LA, Tan CP, et al (2010) PCBP1 Suppresses the Translation of Metastasis-Associated PRL-3 Phosphatase. Cancer Cell 18:52–62. https://doi.org/10.1016/j.ccr.2010.04.028

113. Bardelli A, Saha S, Sager JA, et al (2003) PRL-3 expression in metastatic cancers. Clin Cancer Res 9:5607–5615

114. Kato H, Semba S, Miskad UA, et al (2004) High Expression of PRL-3 Promotes Cancer Cell Motility and Liver Metastasis in Human Colorectal Cancer: A Predictive Molecular Marker of Metachronous Liver and Lung Metastases. Clin Cancer Res 10:7318–7328. https://doi.org/10.1158/1078-0432.CCR-04-0485

115. Polato F, Codegoni A, Fruscio R, et al (2005) PRL-3 Phosphatase Is Implicated in Ovarian Cancer Growth. Clin Cancer Res 11:6835–6839. https://doi.org/10.1158/1078-0432.CCR-04-2357

116. Ming J, Liu N, Gu Y, et al (2009) PRL-3 facilitates angiogenesis and metastasis by increasing ERK phosphorylation and up-regulating the levels and activities of Rho-A/C in lung cancer. Pathology 41:118–126. https://doi.org/10.1080/00313020802579268

117. Hardy S, Wong NN, Muller WJ, et al (2010) Overexpression of the Protein Tyrosine Phosphatase PRL-2 Correlates with Breast Tumor Formation and Progression. Cancer Res 70:8959–8967. https://doi.org/10.1158/0008-5472.CAN-10-2041

118. Radke I, Götte M, Kersting C, et al (2006) Expression and prognostic impact of the protein tyrosine phosphatases PRL-1, PRL-2, and PRL-3 in breast cancer. Br J Cancer 95:347–354. https://doi.org/10.1038/sj.bjc.6603261

119. Ren T, Jiang B, Xing X, et al (2009) Prognostic Significance of Phosphatase of Regenerating Liver-3 Expression in Ovarian Cancer. Pathol Oncol Res 15:555–560. https://doi.org/10.1007/s12253-009-9153-1

120. Reich R, Hadar S, Davidson B (2011) Expression and Clinical Role of Protein of Regenerating Liver (PRL) Phosphatases in Ovarian Carcinoma. IJMS 12:1133–1145. https://doi.org/10.3390/ijms12021133

121. Yeh H-C, Li C-C, Huang C-N, et al (2015) PTP4A3 Independently Predicts Metastasis and Survival in Upper Tract Urothelial Carcinoma Treated with Radical Nephroureterectomy. Journal of Urology 194:1449–1455. https://doi.org/10.1016/j.juro.2015.05.101

122. Sun F, Li W, Wang L, Jiao C (2017) Expression of phosphatase of regenerating liver-3 is associated with prognosis of Wilms' tumor. OTT Volume 10:311–317. https://doi.org/10.2147/OTT.S107076

123. Jiang L, Wang M, Lin S, et al (2020) A Quantitative Proteome Map of the Human Body. Cell 183:269-283.e19. https://doi.org/10.1016/j.cell.2020.08.036

124. Szász AM, Lánczky A, Nagy Á, et al (2016) Cross-validation of survival associated biomarkers in gastric cancer using transcriptomic data of 1,065 patients. Oncotarget 7:49322–49333. https://doi.org/10.18632/oncotarget.10337

125. Nagy Á, Munkácsy G, Győrffy B (2021) Pancancer survival analysis of cancer hallmark genes. Sci Rep 11:6047. https://doi.org/10.1038/s41598-021-84787-5

126. Al-Aidaroos AQO, Zeng Q (2010) PRL-3 phosphatase and cancer metastasis. J Cell Biochem 111:1087–1098. https://doi.org/10.1002/jcb.22913

127. Duciel L, Monraz Gomez LC, Kondratova M, et al (2019) The Phosphatase PRL-3 Is Involved in Key Steps of Cancer Metastasis. Journal of Molecular Biology 431:3056–3067. https://doi.org/10.1016/j.jmb.2019.06.008

128. Rios P, Li X, Köhn M (2013) Molecular mechanisms of the PRL phosphatases: Molecular mechanisms of the PRL phosphatases. FEBS Journal 280:505–524. https://doi.org/10.1111/j.1742-4658.2012.08565.x

129. Campbell AM, Zhang Z-Y (2014) Phosphatase of regenerating liver: a novel target for cancer therapy. Expert Opinion on Therapeutic Targets 18:555–569. https://doi.org/10.1517/14728222.2014.892926

130. Zeng Q, Dong J-M, Guo K, et al (2003) PRL-3 and PRL-1 promote cell migration, invasion, and metastasis. Cancer Res 63:2716–2722

131. Li Q, Bai Y, Lyle LT, et al (2020) Mechanism of PRL2 phosphatase-mediated PTEN degradation and tumorigenesis. PNAS. https://doi.org/10.1073/pnas.2002964117

132. Wang H, Quah SY, Dong JM, et al (2007) PRL-3 Down-regulates PTEN Expression and Signals through PI3K to Promote Epithelial-Mesenchymal Transition. Cancer Res 67:2922–2926. https://doi.org/10.1158/0008-5472.CAN-06-3598

133. Schwering I, Bräuninger A, Distler V, et al (2003) Profiling of Hodgkin's Lymphoma Cell Line L1236 and Germinal Center B Cells: Identification of Hodgkin's Lymphoma-specific Genes. Mol Med 9:85–95. https://doi.org/10.1007/BF03402041

134. Hjort MA, Hov H, Abdollahi P, et al (2018) Phosphatase of regenerating liver-3 (PRL-3) is overexpressed in classical Hodgkin lymphoma and promotes survival

and migration. Exp Hematol Oncol 7:8. https://doi.org/10.1186/s40164-018-0100-2

135. Wei M, Haney MG, Rivas DR, Blackburn JS (2020) Protein tyrosine phosphatase 4A3 (PTP4A3/PRL-3) drives migration and progression of T-cell acute lymphoblastic leukemia in vitro and in vivo. Oncogenesis 9:6. https://doi.org/10.1038/s41389-020-0192-5

136. Garcia EG, Veloso A, Oliveira ML, et al (2021) PRL3 enhances T-cell acute lymphoblastic leukemia growth through suppressing T-cell signaling pathways and apoptosis. Leukemia 35:679–690. https://doi.org/10.1038/s41375-020-0937-3

137. Park JE, Yuen HF, Zhou JB, et al (2013) Oncogenic roles of PRL-3 in FLT3-ITD induced acute myeloid leukaemia. EMBO Mol Med 5:1351–1366. https://doi.org/10.1002/emmm.201202183

138. Zhou J, Chan Z-L, Bi C, et al (2017) LIN28B Activation by PRL-3 Promotes Leukemogenesis and a Stem Cell–like Transcriptional Program in AML. Mol Cancer Res 15:294–303. https://doi.org/10.1158/1541-7786.MCR-16-0275-T

139. Chong PSY, Zhou J, Chooi J-Y, et al (2019) Non-canonical activation of β-catenin by PRL-3 phosphatase in acute myeloid leukemia. Oncogene 38:1508–1519. https://doi.org/10.1038/s41388-018-0526-3

140. Zhou J, Cheong L-L, Liu S-C, et al (2012) The pro-metastasis tyrosine phosphatase, PRL-3 (PTP4A3), is a novel mediator of oncogenic function of BCR-ABL in human chronic myeloid leukemia. Mol Cancer 11:72. https://doi.org/10.1186/1476-4598-11-72

141. Xu J, Wu W, Tang Y, et al (2019) PRL-3 exerts oncogenic functions in myeloid leukemia cells via aberrant dephosphorylation of stathmin and activation of STAT3 signaling. Aging 11:7817–7829. https://doi.org/10.18632/aging.102290

142. Chong PSY, Zhou J, Lim JSL, et al (2019) Interleukin-6 promotes a STAT3-PRL3 feedforward loop via SHP2 repression in Multiple Myeloma. Cancer Res canres.0343.2019. https://doi.org/10.1158/0008-5472.CAN-19-0343

143. Vandsemb EN, Rye MB, Steiro IJ, et al (2021) PRL-3 induces a positive signaling circuit between glycolysis and activation of STAT1/2. FEBS J febs.16058. https://doi.org/10.1111/febs.16058

144. Funato Y, Yoshida A, Hirata Y, et al (2020) The Oncogenic PRL Protein Causes Acid Addiction of Cells by Stimulating Lysosomal Exocytosis. Developmental Cell 1–11. https://doi.org/10.1016/j.devcel.2020.08.009

145. Boedtkjer E, Pedersen SF (2020) The Acidic Tumor Microenvironment as a Driver of Cancer. Annu Rev Physiol 82:103–126. https://doi.org/10.1146/annurev-physiol-021119-034627

146. Shi Y, Xu S, Ngoi NYL, et al (2021) PRL-3 dephosphorylates p38 MAPK to promote cell survival under stress. Free Radical Biology and Medicine S0891584921007656. https://doi.org/10.1016/j.freeradbiomed.2021.10.015

147. Canovas B, Nebreda AR (2021) Diversity and versatility of p38 kinase signalling in health and disease. Nat Rev Mol Cell Biol 22:346–366. https://doi.org/10.1038/s41580-020-00322-w

148. Wang C-Y, Shi J-D, Yang P, et al (2003) Molecular cloning and characterization of a novel gene family of four ancient conserved domain proteins (ACDP). Gene 306:37–44. https://doi.org/10.1016/S0378-1119(02)01210-6

149. Tang R-J, Meng S-F, Zheng X-J, et al (2022) Conserved mechanism for vacuolar magnesium sequestration in yeast and plant cells. Nat Plants. https://doi.org/10.1038/s41477-021-01087-6

150. Funato Y, Miki H (2019) Molecular function and biological importance of CNNM family Mg^{2+} transporters. J Biochem 165:219–225. https://doi.org/10.1093/jb/mvy095

151. Giménez-Mascarell P, González-Recio I, Fernández-Rodríguez C, et al (2019) Current Structural Knowledge on the CNNM Family of Magnesium Transport Mediators. International Journal of Molecular Sciences 20:1135. https://doi.org/10.3390/ijms20051135

152. Chen YS, Kozlov G, Fakih R, et al (2018) The cyclic nucleotide–binding homology domain of the integral membrane protein CNNM mediates dimerization and is required for Mg2+ efflux activity. Journal of Biological Chemistry 293:19998–20007. https://doi.org/10.1074/jbc.RA118.005672

153. Chen YS, Kozlov G, Fakih R, et al (2019) Mg^{2+}-ATP Sensing in CNNM, a Putative Magnesium Transporter. Structure. https://doi.org/10.1016/j.str.2019.11.016

154. Huang Y, Jin F, Funato Y, et al (2021) Structural basis for the Mg2+ recognition and regulation of the CorC Mg2+ transporter. Science Advances 7:eabe6140. https://doi.org/10.1126/sciadv.abe6140

155. Chen YS, Kozlov G, Moeller BE, et al (2021) Crystal structure of an archaeal CorB magnesium transporter. Nat Commun 12:4028. https://doi.org/10.1038/s41467-021-24282-7

156. Stuiver M, Lainez S, Will C, et al (2011) CNNM2, Encoding a Basolateral Protein Required for Renal Mg^{2+} Handling, Is Mutated in Dominant Hypomagnesemia. The

American Journal of Human Genetics 88:333–343. https://doi.org/10.1016/j.ajhg.2011.02.005

157. Arjona FJ, Baaij JHF de, Schlingmann KP, et al (2014) CNNM2 Mutations Cause Impaired Brain Development and Seizures in Patients with Hypomagnesemia. PLOS Genetics 10:e1004267. https://doi.org/10.1371/journal.pgen.1004267

158. Franken GAC, Müller D, Mignot C, et al (2021) Phenotypic and genetic spectrum of patients with heterozygous mutations in Cyclin M2 (CNNM2). Human Mutation n/a: https://doi.org/10.1002/humu.24182

159. Zhang H, Wu Y, Jiang Y (2021) CNNM2-Related Disorders: Phenotype and Its Severity Were Associated With the Mode of Inheritance. Front Pediatr 9:699568. https://doi.org/10.3389/fped.2021.699568

160. Xu X, Hou S, Sun W, et al (2022) Rare hypomagnesemia, seizures, and mental retardation in a 4-month-old patient caused by novel CNNM2 mutation Tyr189Cys: Genetic analysis and review. Molec Gen & Gen Med. https://doi.org/10.1002/mgg3.1898

161. Polok B, Escher P, Ambresin A, et al (2009) Mutations in CNNM4 Cause Recessive Cone-Rod Dystrophy with Amelogenesis Imperfecta. The American Journal of Human Genetics 84:259–265. https://doi.org/10.1016/j.ajhg.2009.01.006

162. Parry DA, Mighell AJ, El-Sayed W, et al (2009) Mutations in CNNM4 Cause Jalili Syndrome, Consisting of Autosomal-Recessive Cone-Rod Dystrophy and Amelogenesis Imperfecta. The American Journal of Human Genetics 84:266–273. https://doi.org/10.1016/j.ajhg.2009.01.009

163. Abu-Safieh L, Alrashed M, Anazi S, et al (2013) Autozygome-guided exome sequencing in retinal dystrophy patients reveals pathogenetic mutations and novel candidate disease genes. Genome Res 23:236–247. https://doi.org/10.1101/gr.144105.112

164. Doucette L, Green J, Black C, et al (2013) Molecular Genetics of Achromatopsia in Newfoundland Reveal Genetic Heterogeneity, Founder Effects and the First Cases of Jalili Syndrome in North America. Ophthalmic Genetics 34:119–129. https://doi.org/10.3109/13816810.2013.763993

165. Coppieters F, Van Schil K, Bauwens M, et al (2014) Identity-by-descent–guided mutation analysis and exome sequencing in consanguineous families reveals unusual clinical and molecular findings in retinal dystrophy. Genetics in Medicine 16:671–680. https://doi.org/10.1038/gim.2014.24

166. Lopez Torres LT, Schorderet D, Valmaggia C, Todorova M (2015) A novel mutation in CNNM4 (G492C) associated with Jalili Syndrome. Acta Ophthalmol 93:n/a-n/a. https://doi.org/10.1111/j.1755-3768.2015.0606

167. Rahimi-Aliabadi S, Daftarian N, Ahmadieh H, et al (2016) A novel mutation and variable phenotypic expression in a large consanguineous pedigree with Jalili syndrome. Eye 30:1424–1432. https://doi.org/10.1038/eye.2016.137

168. Prasad MK, Geoffroy V, Vicaire S, et al (2016) A targeted next-generation sequencing assay for the molecular diagnosis of genetic disorders with orodental involvement. J Med Genet 53:98–110. https://doi.org/10.1136/jmedgenet-2015-103302

169. Wawrocka A, Walczak-Sztulpa J, Badura-Stronka M, et al (2017) Co-occurrence of Jalili syndrome and muscular overgrowth. Am J Med Genet 173:2280–2283. https://doi.org/10.1002/ajmg.a.38318

170. Maia CMF, Machado RA, Gil-da-Silva-Lopes VL, et al (2018) Report of two unrelated families with Jalili syndrome and a novel nonsense heterozygous mutation in CNNM4 gene. European Journal of Medical Genetics 61:384–387. https://doi.org/10.1016/j.ejmg.2018.02.003

171. Hirji N, Bradley PD, Li S, et al (2018) Jalili Syndrome: Cross-sectional and Longitudinal Features of Seven Patients With Cone-Rod Dystrophy and Amelogenesis Imperfecta. American Journal of Ophthalmology 188:123–130. https://doi.org/10.1016/j.ajo.2018.01.029

172. Parveen A, Mirza MU, Vanmeert M, et al (2019) A novel pathogenic missense variant in CNNM4 underlying Jalili syndrome: Insights from molecular dynamics simulations. Molecular Genetics & Genomic Medicine 0:e902. https://doi.org/10.1002/mgg3.902

173. Prasov L, Ullah E, Turriff AE, et al (2020) Expanding the genotypic spectrum of Jalili syndrome: Novel CNNM4 variants and uniparental isodisomy in a north American patient cohort. Am J Med Genet 182:493–497. https://doi.org/10.1002/ajmg.a.61484

174. Khan AO (2020) Phenotype-guided genetic testing of pediatric inherited retinal disease in the United Arab Emirates. Retina 40:1829–1837. https://doi.org/10.1097/IAE.0000000000002675

175. Hyde RA, Kratunova E, Park JC, McAnany JJ (2021) Cone pathway dysfunction in Jalili syndrome due to a novel familial variant of CNNM4 revealed by pupillometry and electrophysiologic investigations. Ophthalmic Genetics 1–9. https://doi.org/10.1080/13816810.2021.2002916

176. Li H, Huang Y, Li J, Xie M (2022) Novel homozygous nonsynonymous variant of CNNM4 gene in a Chinese family with Jalili syndrome. Molec Gen & Gen Med. https://doi.org/10.1002/mgg3.1860

177. Gong H, Amemiya T, Takaya K (2001) Retinal Changes in Magnesium-deficient Rats. Experimental Eye Research 72:23–32. https://doi.org/10.1006/exer.2000.0928

178. Agarwal R, Iezhitsa Igor, Agarwal P (2014) Pathogenetic role of magnesium deficiency in ophthalmic diseases. Biometals 27:5–18. https://doi.org/10.1007/s10534-013-9684-5

179. Luder HU, Gerth-Kahlert C, Ostertag-Benzinger S, Schorderet DF (2013) Dental Phenotype in Jalili Syndrome Due to a c.1312 dupC Homozygous Mutation in the CNNM4 Gene. PLoS ONE 8:e78529. https://doi.org/10.1371/journal.pone.0078529

180. Yamazaki D, Funato Y, Miura J, et al (2013) Basolateral Mg^{2+} Extrusion via CNNM4 Mediates Transcellular Mg^{2+} Transport across Epithelia: A Mouse Model. PLOS Genetics 9:e1003983. https://doi.org/10.1371/journal.pgen.1003983

181. Block I, Müller C, Sdogati D, et al (2019) CFP suppresses breast cancer cell growth by TES-mediated upregulation of the transcription factor DDIT3. Oncogene 38:4560–4573. https://doi.org/10.1038/s41388-019-0739-0

182. Kostantin E, Hardy S, Valinsky WC, et al (2016) Inhibition of PRL-2·CNNM3 Protein Complex Formation Decreases Breast Cancer Proliferation and Tumor Growth. J Biol Chem 291:10716–10725. https://doi.org/10.1074/jbc.M115.705863

183. Yamazaki D, Hasegawa A, Funato Y, et al (2019) Cnnm4 deficiency suppresses Ca 2+ signaling and promotes cell proliferation in the colon epithelia. Oncogene 38:3962–3969. https://doi.org/10.1038/s41388-019-0682-0

184. Simón J, Goikoetxea-Usandizaga N, Serrano-Maciá M, et al (2021) Magnesium accumulation upon cyclin M4 silencing activates microsomal triglyceride transfer protein improving NASH. Journal of Hepatology S0168827821000945. https://doi.org/10.1016/j.jhep.2021.01.043

185. Funato Y, Furutani K, Kurachi Y, Miki H (2018) CrossTalk proposal: CNNM proteins are Na^{+}/Mg^{2+} exchangers playing a central role in transepithelial Mg^{2+} (re)absorption. The Journal of Physiology 596:743–746. https://doi.org/10.1113/JP275248

186. Arjona FJ, de Baaij JHF (2018) CrossTalk opposing view: CNNM proteins are not Na+/Mg2+ exchangers but Mg2+ transport regulators playing a central role in

transepithelial Mg2+ (re)absorption. J Physiol 596:747–750. https://doi.org/10.1113/JP275249

187. Funato Y, Furutani K, Kurachi Y, Miki H (2018) Rebuttal from Yosuke Funato, Kazuharu Furutani, Yoshihisa Kurachi and Hiroaki Miki: CrossTalk. J Physiol 596:751–751. https://doi.org/10.1113/JP275706

188. Arjona FJ, de Baaij JHF (2018) Rebuttal from Francisco J. Arjona and Jeroen H. F. de Baaij: CrossTalk. J Physiol 596:753–754. https://doi.org/10.1113/JP275705

189. Hirata Y, Funato Y, Takano Y, Miki H (2014) Mg^{2+}-dependent Interactions of ATP with the Cystathionine-β-Synthase (CBS) Domains of a Magnesium Transporter. Journal of Biological Chemistry 289:14731–14739. https://doi.org/10.1074/jbc.M114.551176

190. Corral-Rodríguez MÁ, Stuiver M, Abascal-Palacios G, et al (2014) Nucleotide binding triggers a conformational change of the CBS module of the magnesium transporter CNNM2 from a twisted towards a flat structure. Biochemical Journal 464:23–34. https://doi.org/10.1042/BJ20140409

191. Giménez-Mascarell P, Oyenarte I, Hardy S, et al (2017) Structural Basis of the Oncogenic Interaction of Phosphatase PRL-1 with the Magnesium Transporter CNNM2. J Biol Chem 292:786–801. https://doi.org/10.1074/jbc.M116.759944

192. Hardy S, Uetani N, Wong N, et al (2015) The protein tyrosine phosphatase PRL-2 interacts with the magnesium transporter CNNM3 to promote oncogenesis. Oncogene 34:986–995. https://doi.org/10.1038/onc.2014.33

193. Huang Y, Mu K, Teng X, et al (2021) Identification and mechanistic analysis of an inhibitor of the CorC Mg2+ transporter. iScience 24:102370. https://doi.org/10.1016/j.isci.2021.102370

194. Funato Y, Yamazaki D, Mizukami S, et al (2014) Membrane protein CNNM4–dependent Mg^{2+} efflux suppresses tumor progression. J Clin Invest 124:5398–5410. https://doi.org/10.1172/JCI76614

195. Gulerez I, Funato Y, Wu H, et al (2016) Phosphocysteine in the PRL-CNNM pathway mediates magnesium homeostasis. EMBO reports 17:1890–1900. https://doi.org/10.15252/embr.201643393

196. Kazyken D, Magnuson B, Bodur C, et al (2019) AMPK directly activates mTORC2 to promote cell survival during acute energetic stress. Sci Signal 12:eaav3249. https://doi.org/10.1126/scisignal.aav3249

197. Nadler MJS, Hermosura MC, Inabe K, et al (2001) LTRPC7 is a Mg·ATP-regulated divalent cation channel required for cell viability. Nature 411:590–595. https://doi.org/10.1038/35079092

198. Mittermeier L, Demirkhanyan L, Stadlbauer B, et al (2019) TRPM7 is the central gatekeeper of intestinal mineral absorption essential for postnatal survival. PNAS 116:4706–4715. https://doi.org/10.1073/pnas.1810633116

199. Runnels LW, Yue L, Clapham DE (2001) TRP-PLIK, a Bifunctional Protein with Kinase and Ion Channel Activities. Science 291:1043–1047. https://doi.org/10.1126/science.1058519

200. Ryazanova LV, Rondon LJ, Zierler S, et al (2010) TRPM7 is essential for Mg2+ homeostasis in mammals. Nat Commun 1:109. https://doi.org/10.1038/ncomms1108

201. Chubanov V, Ferioli S, Wisnowsky A, et al (2016) Epithelial magnesium transport by TRPM6 is essential for prenatal development and adult survival. eLife 5:e20914. https://doi.org/10.7554/eLife.20914

202. Clark K, Langeslag M, van Leeuwen B, et al (2006) TRPM7, a novel regulator of actomyosin contractility and cell adhesion. The EMBO Journal 25:290–301. https://doi.org/10.1038/sj.emboj.7600931

203. Langeslag M, Clark K, Moolenaar WH, et al (2007) Activation of TRPM7 Channels by Phospholipase C-coupled Receptor Agonists. Journal of Biological Chemistry 282:232–239. https://doi.org/10.1074/jbc.M605300200

204. Brauchi S, Krapivinsky G, Krapivinsky L, Clapham DE (2008) TRPM7 facilitates cholinergic vesicle fusion with the plasma membrane. Proceedings of the National Academy of Sciences 105:8304–8308. https://doi.org/10.1073/pnas.0800881105

205. Abiria SA, Krapivinsky G, Sah R, et al (2017) TRPM7 senses oxidative stress to release Zn^{2+} from unique intracellular vesicles. Proc Natl Acad Sci USA 114:E6079–E6088. https://doi.org/10.1073/pnas.1707380114

206. Vargas-Poussou R, Claverie-Martin F, Prot-Bertoye C, et al (2022) Possible role for rare TRPM7 variants in patients with hypomagnesemia with secondary hypocalcemia. Nephrology Dialysis Transplantation gfac182. https://doi.org/10.1093/ndt/gfac182

207. Paravicini TM, Chubanov V, Gudermann T (2012) TRPM7: A unique channel involved in magnesium homeostasis. The International Journal of Biochemistry & Cell Biology 44:1381–1384. https://doi.org/10.1016/j.biocel.2012.05.010

208. Nikonorova IA, Kornakov NV, Dmitriev SE, et al (2014) Identification of a Mg2+-sensitive ORF in the 5′-leader of TRPM7 magnesium channel mRNA. Nucleic Acids Research 42:12779–12788. https://doi.org/10.1093/nar/gku951

209. Xie J, Sun B, Du J, et al (2011) Phosphatidylinositol 4,5-bisphosphate (PIP2) controls magnesium gatekeeper TRPM6 activity. Sci Rep 1:146. https://doi.org/10.1038/srep00146

210. Runnels LW, Yue L, Clapham DE (2002) The TRPM7 channel is inactivated by PIP_2 hydrolysis. Nat Cell Biol 4:329–336. https://doi.org/10.1038/ncb781

211. Krishnamoorthy M, Wasim L, Buhari FHM, et al (2018) The channel-kinase TRPM7 regulates antigen gathering and internalization in B cells. Sci Signal 11:eaah6692. https://doi.org/10.1126/scisignal.aah6692

212. Seo JB, Jung S-R, Huang W, et al (2015) Charge Shielding of PIP_2 by Cations Regulates Enzyme Activity of Phospholipase C. PLoS ONE 10:e0144432. https://doi.org/10.1371/journal.pone.0144432

213. Thebault S, Alexander RT, Tiel Groenestege WM, et al (2009) EGF Increases TRPM6 Activity and Surface Expression. JASN 20:78–85. https://doi.org/10.1681/ASN.2008030327

214. Gao H, Chen X, Du X, et al (2011) EGF enhances the migration of cancer cells by up-regulation of TRPM7. Cell Calcium 50:559–568. https://doi.org/10.1016/j.ceca.2011.09.003

215. Zou Z-G, Rios FJ, Neves KB, et al (2020) Epidermal growth factor signaling through transient receptor potential melastatin 7 cation channel regulates vascular smooth muscle cell function. Clinical Science 134:2019–2035. https://doi.org/10.1042/CS20200827

216. Groenestege WMT, Thébault S, van der Wijst J, et al (2007) Impaired basolateral sorting of pro-EGF causes isolated recessive renal hypomagnesemia. J Clin Invest 117:2260–2267. https://doi.org/10.1172/JCI31680

217. Matsushita M, Kozak JA, Shimizu Y, et al (2005) Channel Function Is Dissociated from the Intrinsic Kinase Activity and Autophosphorylation of TRPM7/ChaK1. Journal of Biological Chemistry 280:20793–20803. https://doi.org/10.1074/jbc.M413671200

218. Cai N, Bai Z, Nanda V, Runnels LW (2017) Mass Spectrometric Analysis of TRPM6 and TRPM7 Phosphorylation Reveals Regulatory Mechanisms of the Channel-Kinases. Sci Rep 7:42739. https://doi.org/10.1038/srep42739

219. Chubanov V, Waldegger S, Schnitzler MM y, et al (2004) Disruption of TRPM6/TRPM7 complex formation by a mutation in the TRPM6 gene causes hypomagnesemia with secondary hypocalcemia. PNAS 101:2894–2899. https://doi.org/10.1073/pnas.0305252101

220. Schwarz F, Aebi M (2011) Mechanisms and principles of N-linked protein glycosylation. Current Opinion in Structural Biology 21:576–582. https://doi.org/10.1016/j.sbi.2011.08.005

221. Wild R, Kowal J, Eyring J, et al (2018) Structure of the yeast oligosaccharyltransferase complex gives insight into eukaryotic N-glycosylation. Science 359:545–550. https://doi.org/10.1126/science.aar5140

222. Kornfeld R, Kornfeld S (1985) Assembly of Asparagine-Linked Oligosaccharides. Annu Rev Biochem 54:631–664. https://doi.org/10.1146/annurev.bi.54.070185.003215

223. Helenius A, Aebi M (2001) Intracellular Functions of N-Linked Glycans. Science 291:2364–2369. https://doi.org/10.1126/science.291.5512.2364

224. Hou W, Qiu Y, Hashimoto N, et al (2016) A systematic framework to derive N-glycan biosynthesis process and the automated construction of glycosylation networks. BMC Bioinformatics 17:240. https://doi.org/10.1186/s12859-016-1094-6

225. Fujita A, Aoki NP, Shinmachi D, et al (2021) The international glycan repository GlyTouCan version 3.0. Nucleic Acids Research 49:D1529–D1533. https://doi.org/10.1093/nar/gkaa947

226. Voolstra O, Huber A (2014) Post-Translational Modifications of TRP Channels. Cells 3:258–287. https://doi.org/10.3390/cells3020258

227. Pertusa M, Madrid R, Morenilla-Palao C, et al (2012) N-Glycosylation of TRPM8 Ion Channels Modulates Temperature Sensitivity of Cold Thermoreceptor Neurons. Journal of Biological Chemistry 287:18218–18229. https://doi.org/10.1074/jbc.M111.312645

228. Hofherr A, Wagner C, Fedeles S, et al (2014) N-Glycosylation Determines the Abundance of the Transient Receptor Potential Channel TRPP2. Journal of Biological Chemistry 289:14854–14867. https://doi.org/10.1074/jbc.M114.562264

229. Woo SK, Kwon MS, Ivanov A, et al (2013) Complex N-Glycosylation Stabilizes Surface Expression of Transient Receptor Potential Melastatin 4b Protein. Journal of Biological Chemistry 288:36409–36417. https://doi.org/10.1074/jbc.M113.530584

230. Li JV, Ng C-A, Cheng D, et al (2021) Modified N-linked glycosylation status predicts trafficking defective human Piezo1 channel mutations. Commun Biol 4:1038. https://doi.org/10.1038/s42003-021-02528-w

231. Varelas X, Bouchie MP, Kukuruzinska MA (2014) Protein N-glycosylation in oral cancer: Dysregulated cellular networks among DPAGT1, E-cadherin adhesion and

canonical Wnt signaling. Glycobiology 24:579–591. https://doi.org/10.1093/glycob/cwu031

232. Sethi MK, Kim H, Park CK, et al (2015) In-depth N-glycome profiling of paired colorectal cancer and non-tumorigenic tissues reveals cancer-, stage- and EGFR-specific protein N-glycosylation. Glycobiology 25:1064–1078. https://doi.org/10.1093/glycob/cwv042

233. Legler K, Rosprim R, Karius T, et al (2018) Reduced mannosidase MAN1A1 expression leads to aberrant N-glycosylation and impaired survival in breast cancer. Br J Cancer 118:847–856. https://doi.org/10.1038/bjc.2017.472

234. Greco B, Malacarne V, De Girardi F, et al (2022) Disrupting N-glycan expression on tumor cells boosts chimeric antigen receptor T cell efficacy against solid malignancies. Sci Transl Med 14:eabg3072. https://doi.org/10.1126/scitranslmed.abg3072

235. Flynn RA, Pedram K, Malaker SA, et al (2021) Small RNAs are modified with N-glycans and displayed on the surface of living cells. Cell 184:3109-3124.e22. https://doi.org/10.1016/j.cell.2021.04.023

236. Zoltowska K, Webster R, Finlayson S, et al (2013) Mutations in GFPT1 that underlie limb-girdle congenital myasthenic syndrome result in reduced cell-surface expression of muscle AChR. Human Molecular Genetics 22:2905–2913. https://doi.org/10.1093/hmg/ddt145

237. Nakajima K, Ito E, Ohtsubo K, et al (2013) Mass Isotopomer Analysis of Metabolically Labeled Nucleotide Sugars and N- and O-Glycans for Tracing Nucleotide Sugar Metabolisms. Molecular & Cellular Proteomics 12:2468–2480. https://doi.org/10.1074/mcp.M112.027151

238. Würde AE, Reunert J, Rust S, et al (2012) Congenital disorder of glycosylation type Ij (CDG-Ij, DPAGT1-CDG): Extending the clinical and molecular spectrum of a rare disease. Molecular Genetics and Metabolism 105:634–641. https://doi.org/10.1016/j.ymgme.2012.01.001

239. Ganetzky R, Izumi K, Edmondson A, et al (2015) Fetal akinesia deformation sequence due to a congenital disorder of glycosylation. Am J Med Genet 167:2411–2417. https://doi.org/10.1002/ajmg.a.37184

240. Kelleher DJ, Karaoglu D, Mandon EC, Gilmore R (2003) Oligosaccharyltransferase Isoforms that Contain Different Catalytic STT3 Subunits Have Distinct Enzymatic Properties. Molecular Cell 12:101–111. https://doi.org/10.1016/S1097-2765(03)00243-0

241. Goytain A, Quamme GA (2005) Identification and characterization of a novel mammalian Mg2+ transporter with channel-like properties. BMC Genomics 6:48. https://doi.org/10.1186/1471-2164-6-48

242. Zhou H, Clapham DE (2009) Mammalian MagT1 and TUSC3 are required for cellular magnesium uptake and vertebrate embryonic development. PNAS 106:15750–15755. https://doi.org/10.1073/pnas.0908332106

243. Cherepanova NA, Shrimal S, Gilmore R (2014) Oxidoreductase activity is necessary for N-glycosylation of cysteine-proximal acceptor sites in glycoproteins. Journal of Cell Biology 206:525–539. https://doi.org/10.1083/jcb.201404083

244. Li F-Y, Chaigne-Delalande B, Kanellopoulou C, et al (2011) Second messenger role for Mg^{2+} revealed by human T-cell immunodeficiency. Nature 475:471–476. https://doi.org/10.1038/nature10246

245. Blommaert E, Péanne R, Cherepanova NA, et al (2019) Mutations in MAGT1 lead to a glycosylation disorder with a variable phenotype. Proc Natl Acad Sci USA 116:9865–9870. https://doi.org/10.1073/pnas.1817815116

246. Matsuda-Lennikov M, Biancalana M, Zou J, et al (2019) Magnesium transporter 1 (MAGT1) deficiency causes selective defects in N-linked glycosylation and expression of immune-response genes. J Biol Chem jbc.RA119.008903. https://doi.org/10.1074/jbc.RA119.008903

247. Brault J, Liu TQ, Bello EA, et al (2021) CRISPR-targeted MAGT1 insertion restores XMEN patient hematopoietic stem cells and lymphocytes. Blood blood.2021011192. https://doi.org/10.1182/blood.2021011192

248. Goytain A, Quamme GA (2008) Identification and characterization of a novel family of membrane magnesium transporters, MMgT1 and MMgT2. American Journal of Physiology-Cell Physiology 294:C495–C502. https://doi.org/10.1152/ajpcell.00238.2007

249. Christianson JC, Olzmann JA, Shaler TA, et al (2012) Defining human ERAD networks through an integrative mapping strategy. Nat Cell Biol 14:93–105. https://doi.org/10.1038/ncb2383

250. Guna A, Volkmar N, Christianson JC, Hegde RS (2018) The ER membrane protein complex is a transmembrane domain insertase. Science 359:470–473. https://doi.org/10.1126/science.aao3099

251. Chitwood PJ, Juszkiewicz S, Guna A, et al (2018) EMC Is Required to Initiate Accurate Membrane Protein Topogenesis. Cell 175:1507-1519.e16. https://doi.org/10.1016/j.cell.2018.10.009

252. Braunger K, Pfeffer S, Shrimal S, et al (2018) Structural basis for coupling protein transport and N-glycosylation at the mammalian endoplasmic reticulum. Science 360:215–219. https://doi.org/10.1126/science.aar7899

253. Goytain A, Hines RM, Quamme GA (2008) Huntingtin-interacting Proteins, HIP14 and HIP14L, Mediate Dual Functions, Palmitoyl Acyltransferase and Mg^{2+} Transport. Journal of Biological Chemistry 283:33365–33374. https://doi.org/10.1074/jbc.M801469200

254. Lemarié FL, Caron NS, Sanders SS, et al (2021) Rescue of aberrant huntingtin palmitoylation ameliorates mutant huntingtin-induced toxicity. Neurobiology of Disease 158:105479. https://doi.org/10.1016/j.nbd.2021.105479

255. Ryazanova LV, Rondon LJ, Zierler S, et al (2010) TRPM7 is essential for Mg^{2+} homeostasis in mammals. Nature Communications 1:109. https://doi.org/10.1038/ncomms1108

256. Yoshida A, Funato Y, Miki H (2018) Phosphatase of regenerating liver maintains cellular magnesium homeostasis. Biochem J 475:1129–1139. https://doi.org/10.1042/BCJ20170756

257. Baaij JHF de, Stuiver M, Meij IC, et al (2012) Membrane Topology and Intracellular Processing of Cyclin M2 (CNNM2). J Biol Chem 287:13644–13655. https://doi.org/10.1074/jbc.M112.342204

258. Arjona FJ, Baaij JHF de (2018) CrossTalk opposing view: CNNM proteins are not Na^{+}/Mg^{2+} exchangers but Mg^{2+} transport regulators playing a central role in transepithelial Mg2+ (re)absorption. The Journal of Physiology 596:747–750. https://doi.org/10.1113/JP275249

259. Downward J (1990) The ras superfamily of small GTP-binding proteins. Trends in Biochemical Sciences 15:469–472. https://doi.org/10.1016/0968-0004(90)90300-Z

260. Newman CMH, Magee AI (1993) Posttranslational processing of the ras superfamily of small GTP-binding proteins. Biochimica et Biophysica Acta (BBA) - Reviews on Cancer 1155:79–96. https://doi.org/10.1016/0304-419X(93)90023-6

261. Nooren IMA, Thornton JM (2003) Diversity of protein–protein interactions. The EMBO Journal 22:3486–3492. https://doi.org/10.1093/emboj/cdg359

262. Sharma A, Saini M, Kundu S, Thelma BK (2020) Computational insight into the three-dimensional structure of ADP ribosylation factor like protein 15, a novel susceptibility gene for rheumatoid arthritis. Journal of Biomolecular Structure and Dynamics 0:1–16. https://doi.org/10.1080/07391102.2020.1860826

263. Baker NA, Sept D, Joseph S, et al (2001) Electrostatics of nanosystems: Application to microtubules and the ribosome. PNAS 98:10037–10041. https://doi.org/10.1073/pnas.181342398

264. Harada Y, Ohkawa Y, Kizuka Y, Taniguchi N (2019) Oligosaccharyltransferase: A Gatekeeper of Health and Tumor Progression. International Journal of Molecular Sciences 20:6074. https://doi.org/10.3390/ijms20236074

265. Gupta R, Jung E, Brunak S (2004) Prediction of N-glycosylation sites in human proteins. In preparation

266. Klaver E, Zhao P, May M, et al (2019) Selective inhibition of N-linked glycosylation impairs receptor tyrosine kinase processing. Disease Models & Mechanisms 12:. https://doi.org/10.1242/dmm.039602

267. Popov M, Li J, Reithmeier RAF (2000) Resolution of Glycoproteins by a Lectin Gel-Shift Assay. Analytical Biochemistry 279:90–95. https://doi.org/10.1006/abio.1999.4443

268. Amr S, Heisey C, Zhang M, et al (2007) A Homozygous Mutation in a Novel Zinc-Finger Protein, ERIS, Is Responsible for Wolfram Syndrome 2. The American Journal of Human Genetics 81:673–683. https://doi.org/10.1086/520961

269. Bajar BT, Wang ES, Lam AJ, et al (2016) Improving brightness and photostability of green and red fluorescent proteins for live cell imaging and FRET reporting. Scientific Reports 6:20889. https://doi.org/10.1038/srep20889

270. Zhang Y, Werling U, Edelmann W (2012) SLiCE: a novel bacterial cell extract-based DNA cloning method. Nucleic Acids Res 40:e55–e55. https://doi.org/10.1093/nar/gkr1288

271. Goedhart J, von Stetten D, Noirclerc-Savoye M, et al (2012) Structure-guided evolution of cyan fluorescent proteins towards a quantum yield of 93%. Nature Communications 3:751. https://doi.org/10.1038/ncomms1738

272. Bagci H, Sriskandarajah N, Robert A, et al (2020) Mapping the proximity interaction network of the Rho-family GTPases reveals signalling pathways and regulatory mechanisms. Nature Cell Biology 22:120–134. https://doi.org/10.1038/s41556-019-0438-7

273. Knight JDR, Choi H, Gupta GD, et al (2017) ProHits-viz: a suite of web tools for visualizing interaction proteomics data. Nature Methods 14:645–646. https://doi.org/10.1038/nmeth.4330

274. Mi H, Muruganujan A, Ebert D, et al (2019) PANTHER version 14: more genomes, a new PANTHER GO-slim and improvements in enrichment analysis tools. Nucleic Acids Res 47:D419–D426. https://doi.org/10.1093/nar/gky1038

275. Eswar N, Eramian D, Webb B, et al (2008) Protein Structure Modeling with MODELLER. In: Kobe B, Guss M, Huber T (eds) Structural Proteomics: High-Throughput Methods. Humana Press, Totowa, NJ, pp 145–159

276. Pettersen EF, Goddard TD, Huang CC, et al (2004) UCSF Chimera—A visualization system for exploratory research and analysis. Journal of Computational Chemistry 25:1605–1612. https://doi.org/10.1002/jcc.20084

277. Shen M, Sali A (2006) Statistical potential for assessment and prediction of protein structures. Protein Science 15:2507–2524. https://doi.org/10.1110/ps.062416606

278. Maier JA, Martinez C, Kasavajhala K, et al (2015) ff14SB: Improving the accuracy of protein side chain and backbone parameters from ff99SB. J Chem Theory Comput 11:3696–3713. https://doi.org/10.1021/acs.jctc.5b00255

279. Emsley P, Lohkamp B, Scott WG, Cowtan K (2010) Features and development of Coot. Acta Cryst D 66:486–501. https://doi.org/10.1107/S0907444910007493

280. Giménez-Mascarell P, Oyenarte I, González-Recio I, et al (2019) Structural Insights into the Intracellular Region of the Human Magnesium Transport Mediator CNNM4. International Journal of Molecular Sciences 20:6279. https://doi.org/10.3390/ijms20246279

281. Ritchie DW, Kemp GJL (2000) Protein docking using spherical polar Fourier correlations. Proteins: Structure, Function, and Bioinformatics 39:178–194. https://doi.org/10.1002/(SICI)1097-0134(20000501)39:2<178::AID-PROT8>3.0.CO;2-6

282. Chuang G-Y, Kozakov D, Brenke R, et al (2008) DARS (Decoys As the Reference State) Potentials for Protein-Protein Docking. Biophysical Journal 95:4217–4227. https://doi.org/10.1529/biophysj.108.135814

283. Yu X, Martinez M, Gable AL, et al (2015) webSDA: a web server to simulate macromolecular diffusional association. Nucleic Acids Res 43:W220–W224. https://doi.org/10.1093/nar/gkv335

284. Elcock AH, Gabdoulline RR, Wade RC, McCammon JA (1999) Computer simulation of protein-protein association kinetics: acetylcholinesterase-fasciculin11Edited by B. Honig. Journal of Molecular Biology 291:149–162. https://doi.org/10.1006/jmbi.1999.2919

285. Gabdoulline RR, Wade RC (2009) On the Contributions of Diffusion and Thermal Activation to Electron Transfer between Phormidium laminosum Plastocyanin and Cytochrome f: Brownian Dynamics Simulations with Explicit Modeling of Nonpolar Desolvation Interactions and Electron Transfer Events. J Am Chem Soc 131:9230–9238. https://doi.org/10.1021/ja809567k

286. Dolinsky TJ, Nielsen JE, McCammon JA, Baker NA (2004) PDB2PQR: an automated pipeline for the setup of Poisson–Boltzmann electrostatics calculations. Nucleic Acids Res 32:W665–W667. https://doi.org/10.1093/nar/gkh381

287. Schneider CA, Rasband WS, Eliceiri KW (2012) NIH Image to ImageJ: 25 years of image analysis. Nature Methods 9:671–675. https://doi.org/10.1038/nmeth.2089

288. Sanjana NE, Shalem O, Zhang F (2014) Improved vectors and genome-wide libraries for CRISPR screening. Nature Methods 11:783–784. https://doi.org/10.1038/nmeth.3047

289. Konermann S, Brigham MD, Trevino AE, et al (2015) Genome-scale transcriptional activation by an engineered CRISPR-Cas9 complex. Nature 517:583–588. https://doi.org/10.1038/nature14136

290. Donaldson JG, Jackson CL (2011) ARF family G proteins and their regulators: roles in membrane transport, development and disease. Nature Reviews Molecular Cell Biology 12:362–375. https://doi.org/10.1038/nrm3117

291. Wilhelmi I, Grunwald S, Gimber N, et al (2020) The ARFRP1-dependent Golgi scaffolding protein GOPC is required for insulin secretion from pancreatic β-cells. Molecular Metabolism 101151. https://doi.org/10.1016/j.molmet.2020.101151

292. Ben-Tekaya H, Kahn RA, Hauri H-P (2010) ADP Ribosylation Factors 1 and 4 and Group VIA Phospholipase A2 Regulate Morphology and Intraorganellar Traffic in the Endoplasmic Reticulum–Golgi Intermediate Compartment. MBoC 21:4130–4140. https://doi.org/10.1091/mbc.e10-01-0022

293. Zheng C, Page RC, Das V, et al (2013) Structural Characterization of Carbohydrate Binding by LMAN1 Protein Provides New Insight into the Endoplasmic Reticulum Export of Factors V (FV) and VIII (FVIII). J Biol Chem 288:20499–20509. https://doi.org/10.1074/jbc.M113.461434

294. Shen X, Hong M-S, Moss J, Vaughan M (2007) BIG1, a brefeldin A-inhibited guanine nucleotide-exchange protein, is required for correct glycosylation and function of integrin β1. PNAS 104:1230–1235. https://doi.org/10.1073/pnas.0610535104

295. Singh R, Almutairi MM, Pacheco-Andrade R, et al (2015) Impact of Hybrid and Complex N-Glycans on Cell Surface Targeting of the Endogenous Chloride Cotransporter Slc12a2. In: International Journal of Cell Biology. https://www.hindawi.com/journals/ijcb/2015/505294/. Accessed 7 Jan 2021

296. Hayashi H, Yamashita Y (2011) Role of N-glycosylation in cell surface expression and protection against proteolysis of the intestinal anion exchanger SLC26A3.

American Journal of Physiology-Cell Physiology 302:C781–C795. https://doi.org/10.1152/ajpcell.00165.2011

297. Cohen DM (2006) Regulation of TRP channels by N-linked glycosylation. Seminars in Cell & Developmental Biology 17:630–637. https://doi.org/10.1016/j.semcdb.2006.11.007

298. Dennis JW, Lau KS, Demetriou M, Nabi IR (2009) Adaptive Regulation at the Cell Surface by N-Glycosylation. Traffic 10:1569–1578. https://doi.org/10.1111/j.1600-0854.2009.00981.x

299. Gabius H-J, Kayser K (2014) Introduction to glycopathology: the concept, the tools and the perspectives. Diagn Pathol 9:4. https://doi.org/10.1186/1746-1596-9-4

300. Chang Q, Hoefs S, Kemp AW van der, et al (2005) The ß-Glucuronidase Klotho Hydrolyzes and Activates the TRPV5 Channel. Science 310:490–493. https://doi.org/10.1126/science.1114245

301. Leunissen EHP, Nair AV, Büll C, et al (2013) The Epithelial Calcium Channel TRPV5 Is Regulated Differentially by Klotho and Sialidase. J Biol Chem 288:29238–29246. https://doi.org/10.1074/jbc.M113.473520

302. Voets T, Nilius B, Hoefs S, et al (2004) TRPM6 Forms the Mg^{2+} Influx Channel Involved in Intestinal and Renal Mg^{2+} Absorption. J Biol Chem 279:19–25. https://doi.org/10.1074/jbc.M311201200

303. Chery M, Biancalana V, Philippe C, et al (1994) Hypomagensemia with secondary hypocalcemia in a female with balanced X;9 translocation: mapping of the Xp22 chromosome breakpoint. Hum Genet 93:587–591. https://doi.org/10.1007/BF00202829

304. Hashizume O, Funato Y, Yamazaki D, Miki H (2020) Excessive Mg^{2+} Impairs Intestinal Homeostasis by Enhanced Production of Adenosine Triphosphate and Reactive Oxygen Species. Antioxidants & Redox Signaling 33:20–34. https://doi.org/10.1089/ars.2019.7951

305. Mahajan A, Go MJ, Zhang W, et al (2014) Genome-wide trans-ancestry meta-analysis provides insight into the genetic architecture of type 2 diabetes susceptibility. Nature Genetics 46:234–244. https://doi.org/10.1038/ng.2897

306. Teslovich TM, Musunuru K, Smith AV, et al (2010) Biological, clinical and population relevance of 95 loci for blood lipids. Nature 466:707–713. https://doi.org/10.1038/nature09270

307. Willer CJ, Schmidt EM, Sengupta S, et al (2013) Discovery and refinement of loci associated with lipid levels. Nature Genetics 45:1274–1283. https://doi.org/10.1038/ng.2797

308. Zhao J, Wang M, Deng W, et al (2017) ADP-ribosylation factor-like GTPase 15 enhances insulin-induced AKT phosphorylation in the IR/IRS1/AKT pathway by interacting with ASAP2 and regulating PDPK1 activity. Biochemical and Biophysical Research Communications 486:865–871. https://doi.org/10.1016/j.bbrc.2017.03.079

309. Uetani N, Hardy S, Gravel S-P, et al (2017) PRL2 links magnesium flux and sex-dependent circadian metabolic rhythms. JCI Insight 2:. https://doi.org/10.1172/jci.insight.91722

310. Monteilh-Zoller MK, Hermosura MC, Nadler MJS, et al (2003) TRPM7 Provides an Ion Channel Mechanism for Cellular Entry of Trace Metal Ions. Journal of General Physiology 121:49–60. https://doi.org/10.1085/jgp.20028740

311. Jin J, Wu L-J, Jun J, et al (2012) The channel kinase, TRPM7, is required for early embryonic development. Proceedings of the National Academy of Sciences 109:E225–E233. https://doi.org/10.1073/pnas.1120033109

312. Komiya Y, Runnels LW (2015) TRPM channels and magnesium in early embryonic development. Int J Dev Biol 59:281–288. https://doi.org/10.1387/ijdb.150196lr

313. Dorovkov MV, Ryazanov AG (2004) Phosphorylation of Annexin I by TRPM7 Channel-Kinase. Journal of Biological Chemistry 279:50643–50646. https://doi.org/10.1074/jbc.C400441200

314. Abed E, Moreau R (2007) Importance of melastatin-like transient receptor potential 7 and cations (magnesium, calcium) in human osteoblast-like cell proliferation. Cell Prolif 40:849–865. https://doi.org/10.1111/j.1365-2184.2007.00476.x

315. Sahni J, Scharenberg AM (2008) TRPM7 Ion Channels Are Required for Sustained Phosphoinositide 3-Kinase Signaling in Lymphocytes. Cell Metabolism 8:84–93. https://doi.org/10.1016/j.cmet.2008.06.002

316. Wang J, Liao Q, Zhang Y, et al (2014) TRPM7 is required for ovarian cancer cell growth, migration and invasion. Biochemical and Biophysical Research Communications 454:547–553. https://doi.org/10.1016/j.bbrc.2014.10.118

317. Chen L, Cao R, Wang G, et al (2017) Downregulation of TRPM7 suppressed migration and invasion by regulating epithelial–mesenchymal transition in prostate cancer cells. Med Oncol 34:127. https://doi.org/10.1007/s12032-017-0987-1

318. Baldoli E, Castiglioni S, Maier JAM (2013) Regulation and Function of TRPM7 in Human Endothelial Cells: TRPM7 as a Potential Novel Regulator of Endothelial Function. PLoS ONE 8:e59891. https://doi.org/10.1371/journal.pone.0059891

319. Su L-T, Liu W, Chen H-C, et al (2011) TRPM7 regulates polarized cell movements. Biochemical Journal 434:513–521. https://doi.org/10.1042/BJ20101678

320. Luanpitpong S, Rodboon N, Samart P, et al (2020) A novel TRPM7/O-GlcNAc axis mediates tumour cell motility and metastasis by stabilising c-Myc and caveolin-1 in lung carcinoma. British Journal of Cancer 1–13. https://doi.org/10.1038/s41416-020-0991-7

321. Voringer S, Schreyer L, Nadolni W, et al (2019) Inhibition of TRPM7 blocks MRTF/SRF-dependent transcriptional and tumorigenic activity. Oncogene 1–17. https://doi.org/10.1038/s41388-019-1140-8

322. Guilbert A, Gautier M, Dhennin-Duthille I, et al (2009) Evidence that TRPM7 is required for breast cancer cell proliferation. American Journal of Physiology-Cell Physiology 297:C493–C502. https://doi.org/10.1152/ajpcell.00624.2008

323. Liu K, Xu S-H, Chen Z, et al (2018) TRPM7 overexpression enhances the cancer stem cell-like and metastatic phenotypes of lung cancer through modulation of the Hsp90α/uPA/MMP2 signaling pathway. BMC Cancer 18:1167. https://doi.org/10.1186/s12885-018-5050-x

324. Su L-T, Agapito MA, Li M, et al (2006) TRPM7 Regulates Cell Adhesion by Controlling the Calcium-dependent Protease Calpain. Journal of Biological Chemistry 281:11260–11270. https://doi.org/10.1074/jbc.M512885200

325. Abed E, Moreau R (2009) Importance of melastatin-like transient receptor potential 7 and magnesium in the stimulation of osteoblast proliferation and migration by platelet-derived growth factor. American Journal of Physiology-Cell Physiology 297:C360–C368. https://doi.org/10.1152/ajpcell.00614.2008

326. Yankaskas CL, Bera K, Stoletov K, et al (2021) The fluid shear stress sensor TRPM7 regulates tumor cell intravasation. Sci Adv 7:eabh3457. https://doi.org/10.1126/sciadv.abh3457

327. Zolotarov Y, Ma C, González-Recio I, et al (2021) ARL15 modulates magnesium homeostasis through N-glycosylation of CNNMs. Cell Mol Life Sci 78:5427–5445. https://doi.org/10.1007/s00018-021-03832-8

328. Kubota T, Shindo Y, Tokuno K, et al (2005) Mitochondria are intracellular magnesium stores: investigation by simultaneous fluorescent imagings in PC12 cells. Biochimica et Biophysica Acta (BBA) - Molecular Cell Research 1744:19–28. https://doi.org/10.1016/j.bbamcr.2004.10.013

329. Chubanov V, Mederos y Schnitzler M, Meißner M, et al (2012) Natural and synthetic modulators of SK (Kca2) potassium channels inhibit magnesium-dependent activity of the kinase-coupled cation channel TRPM7: Pharmacological targeting of TRPM7. British Journal of Pharmacology 166:1357–1376. https://doi.org/10.1111/j.1476-5381.2012.01855.x

330. Sawicka K, Pyronneau A, Chao M, et al (2016) Elevated ERK/p90 ribosomal S6 kinase activity underlies audiogenic seizure susceptibility in fragile X mice. Proc Natl Acad Sci USA 113:E6290–E6297. https://doi.org/10.1073/pnas.1610812113

331. Go CD, Knight JDR, Rajasekharan A, et al (2021) A proximity-dependent biotinylation map of a human cell. Nature 595:120–124. https://doi.org/10.1038/s41586-021-03592-2

332. Hermosura MC, Monteilh-Zoller MK, Scharenberg AM, et al (2002) Dissociation of the store-operated calcium current I _CRAC_ and the Mg-nucleotide-regulated metal ion current MagNuM. The Journal of Physiology 539:445–458. https://doi.org/10.1113/jphysiol.2001.013361

333. Schmitz C, Perraud A-L, Johnson CO, et al (2003) Regulation of Vertebrate Cellular Mg^{2+} Homeostasis by TRPM7. Cell 114:191–200. https://doi.org/10.1016/S0092-8674(03)00556-7

334. Demeuse P, Penner R, Fleig A (2006) TRPM7 Channel Is Regulated by Magnesium Nucleotides via its Kinase Domain. Journal of General Physiology 127:421–434. https://doi.org/10.1085/jgp.200509410

335. Yee N (2017) Role of TRPM7 in Cancer: Potential as Molecular Biomarker and Therapeutic Target. Pharmaceuticals 10:39. https://doi.org/10.3390/ph10020039

336. Meng S, Alanazi R, Ji D, et al (2021) Role of TRPM7 kinase in cancer. Cell Calcium 96:102400. https://doi.org/10.1016/j.ceca.2021.102400

337. Middelbeek J, Kuipers AJ, Henneman L, et al (2012) TRPM7 Is Required for Breast Tumor Cell Metastasis. Cancer Res 72:4250–4261. https://doi.org/10.1158/0008-5472.CAN-11-3863

338. Jiang J, Li M-H, Inoue K, et al (2007) Transient Receptor Potential Melastatin 7–like Current in Human Head and Neck Carcinoma Cells: Role in Cell Proliferation. Cancer Res 67:10929–10938. https://doi.org/10.1158/0008-5472.CAN-07-1121

339. Lainez S, Schlingmann KP, van der Wijst J, et al (2014) New TRPM6 missense mutations linked to hypomagnesemia with secondary hypocalcemia. Eur J Hum Genet 22:497–504. https://doi.org/10.1038/ejhg.2013.178

340. Gungabeesoon J, Tremblay ML, Uetani N (2016) Localizing PRL-2 expression and determining the effects of dietary Mg2+ on expression levels. Histochem Cell Biol 146:99–111. https://doi.org/10.1007/s00418-016-1427-6

341. Costantini LM, Baloban M, Markwardt ML, et al (2015) A palette of fluorescent proteins optimized for diverse cellular environments. Nat Commun 6:7670. https://doi.org/10.1038/ncomms8670

342. Younis I, Berg M, Kaida D, et al (2010) Rapid-Response Splicing Reporter Screens Identify Differential Regulators of Constitutive and Alternative Splicing. Mol Cell Biol 30:1718–1728. https://doi.org/10.1128/MCB.01301-09

343. Ran FA, Hsu PD, Wright J, et al (2013) Genome engineering using the CRISPR-Cas9 system. Nat Protoc 8:2281–2308. https://doi.org/10.1038/nprot.2013.143

344. Ford ES, Mokdad AH (2003) Dietary Magnesium Intake in a National Sample of U.S. Adults. The Journal of Nutrition 133:2879–2882. https://doi.org/10.1093/jn/133.9.2879

345. Franken GAC, Seker M, Bos C, et al (2021) Cyclin M2 (CNNM2) knockout mice show mild hypomagnesaemia and developmental defects. Scientific Reports 11:8217. https://doi.org/10.1038/s41598-021-87548-6

346. Schlingmann KP, Weber S, Peters M, et al (2002) Hypomagnesemia with secondary hypocalcemia is caused by mutations in TRPM6 , a new member of the TRPM gene family. Nature Genetics 31:166. https://doi.org/10.1038/ng889

347. Stark C, Breitkreutz B-J, Reguly T, et al (2006) BioGRID: a general repository for interaction datasets. Nucleic Acids Res 34:D535-539. https://doi.org/10.1093/nar/gkj109

348. Schmidt E, Narangoda C, Nörenberg W, et al (2022) Structural mechanism of TRPM7 channel regulation by intracellular magnesium. Cell Mol Life Sci 79:225. https://doi.org/10.1007/s00018-022-04192-7

349. Overton JD, Komiya Y, Mezzacappa C, et al (2015) Hepatocystin is Essential for TRPM7 Function During Early Embryogenesis. Scientific Reports 5:18395. https://doi.org/10.1038/srep18395

350. Bai Z, Feng J, Franken GAC, et al (2021) CNNM proteins selectively bind to the TRPM7 channel to stimulate divalent cation entry into cells. PLoS Biol 19:e3001496. https://doi.org/10.1371/journal.pbio.3001496